PERFORMANCE CHARACTERISTICS OF A NOVEL UNIFLOW-SCAVENGED GASOLINE DIRECT-INJECTION TWO-STROKE ENGINE

by

STEVEN HAROLD IRWIN REYNOLDS

A thesis submitted to the

Department of Mechanical and Materials Engineering

in conformity with the requirements

for the degree of Master of Science (Engineering)

Queen's University

Kingston, Ontario, Canada

June 2007

Your file Votre référence
ISBN: 978-0-494-30276-7
Our file Notre référence
ISBN: 978-0-494-30276-7

Abstract

The performance characteristics of a novel uniflow-scavenged gasoline direct-injection two-stroke engine are presented in this thesis. The feature that makes this engine novel is the engine head. It contains multiple passive check valves used to control airflow into the cylinder. A thin platelet is contained within the check valve cavity that reacts to the pressure difference across the engine head. When the intake plenum pressure is higher than the cylinder pressure, air flows through the check valve. When the intake plenum pressure is lower than the cylinder pressure, airflow is not permitted through the check valve. This engine head design provides asymmetrical intake valve timing and abolishes the need for traditional cams and the associated valve train. In combination with an external Roots-type supercharger and exhaust ports at the base of the cylinder wall, the novel head provides top-down uniflow air scavenging. The engine is equipped with gasoline direct injection to eliminate fuel short-circuiting, a common problem with traditional two-stroke engines.

Motoring tests were performed to identify check valve characteristics and revealed that the platelets have a finite closing time that is dependent on engine speed. The engine was connected to a hydraulic dynamometer for fired engine tests. The head design was validated at low engine speeds ranging from 1250 to 2000 rpm. Both indicated torque and indicated specific fuel consumption performance diminished with increasing engine speed, revealing that improvements in engine scavenging and mixture preparation are necessary.

Acknowledgments

I would like to thank Professor Gaby Ciccarelli for the opportunity to work on this project and the guidance that he offered during my time in the combustion lab. I would also like to thank my parents and brother for their support. I am very fortunate to have a family that inspires me to be a better person. I would like to recognise the graduate students that I have had the pleasure of working with in the combustion lab. I am grateful for their sound advice and friendship over the past two years. Much thanks also goes to the office staff, department technicians, and machine shop staff of McLaughlin Hall who helped to make this project possible.

Table of Contents

List of Tables

List of Figures

Nomenclature

Symbols

a	Crankshaft radius
A_{ref}	Reference area
b	Cylinder bore
C_d	Discharge coefficient
C_f	Flow coefficient
C_p	Specific heat at constant pressure
D	Diameter
e	Charge amplifier voltage output
l	Connecting rod length
m	Slope
$\dot{m}$	Mass flow rate
$\dot{m}_a$	Air mass flow rate
$\dot{m}_{au}$	Uncorrected air mass flow rate
$\dot{m}_f$	Fuel mass flow rate
$\dot{m}_i$	Ideal mass flow rate
n	Polytropic exponent
n_R	Number of crankshaft revolutions per power stroke
N	Engine speed
p	Pressure
p_c	Cylinder pressure

p_i	Initial pressure
p_r	Pressure ratio
p_{01}	Atmospheric pressure
p_2	Static pressure downstream from the valve
P_b	Brake power
$P_{density}$	Power density
P_f	Friction power
P_i	Indicated power
P_s	Supercharger power
Q_a	Volumetric air flow rate
Q_{HV}	Fuel heating value
r_c	Compression ratio
R	Gas constant
s	Stroke
s_a	Adjusted stroke
T	Temperature
T_{amb}	Ambient temperature
T_i	Indicated torque
V	Volume
V_c	Clearance volume
V_d	Displacement volume
V_i	Initial volume
W_i	Indicated work

x	bar/volt value
z	Intercept
ϕ	Equivalence ratio
γ	Specific heat ratio
η_c	Combustion efficiency
η_{sc}	Scavenging efficiency
η_t	Thermal efficiency
Λ	Delivery ratio
θ	Crankshaft angle
ρ	Air density
σ_{IMEP}	Standard deviation in indicated mean effective pressure

Abbreviations

2S	Two-stroke engine
4S	Four-stroke engine
AA	Air-assist fuel injection
aBDC	After bottom dead centre
AC	Alternating current
AF	Air-fuel ratio
AF_s	Stoichiometric air-fuel ratio
aTDC	After top dead centre
bBDC	Before bottom dead centre
BDC	Bottom dead centre
BMEP	Brake mean effective pressure

BSFC	Brake specific fuel consumption
bTDC	Before top dead centre
CAI	Controlled auto ignition
CI	Compression ignition
CO_2	Carbon dioxide
COV	Coefficient of variation
CV	Constant velocity
DAQ	Data acquisition
ECU	Engine control unit
ELEVATE	European low emission V4 automotive two-stroke engine
EOI	End of injection
FR	Fuel flow rate
GDI	Gasoline direct injection
HP	High-pressure fuel only injection
IC	Internal combustion
ID	Inside diameter
IMEP	Indicated mean effective pressure
ISFC	Indicated specific fuel consumption
MBT	Maximum brake torque
MEP	Mean effective pressure
MPFI	Multi-port fuel injection
NO_x	Nitrogen oxides
NI	National Instruments

OCP	Orbital combustion process
PFI	Port fuel injection
PW	Fuel pulse width
rpm	Revolutions per minute
SFC	Specific fuel consumption
SI	Spark ignition
SMD	Sauter mean diameter
SOI	Start of injection
TDC	Top dead centre

Chapter 1 Introduction

The internal combustion (IC) engine has been converting fuel into useable mechanical work for the last two centuries and still remains one of the most utilized prime movers in the world. As such, there is a continuous effort to improve the IC engine through the use of innovative design, materials, manufacturing techniques, and fuels. The objective of this thesis is to report on the performance of a novel two-stroke IC engine that is being researched in the IC engine laboratory in the Department of Mechanical and Materials Engineering at Queen's University.

The "novel engine," as it will be referred to throughout this thesis, is a gasoline direct-injection (GDI) two-stroke engine that uses top-down uniflow scavenging. The feature that makes this engine novel is its use of multiple passive check valves in the engine head to control airflow into the cylinder as described in the patent by Hans Ohlman [1]. Each check valve contains a thin steel platelet that reacts to the pressure difference across it.

When the cylinder pressure is greater than the intake plenum pressure, the platelet seats against the head and stops the airflow into the cylinder. When the intake plenum pressure is greater than the cylinder pressure, the platelet rests on the retaining plate and permits the airflow into the cylinder. This simple engine head design provides a means for controlling the incoming air charge without the use of cams and valve train.

Two-stroke engines have the characteristic of producing a power stroke for every revolution of the crankshaft opposed to every two revolutions for four-stroke engines. Theoretically, a two-stroke engine has the potential to produce twice the power of a four stroke for the same displacement. In reality this is not possible due to the challenge of

replacing the combustion products from the previous cycle with a new charge for the next cycle.

Traditional two-strokes have been plagued with high fuel consumption caused by a fuel short-circuiting where part of the air-fuel mixture escapes out of the exhaust before it has a chance to combust. With the application of gasoline direct injection, fuel injection can be controlled to eliminate short-circuiting and reduce fuel consumption.

With the power density gains of the two-stroke cycle, elimination of short-circuiting with GDI, and simplified head design, there is motivation to develop a simple, light, and fuel efficient two-stroke engine. To date the development of this engine has been documented in multiple papers focused on scavenging, airflow, and apparatus development [2-7]. Other in-depth studies have also been completed; in 2005 Rival [8] completed a master's thesis on the scavenging of this engine and in 2007 Ohlmann [9] completed a master's thesis on the development of this engine. The thesis presented here is a continuation of the work carried out by Ohlmann.

The engine's first successful run was in 2005, as described by Ohlmann, but it was apparent that an improved test apparatus was needed for any further testing. As a result, the apparatus was substantially improved during this project so that the objectives of measuring engine performance could be achieved. A new supercharger and surge tank were added and the following engine components were improved: intake system, fuel injection assembly, starting system, dynamometer connection, data acquisition system, and cooling system. With these improvements, the engine operated reliably so that performance could be measured. Even though much research and design work went into

improving the current apparatus, the focus of this thesis is on the measurement analysis of the engine performance.

Many tests were done throughout the course of this project. Airflow and motoring tests were performed on the engine head to gain insight into the characteristics of the check valve design. These results showed how the check valve performance changed with different check valve components. Multiple fired engine tests were done to reveal the operating characteristics of this engine and to measure performance. The engine was operated in homogeneous charge mode since the engine was still in the proof of principle stage and the engine lacked the architecture necessary for stratified charge mode. The improved engine test apparatus, airflow tests, motoring tests, and fired engine tests performed during this project contribute to the development of this novel engine. The result of this work provides, for the first time, the engine performance at low speed for this novel engine.

This thesis first presents a background in internal combustion engines and reviews current two-stroke GDI technology. The apparatus, results, and conclusions are then presented. The results considered important are discussed in depth while the other results are listed for reference. Conclusions based on the experimental results are presented and some recommendations for future work on this engine are offered.

Chapter 2 Background and Theory

2.1 Internal Combustion Engine Fundamentals

A review of IC engine fundamentals is required before presenting a cycle specific discussion. Simply put, an IC engine ignites an air-fuel mixture in a combustion chamber and converts the energy release into useable mechanical work. Traditionally, internal combustion engines use a piston in cylinder arrangement to contain the reaction in a variable volume. The piston is connected to a crankshaft via a connecting rod that changes linear motion to rotational motion and hence creates a torque on the crankshaft. The main stages of the engine cycle are intake, compression, power and exhaust; the stages will be reviewed independently for both the four-stroke engine and two-stroke engine. These two types of engines can operate with different fuels and different thermodynamic cycles. Typical spark ignition (SI) engines operate with the Otto cycle where a pre-mixed air-fuel mixture burns at constant volume while compression ignition (CI) engines operate with the Diesel cycle where fuel is injected directly into the cylinder and burned at a constant pressure.

Figure 2.1 shows the geometric relations required to define the properties of an engine. The bore, b, and stroke, s, are used to define the displacement volume, V_d, of the engine, via Eq. 2.1. The clearance volume, V_c, is the volume of the cylinder when the piston is at top dead centre (TDC).

$$V_d = \frac{\pi b^2}{4} s \qquad (2.1)$$

The compression ratio, r_c, is defined in Eq. 2.2 as the total volume in the cylinder when the piston is at bottom dead centre (BDC) divided by the clearance volume. For

two-stroke engines, the exhaust port stays open for part of the piston's upward stroke resulting in no compression. Therefore, an "effective compression ratio" is calculated using the adjusted stroke, s_a, see Figure 2.1.

$$r_c = \frac{V_c + V_d}{V_c} \quad (2.2)$$

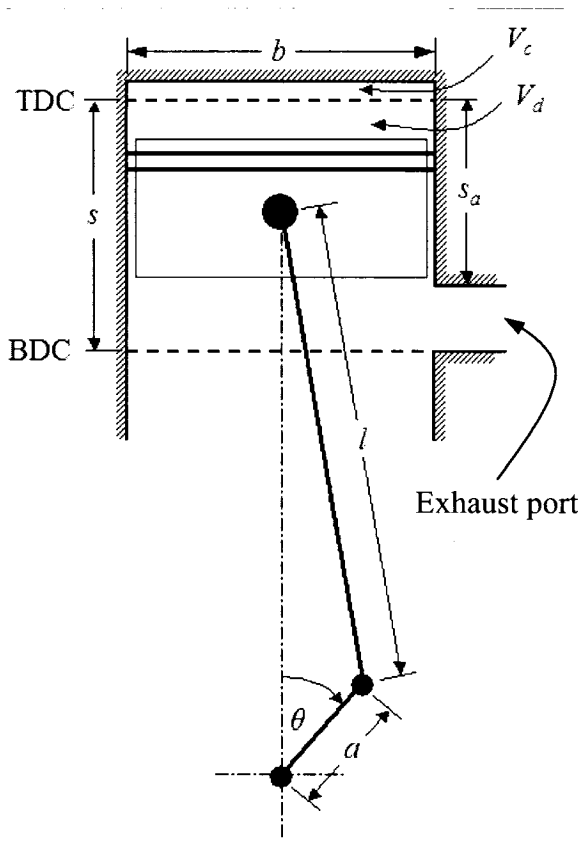

b - bore

s - stroke

s_a – adjusted stroke

l – connecting rod length

a – crankshaft radius (a = s/2)

V_c – clearance volume

V_d – displacement volume

θ - crankshaft angle

TDC – top dead centre

BDC – bottom dead centre

Figure 2.1: Engine geometric relations.

2.1.1 Four-Stroke Cycle Engine

Despite the fact that this thesis focuses on two-stroke technology, it is necessary that a brief review of four-stroke SI engine theory be presented for comparison purposes. In a four-stroke engine, four strokes of the piston, and hence two revolutions of the

crankshaft, are required for a single combustion event: intake, compression, power, and exhaust. The exhaust and intake strokes form the gas exchange period where the exhaust products from the previous combustion event are replaced with a fresh charge. The four strokes are shown in Figure 2.2. The valves permit the gas exchange, the cylinder contains the combustion, and the piston does work on the crankshaft.

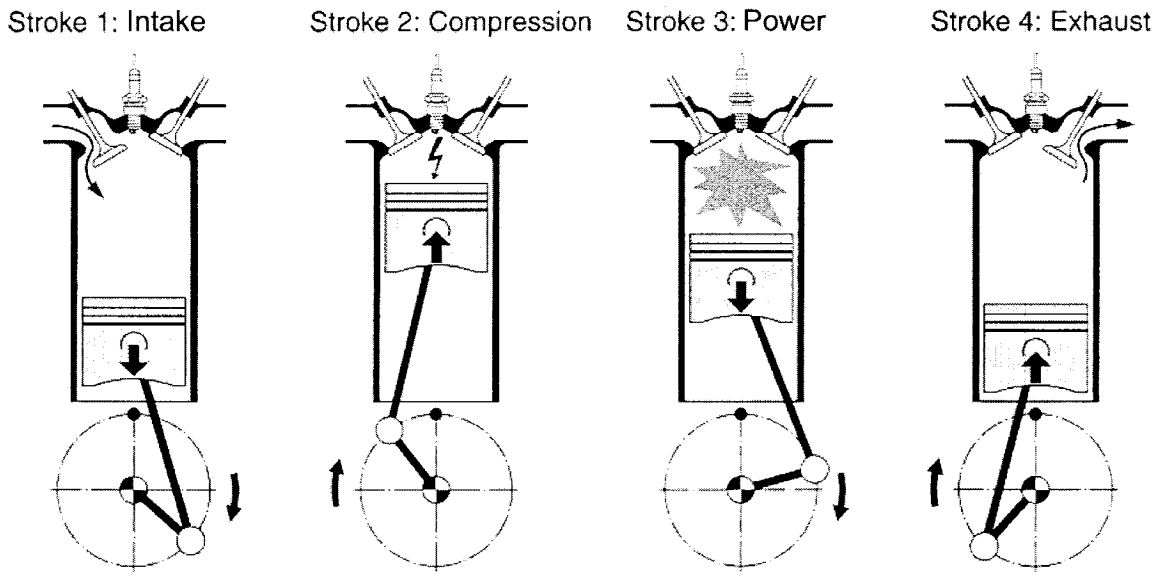

Figure 2.2: Main stages of a four-stroke engine cycle, adapted from [10].

During the intake stroke, the intake valve opens and the piston moves towards BDC. This increases the cylinder volume and creates a pressure lower than that of the intake. The intake charge flows from the intake plenum through the intake valve and into the cylinder. The intake charge can be a premixed air-fuel mixture as with carbureted or port fuel-injection (PFI) engines, or pure air as with diesel or GDI engines.

During the compression stroke the intake and exhaust valves are closed. The piston moves towards TDC and compresses the air-fuel mixture. The mixture is ignited by a spark plug late in the compression stroke and the air-fuel mixture starts to burn. The valves remain closed as the piston begins the power stroke. The hot, high-pressure

combustion gases push the piston towards BDC to do work on the crankshaft. At the end of the power stroke the exhaust valve opens and the piston begins to move towards TDC, pushing the combustion products through the exhaust valve into the exhaust system.

The cycle then begins again when the piston moves back towards BDC and a fresh charge enters the cylinder. The important thing to note is that two strokes during the cycle have been sacrificed for the purpose of the gas exchange process: a stroke for inducting a fresh charge and another stroke for exhausting the combustion products. As will be seen, two-stroke engines manage the gas exchange process very differently than four-stroke engines. For further reading on four-stroke engines refer to [11].

2.1.2 Two-Stroke Cycle Engine

The two-stroke cycle engine produces a power pulse every two strokes of the piston or one revolution of the crankshaft. As a result, typical two-stroke power densities can be 60% greater than that of a four-stroke [12]. Figure 2.3 shows the operation of a typical traditional crankcase scavenged spark ignition two-stroke engine.

The power stroke begins as the piston passes TDC with the high-temperature and high-pressure combustion gases pushing the piston down, turning the crankshaft. At about 60° before BDC (bBDC) the exhaust ports open and the hot combustion gases escape, reducing the cylinder pressure to that of the exhaust system. At that time, the intake ports, also referred to as the scavenge ports, open and a fresh charge flows into the cylinder, scavenging the combustion products and displacing them out the exhaust ports.

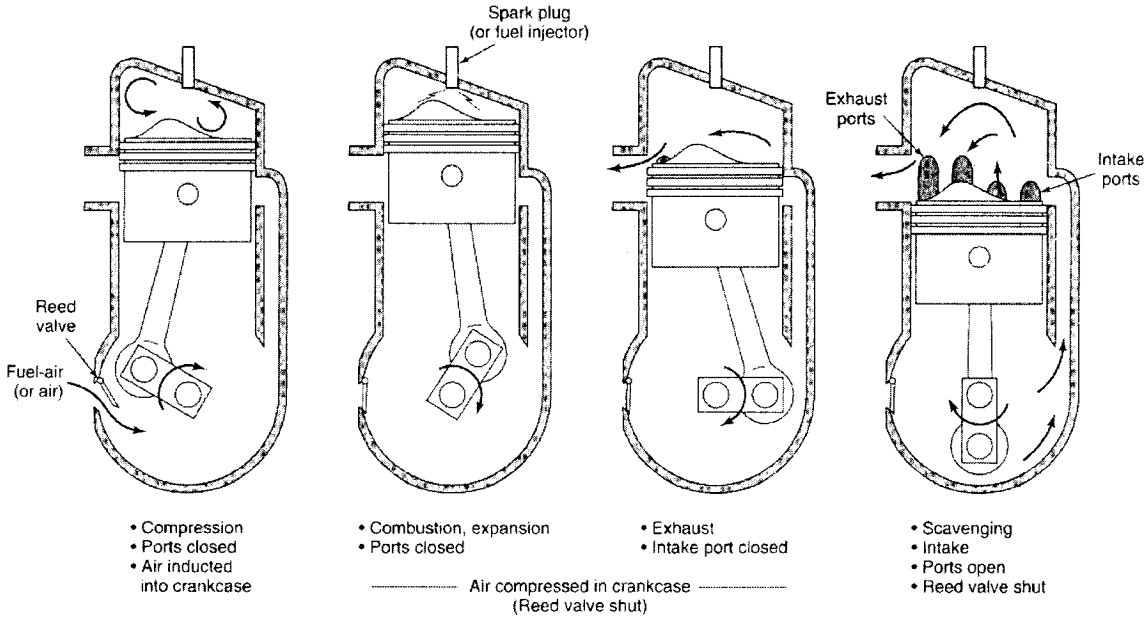

Figure 2.3: Two-stroke engine operation [13].

The compression stroke begins just after the piston passes through BDC. The piston moves up, closing the scavenge port followed by the exhaust port, and finally compresses the air-fuel mixture in preparation for ignition. Just before TDC the compressed mixture is ignited and the cycle repeats itself. Note that the fresh charge must be delivered to the cylinder at a pressure high enough to scavenge the combustion products. For the engine shown in Figure 2.3, the fresh charge is compressed in the crankcase.

Important to note is that the gas exchange process takes place at BDC, positioned between the power stroke and the compression stroke. The gas exchange process starts when the exhaust ports open and ends when both the exhaust ports and scavenge ports close. The two sections that make up the gas exchange process are blowdown and scavenging. Blowdown occurs first and refers to the period from exhaust port open to

scavenge port open. During this time, high-pressure exhaust gas escapes through the exhaust port and the cylinder pressure becomes almost equal to the exhaust pressure.

Scavenging starts when the scavenge ports open and ends when both the exhaust and scavenge ports close. It is during scavenging that a fresh intake charge enters the cylinder to displace the combustion products in preparation for the next combustion event. As a result, effective scavenging is critical for the successful operation of a two-stroke engine and has been the focus of much two-stroke engine research.

2.1.3 Performance Definitions

Indicated Power

The indicted power, P_i, for an engine represents the rate of work done on the piston by the combustion gases in the cylinder. This differs from the brake power, P_b, that is the power available at the crankshaft, by the amount of the friction power, P_f, see Eq. 2.3. Friction power is a result of the engine bearings, piston friction, and engine accessories.

$$P_i = P_b + P_f \quad (2.3)$$

To find the indicated power, P_i, the indicated work per cycle, W_i, must be calculated first. The indicated work per cycle is represented by the area within the pV curve, or indicator diagram, shown in Figure 2.4. This area is found by integrating the pV curve for one cycle.

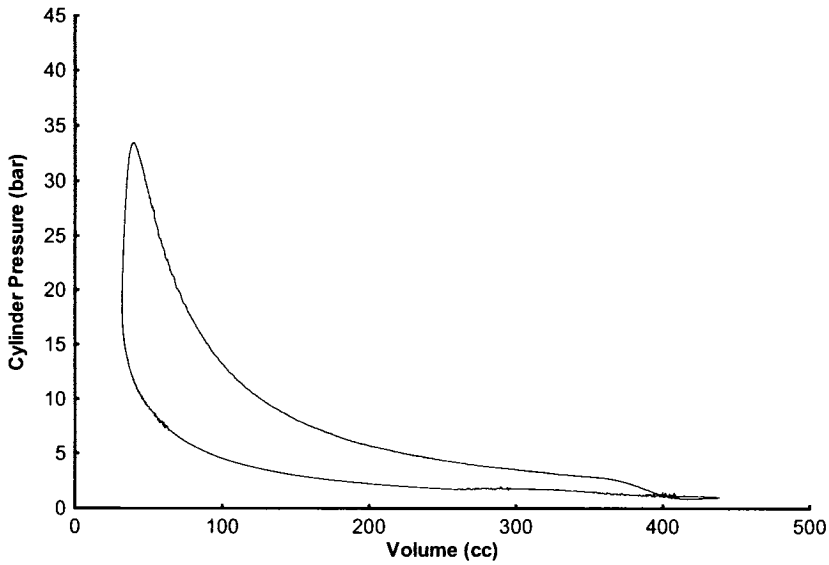

Figure 2.4: Indicator diagram for the novel two-stroke engine at 2000 rpm and 5.5 ms fuel pulse width.

The indicator diagram is plotted using pressure data and crank angle data. The crank angle data is converted into an associated volume using Eq. 2.4 (see section 2.1 for variable definitions).

$$V(\theta) = V_C + \frac{\pi b^2}{4}\left(l + a - \left(a\cos\theta + \left(l^2 - a^2\sin^2\theta\right)^{\frac{1}{2}}\right)\right) \qquad (2.4)$$

The indicated power per cylinder is found using the indicated work per cycle, engine speed, N, in revolutions per minute (rpm), and n_R as shown in Eq. 2.5. The variable, n_R, is the number of crankshaft revolutions per power stroke, $n_R = 1$ for a two-stroke engine. The indicated torque, T_i, is related to the indicated power by Eq. 2.6. Note that the indicated torque is independent of the engine speed.

$$P_i = \frac{W_i N}{n_R 60} \qquad (2.5)$$

$$T_i = \frac{W_i}{2\pi} = \frac{P_i 30 n_R}{\pi N} \qquad (2.6)$$

Mean Effective Pressure

The mean effective pressure (MEP) is defined as a constant pressure that would produce the same power per cycle if it acted on the piston for the power stroke. It can also be interpreted as the work per cycle normalized by the displacement volume. This term allows engines of different displacements to be compared. The indicated mean effective pressure (IMEP) uses the indicated power while the brake mean effective pressure (BMEP) uses the brake power. The IMEP is defined in Eq. 2.7.

$$IMEP = \frac{W_i}{V_d} = \frac{2\pi T_i}{V_d} = \frac{P_i 60 n_R}{V_d N} \qquad (2.7)$$

Specific Fuel Consumption

Specific fuel consumption (SFC) compares the fuel burned by the engine to the power output. It is calculated using the fuel mass flow rate, $\dot{m}_f$, divided by the power. As with the mean effective pressure, indicated specific fuel consumption (ISFC) uses the indicated power while the brake specific fuel consumption (BSFC) uses the brake power. The ISFC is presented in Eq. 2.8.

$$ISFC = \frac{\dot{m}_f}{P_i} \qquad (2.8)$$

Indicated Thermal Efficiency and Fuel Conversion Efficiency

The indicated thermal efficiency is a measure of how well the available energy from the fuel is converted into usable work. It is defined as the indicated power divided by the product of the fuel mass flow rate, lower heating value of the fuel, Q_{HV}, and the combustion efficiency, η_c. Since a portion of the fuel energy provided is not burnt

during combustion, the combustion efficiency represents the fraction of fuel that is burnt during combustion. The lower heating value is used since the water in the combustion products is in a gas state when it leaves the cylinder.

$$\eta_t = \frac{P_i}{\dot{m}_f Q_{HV} \eta_c} \qquad (2.9)$$

An efficiency that compares the power to the whole energy provided by the fuel is the fuel conversion efficiency, η_f, where the combustion efficiency is unity.

$$\eta_f = \frac{P_i}{\dot{m}_f Q_{HV}} = \frac{1}{ISFC \cdot Q_{HV}} \qquad (2.10)$$

Air Flow

The air mass flow rate, $\dot{m}_a$, delivered to the engine is obtained by multiplying the volumetric air flow rate, Q_a, by the air density, ρ, at atmospheric conditions.

$$\dot{m}_a = Q_a \rho \qquad (2.11)$$

Air-fuel Ratio

The air-fuel ratio, *AF*, is the mass ratio between the air and fuel being burnt in an engine at a given time. During engine testing it can be defined using the air mass flow rate, $\dot{m}_a$, and the fuel mass flow rate, $\dot{m}_f$.

$$AF = \frac{\dot{m}_a}{\dot{m}_f} \qquad (2.12)$$

The stoichiometric air-fuel ratio, AF_s, occurs when the fuel burns completely producing only carbon dioxide and water. For example, the stoichiometric air-fuel ratio for gasoline is 14.6 [11].

Equivalence Ratio

The equivalence ratio, ϕ, indicates how fuel rich or fuel lean the air-fuel mixture is. It is defined as the stoichiometric air-fuel ratio divided by the actual air-fuel ratio. Usually when an engine is running, the equivalence ratio is calculated using the fuel mass flow rate and the air mass flow rate. An equivalence ratio greater than one is fuel rich.

$$\phi = \frac{AF_s}{AF} = \frac{AF_S}{\dot{m}_a / \dot{m}_f} = \frac{AF_S \dot{m}_f}{\dot{m}_a} \qquad (2.13)$$

Coefficient of Variation

The coefficient of variation (COV) is a value indicating variability in data expressed as a percent. It is defined as the standard deviation, σ, divided by the mean, $\bar{x}$. For engine applications, the COV in IMEP indicates cycle-to-cycle variation in work produced per cycle. The "n-1" method is used to calculate the standard deviation since only a sample of combustion cycles are taken.

$$COV_{IMEP} = \frac{\sigma_{IMEP}}{IMEP} \times 100 \qquad (2.14)$$

2.2 Scavenging

Scavenging is critical for the successful operation of a two-stroke engine. The incoming charge during scavenging must effectively remove the combustion products from the cylinder and replace them with a fresh charge. Ideally the fresh charge would perfectly

displace all of the combustion products, but in reality the charge displaces some of the combustion products and mixes with the rest. As a result, the trapped charge becomes a combination of fresh charge and combustion products from the previous cycle, also known as residual gas.

Two important terms used to define scavenging performance are delivery ratio and scavenging efficiency. The delivery ratio, Λ, compares the amount of fresh charge delivered to the cylinder to the reference mass required for ideal charging at any instant. The reference mass is defined as the displaced volume multiplied by the ambient density since the displaced volume is relatively easy to find. In reality the trapped volume should be used to find the delivery ratio.

$$\Lambda = \frac{\text{mass of fresh charge delivered}}{\text{displaced volume} \times \text{ambient density}} \qquad (2.15)$$

Scavenging efficiency (η_{sc}) compares the mass of fresh charge retained to the mass of cylinder charge. It represents how effectively the residual gas has been replaced with fresh charge.

$$\eta_{sc} = \frac{\text{mass of fresh charge retained}}{\text{mass of cylinder charge}} \qquad (2.16)$$

Many theoretical models have been presented to help understand the mixing that occurs during scavenging. Two of the more fundamental models for scavenging are the perfect displacement model and the perfect mixing model [12].

The perfect displacement model is the ideal case where the fresh charge perfectly displaces the combustion products. This model assumes that the process is at a constant cylinder volume and pressure, the entering fresh charge perfectly displaces the burnt gas,

no mass or heat crosses the boundary between the fresh charge and burnt gas, and the cylinder walls are adiabatic. Perfect displacement never happens in reality since the incoming charge mixes with the combustion products.

Alternatively, the perfect mixing model assumes that the fresh charge immediately mixes with the contents of the cylinder, forming a homogeneous mixture within the cylinder. Also, the instantaneous composition of the gas leaving the exhaust port is the same homogeneous mixture. Other assumptions for this model are that the process is at a constant cylinder volume and pressure, the cylinder walls are adiabatic, the two gases obey the ideal gas law, the gases have the same molecular weights, and have the same constant specific heat capacity. Perfect mixing is also not accurate since some of the charge displaces the combustion products in the early stages of scavenging. These two models form boundaries for scavenging performance: the perfect displacement model acts as an upper limit while the perfect mixing model forms the lower limit.

For the perfect displacement model, the relationship between delivery ratio and scavenging efficiency is such that for $\Lambda \leq 1$, $\eta_{sc} = \Lambda$ and for $\Lambda > 1$, $\eta_{sc} = 1$. For the perfect mixing model the relationship is a little more complex resulting in $\eta_{sc} = 1 - e^{-\Lambda}$. From these relations, the scavenging efficiency can be plotted versus delivery ratio as shown in Figure 2.5. A full explanation and derivation for the relations is available in the references provided [12, 14].

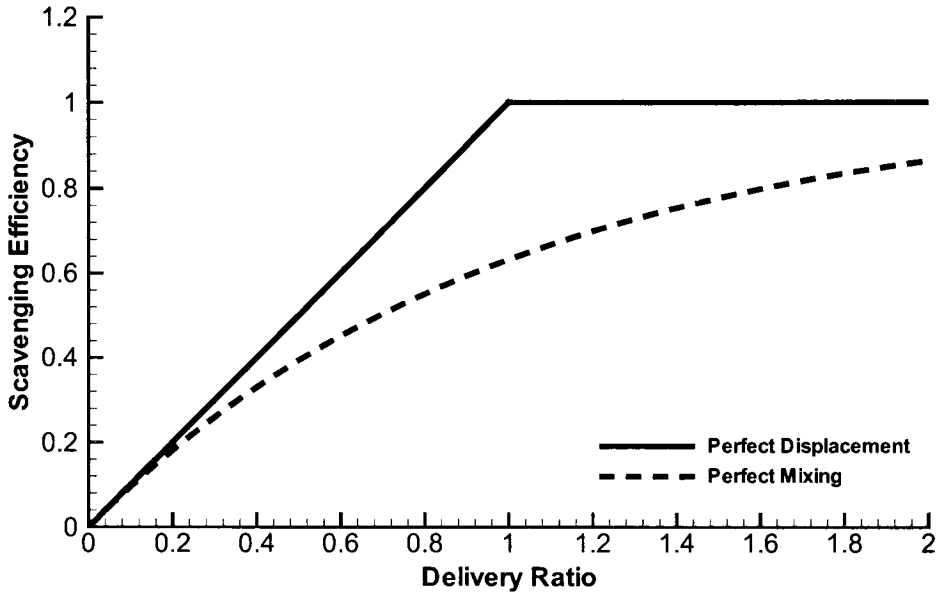

Figure 2.5: Scavenging efficiency versus delivery ratio for both mixing models.

Several methods have been used to scavenge two-stroke engines. Three common layouts for scavenging are illustrated in Figure 2.6.

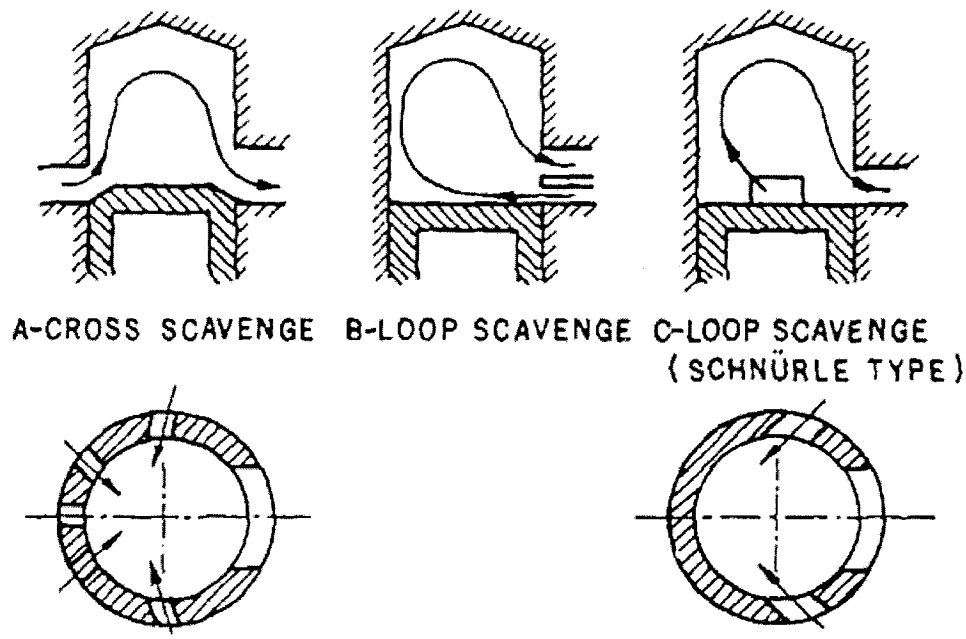

Figure 2.6: Scavenging layouts for a two-stroke engine, from Sher [14].

One of the most basic layouts is the cross scavenging system with ports on opposite sides of the cylinder. The incoming charge flows in one side and out the other as shown in Figure 2.6A. The piston usually has a deflector to deflect incoming air up in order to reduce short-circuiting. The term short-circuiting refers to the phenomenon where some air-fuel charge escapes out the exhaust before it can be compressed and burned.

Loop scavenging is another method where the ports direct flow towards the wall opposite of the exhaust. The scavenge charge flows up and around the opposing cylinder wall in a loop type flow pattern. MAN, a large-bore diesel engine manufacturer, used loop scavenging for their diesel engines by locating the scavenge ports directly below the exhaust ports as shown in Figure 2.6B. This presented a long flow path for the intake charge and required that the charge have a high initial momentum for effective scavenging. Schnurle devised another loop scavenging method, Figure 2.6C, that uses scavenge ports located on either side of the exhaust port. The flow path length is reduced compared to the MAN layout and as a result, the scavenging was less dependent on a high momentum intake charge [12]. Schnurle loop scavenging also reduces the number of crank angles required for scavenging. This method is very common for small crankcase scavenged two-stroke engines.

An inherent disadvantage for cross and loop scavenging is that the exhaust and scavenge port opening is symmetrical about BDC and therefore, the exhaust ports close after the scavenge ports during the compression stroke. As a result, engines using this type of scavenging are prone to short-circuiting since, for a short time, the scavenged charge is open to flow out the exhaust. As well, the engine cannot be supercharged in the

traditional way since the cylinder pressure at the start of compression equals the exhaust pressure. For these reasons, it is desirable that the scavenge ports remain open after the exhaust ports close.

A scavenging method that differs significantly from the cross and loop is uniflow scavenging. This can be achieved with poppet valves in the engine head and ports in the cylinder wall. As a result of the valves, the advantage of unsymmetrical scavenge port timing is possible. Two methods for uniflow scavenging can be used with this layout: the fresh charge can enter through the valves at the top and push the burnt gas down and out the cylinder wall ports, or the fresh charge can enter through the ports and push the burnt gas up and out the valves at the top.

In 1881 Clerk used the top-down uniflow scavenging design for his relatively successful two-stroke engine. From the 1950's until the 1990's Detroit Diesel Corporation produced a bottom-up uniflow scavenged two-stroke diesel engine for on-highway use. Figure 2.7 shows the uniflow designs used by Clerk and Detroit Diesel.

Bottom up uniflow scavenging tends to be used for diesel applications since a swirling motion can be induced by scavenge port design. The swirl also forces the charge outward towards the cylinder wall to eliminate unwanted pockets of residual gas that can occur immediately above the scavenge ports [12]. A disadvantage to this design is that there is potential for an unscavenged core of residual gas in the centre of the cylinder. Also, the poppet valve is exposed to the high temperature exhaust flow.

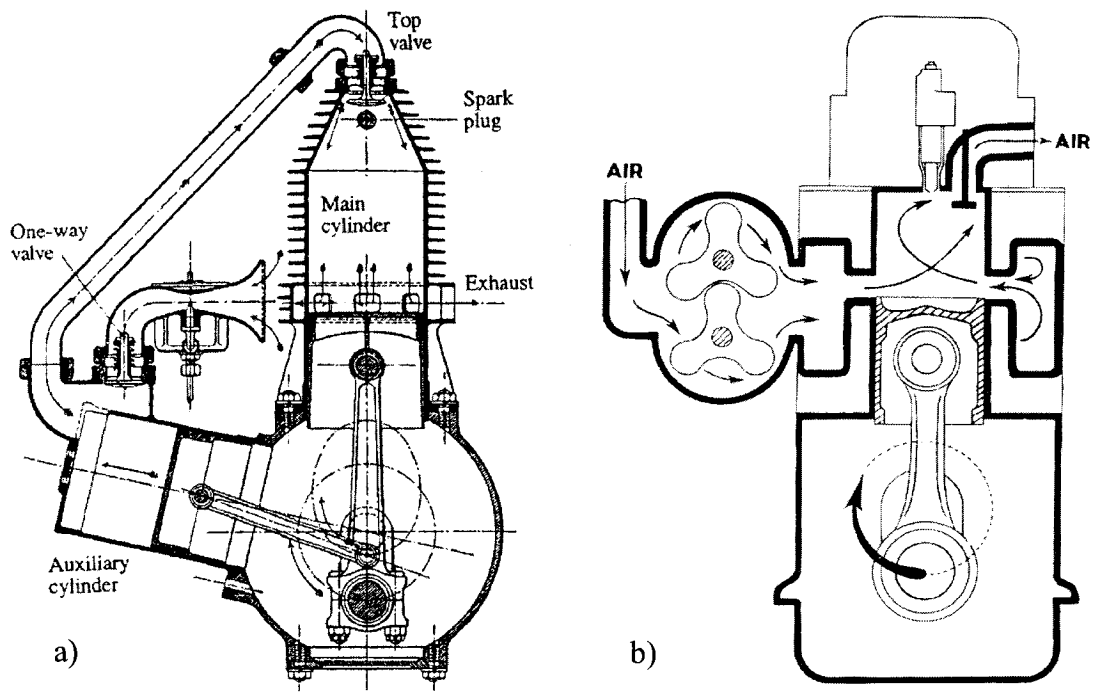

Figure 2.7: Two types of uniflow scavenging: a) Clerk's engine with top-down uniflow scavenging [12]; b) Detroit Diesel's bottom-up uniflow scavenging [15].

2.3 Engine charging

Two-stroke engines require a higher scavenge pressure than exhaust pressure so that the scavenge charge flows into the cylinder during scavenging. Therefore, a means of charging the air-fuel mixture, or pure air in the case of GDI and diesel engines, must be employed. Many methods such as a crankcase scavenge pump, stepped piston design, superchargers and turbochargers have been used for scavenging [12, 16].

Crankcase scavenged engines are very popular due to their simplicity and ability to be used in any orientation; the simplest design uses only three moving parts since the piston controls the intake and exhaust ports. Figure 2.3 shown earlier provides a cross section of a typical crankcase scavenged engine. Applications include motorbikes, trimmers, and motorboats. These engines use ports in the cylinder walls and a reed valve in the crankcase to control the gas exchange process through the engine. The bottom side

of the piston is used to pressurize the crankcase during the power stroke so that high pressure can be used for scavenging.

Reed valves (one-way valves) are located in the side of the sealed crankcase so that a charge can be held during the power stroke. As the piston moves down, the exhaust ports open and blowdown occurs. Then the piston uncovers the scavenge ports and the higher-pressure charge from the crankcase forces the combustion products out through exhaust ports. The piston changes direction and goes up, closing the scavenge ports, the exhaust ports close, and finally compresses the charge in preparation for ignition. Meanwhile the crankcase pressure decreases to that lower than ambient and a charge is drawn through the reed valves into the crankcase, ready to be compressed after the piston starts moving down again.

The crankcase scavenging arrangement prevents these types of engines from using conventional wet-sump lubrication and therefore the lubricating oil must be mixed with the incoming air and burned with the air-fuel mixture. For conventional loop type carburetted engines of this design, short-circuiting is a problem that increases fuel consumption and unburned hydrocarbon emissions. As mentioned above, the port symmetry about BDC is not desirable and some manufacturers have used fluid diodes, special exhaust port valves, and tuned exhaust pipes to reduce this symmetry problem. In fact, exhaust tuning is very important for two-stroke engines of this design. Tuning produces an expansion wave in the exhaust at the time when the scavenge port opens and a compression wave when the exhaust port closes, both of these aid in scavenging.

Externally charged two-stroke engines use an external supercharger, piston pump, turbocharger, or other pump as a pressure source to purge the combustion products during

scavenging. This system keeps the crankcase open for a conventional lubrication system. Also, it avoids the need for lubricating oil in the air-fuel mixture that can be a source of hydrocarbon emissions. Another feature of this design is that the external pump can be efficiently designed to meet the charging requirements of the engine. Four-stroke engines use the normal power piston to do the pumping. The piston is designed for the high pressures experienced during the power stroke and not optimized for the scavenging process. In Figure 2.8, Ricardo et. al. [16] shows an interesting comparison between the power required to scavenge a two-stroke versus a four-stroke over an engine speed range. He assumes 40% of the mechanical friction power happens during the intake and exhaust strokes (more friction power occurs during the compression and power stroke due to higher pressures) and adds this to the pumping work. The graph indicates that a two-stroke engine is favourable at low engine speeds, lower than where curves B and D intersect.

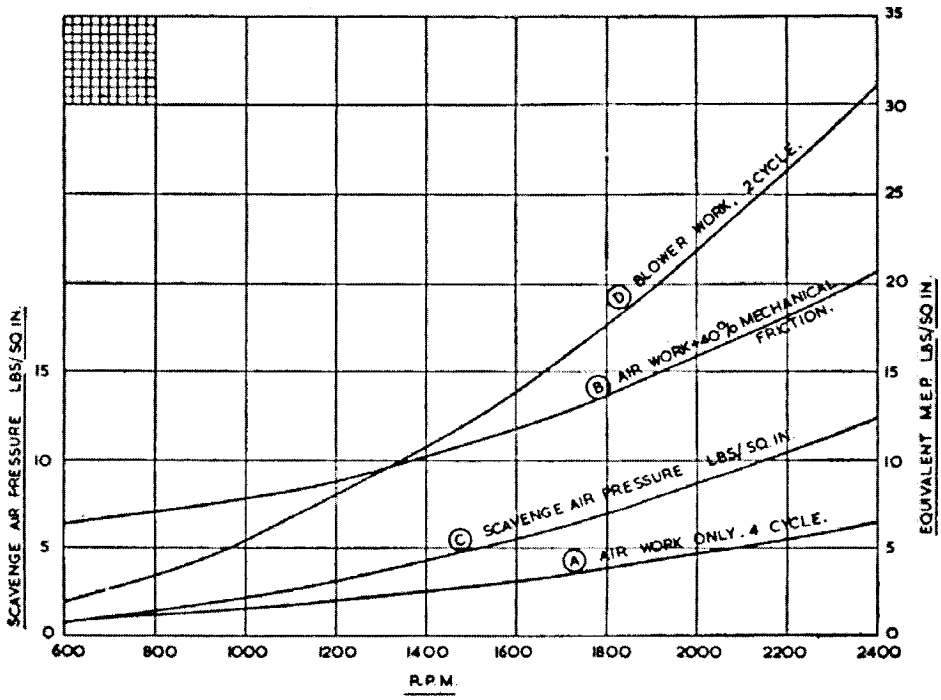

Fig. 10.1.—Comparison curves of work done in emptying and filling the cylinders of typical two- and four-cycle engines of the same power

(A) 4-cycle engine ; air-pumping work only. Volumetric efficiency 80 per cent at s.t.p.

(B) 4-cycle engine ; air-pumping work + 40 per cent of mechanical friction

(C) 2-cycle engine ; scavenge air pressure (lb/in²).

(D) 2-cycle engine ; total blower work allowing for 50 per cent excess air, i.e. 1·2 swept volumes at s.t.p. and assuming an overall blower efficiency of 60 per cent

Figure 2.8: Ricardo's comparison between the work required to scavenge a two-stroke and four-stroke engine [16].

2.4 Combustion

Before airflow and mixing are discussed, it is important to talk about how the air-fuel mixture burns in the gasoline engine and briefly touch on the diesel engine. Traditional carburetted and PFI engines operate such that a premixed homogeneous air-fuel mixture is ingested into the cylinder, compressed to one-ninth (1/9) of its initial volume, and then ignited. The flame starts at the spark plug and propagates radially outward as a thin turbulent reaction zone. It consumes the air-fuel mixture, leaving the combustion

products behind, and extinguishes at the cylinder wall. This process takes place at near constant volume conditions with the bulk of combustion occurring over 25° crankshaft rotation [17]. Mixture preparation differs slightly for GDI engines with stratified charge since only the portion of the volume around the spark plug contains a relatively rich, ignitable mixture.

The flame speed depends on the mixture characteristics, i.e. laminar burning velocity, and the flow characteristics, i.e. turbulence, at the time of ignition. Pressure, temperature, equivalence ratio, and residual gas are all factors that determine the laminar burning velocity. The equivalence ratio is defined in section 2.1.3. Recall that an equivalence ratio greater than unity indicates a fuel rich mixture. Figure 2.9a shows a graph relating laminar burning velocity to fuel-air equivalence ratio for some common fuels at 1 atm and 300K [18, 19]. Notice that for gasoline, the burning velocity peaks on the rich side and hence, maximum torque usually occurs with this equivalence ratio. Unfortunately, exhaust emissions are usually minimised on the fuel lean side, so engine tuning depends on the application of the engine. Figure 2.9b shows the relation between the burned gas mole fraction in the unburned mixture and the laminar burning velocity, where the fuel is gasoline [20]. This indicates that the residual gas acts as a diluent and decreases the flame speed. This relation is very relevant for two-stroke discussions since scavenging inherently leaves a mix of fresh charge and residual gas in the cylinder for combustion.

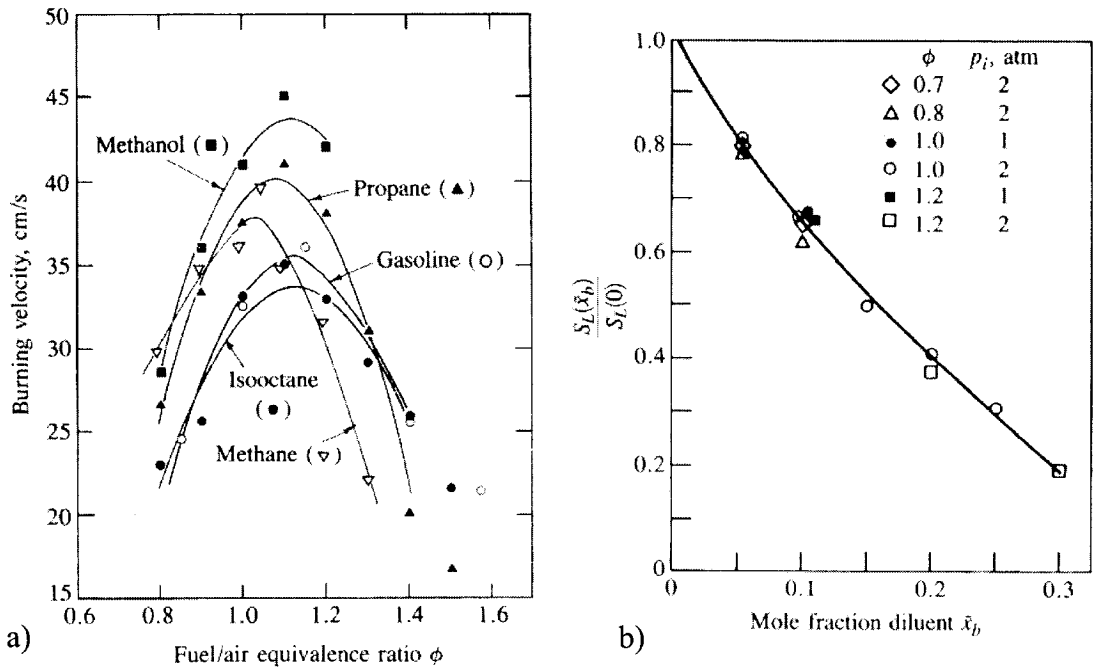

Figure 2.9: a) Laminar burning velocity as a function of equivalence ratio [18, 19]; b) Normalized laminar burning velocity as a function of mole fraction diluent, i.e. residual gas [20]. Both graphs reproduced from Heywood [11].

Not all fuel burns during combustion. Recall that the combustion efficiency represents the fraction of fuel that burns during combustion. Figure 2.10 also from Heywood [11], shows how equivalence ratio affects combustion efficiency. It can be seen that combustion efficiency drops significantly with increased equivalence ratio.

Diesel operation could be an alternative to consider for this novel engine; therefore, a brief discussion of diesel combustion is presented. Diesel engines operate differently than gasoline engines since the diesel cycle burns with a diffusion flame. Pure air is compressed to one-sixteenth (1/16) of its initial volume, so that the air reaches the auto-ignition temperature of diesel. Just before TDC, diesel is injected directly into the cylinder through tiny holes at the injector tip, producing jets that spray radially into the hot air. As the jets penetrate the air, the fuel burns rapidly as a diffusion flame. Proper

air motion is necessary to remove combustion products from the fuel source, and to replace them with fresh air to mix with the fuel and burn.

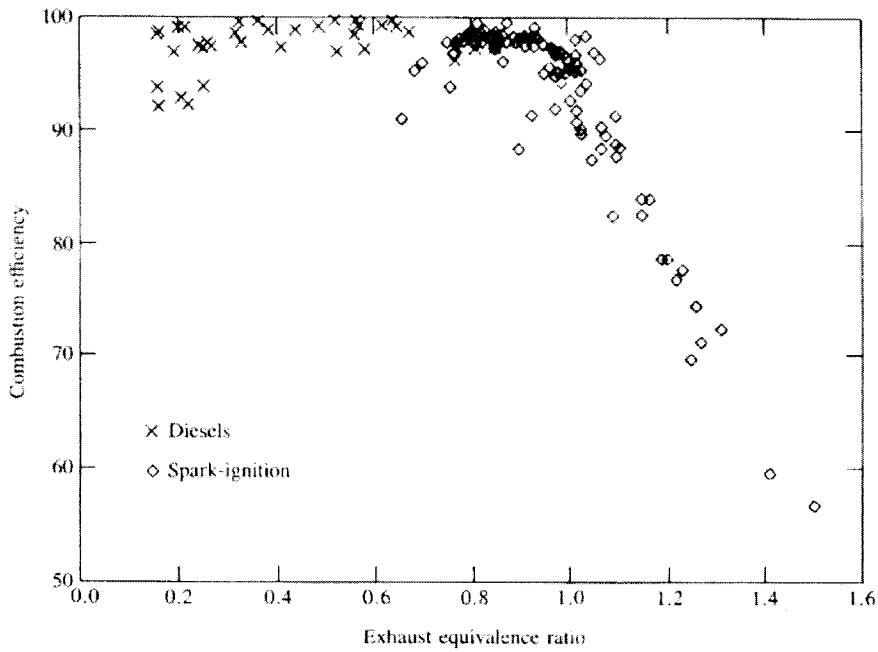

Figure 2.10: Combustion efficiency versus equivalence ratio, from Heywood [11].

2.5 In-Cylinder Charge Motion

With both engine cycles, charge motion in the cylinder is crucial to the combustion process. The charge movement, created by the induction process and combustion chamber design, aids in fuel evaporation, air-fuel mixing, and creates turbulence at the end of compression that is required for effective burning. The air motion required by an engine depends on the type of fuel being burned and engine design. Carburetted and PFI engines have a different airflow than GDI engines and hence, require a different intake, piston, and combustion chamber design to create this flow. The three main flow techniques used to create bulk airflow are swirl, squish, and tumble.

Swirl is defined as a bulk airflow rotating about the axis of the cylinder with an angular momentum. It can be produced by directing the intake (or scavenge) flow tangentially into the cylinder, as shown in Figure 2.11, or by inducing flow angular momentum in the intake port before entry into the cylinder. The Detroit Diesel engine discussed above uses its scavenge ports to create swirl by directing the airflow tangentially into the cylinder. Swirl is also used in GDI engines using stratified charge modes since it can suspend fuel within the centre of the flow. Swirl can remain in the cylinder through compression and even through the power stroke [21].

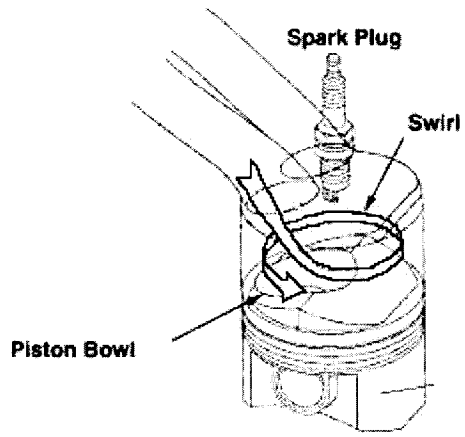

Figure 2.11: Swirl charge flow, adapted from [22].

Another flow technique, usually used in conjunction with swirl, is squish. A bowl in the piston or similar chamber in the engine head is used to provide squish, as shown in Figure 2.12. When the piston moves to TDC it forces the charge from the peripheral towards the centre of the cylinder. Squish is usually used to intensify swirl since a decrease in flow radius increases the angular velocity due to conservation of angular momentum.

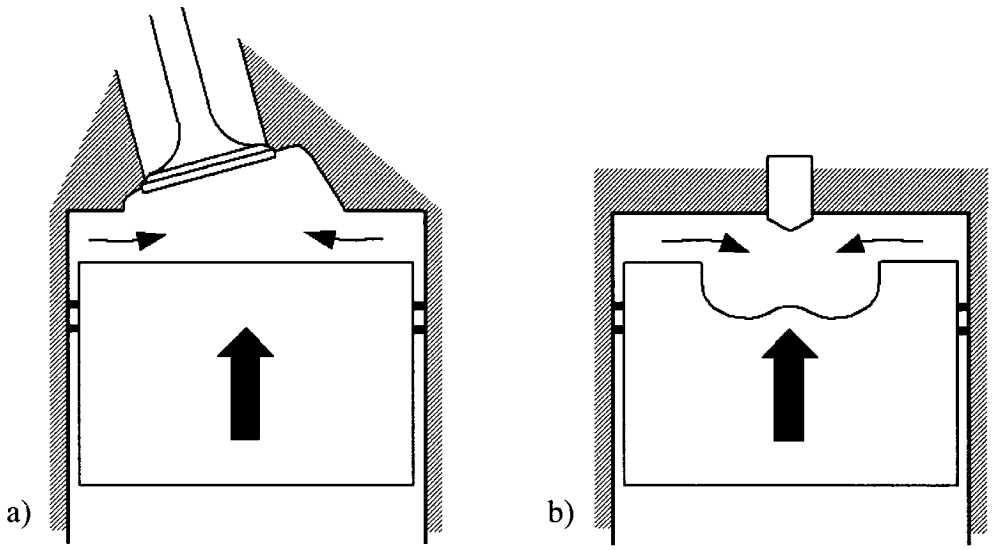

Figure 2.12: Squish flow path. a) SI combustion chamber in the head. b) Diesel combustion chamber in the piston.

Finally, tumble is defined as the bulk airflow rotating about an axis that is normal to the cylinder axis as shown in Figure 2.13. Tumble is used in GDI engines for directing the fuel towards the spark plug. Tumble also results in a high turbulence intensity at the end of compression [21]. This is because the bulk flow gets broken up into smaller vortices as the piston moves towards TDC.

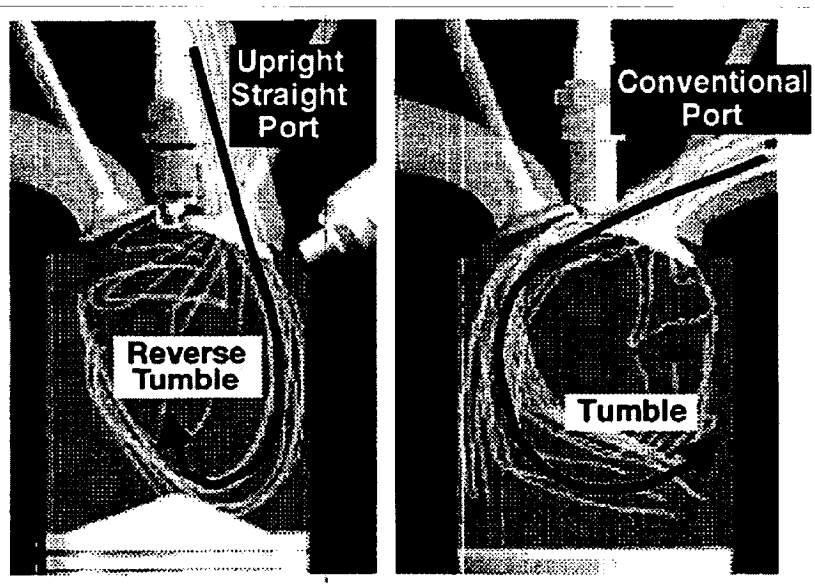

Figure 2.13: Mitsubishi's Tumble and Reverse Tumble airflow [23].

2.6 Fuel Injection

GDI engines have taken the fuel delivery approach that diesels use by injecting the fuel directly into the cylinder. As a result, the fuel has a shorter time to evaporate and mix with the air than traditional PFI engines. Therefore, an injector must break up the fuel delivered into many droplets so that the surface area is increased to achieve higher evaporation and mixing rates. A measure of fuel injector performance is the Sauter mean diameter (SMD). It is defined as the diameter of a sphere that has the same volume-to-area as the particle or spray of interest. It indicates how fine the spray is or how well the surface area has been increased relative to the volume. Increasing the surface area of the fuel injected reduces evaporation time. SMD requirements generally depend on the time available for mixing. PFI engines have a relatively long time for mixing and operate with an SMD of about 120-200 μm while GDI engines have shorter mixing time and require an SMD of less than 20 μm [21].

Obtaining the required droplet size can be done by two methods, either high-pressure fuel only injectors or air-assist injectors that use low-pressure fuel and low-pressure air. High-pressure fuel injectors are usually solenoid activated similar to PFI injectors but require pressures of 40-200 bar to achieve SMDs less than 20 μm. High-pressure injectors can have a fan spray pattern, swirl pattern, or a multi-hole plume pattern. Air-assist injectors use a low air rail pressure of about 6.5 bar and fuel pressure from 7.2-10 bar [21]. The fuel is mixed with the air and injected into the cylinder with the required droplet size. The advantage of air-assist injection is that low pressure PFI technology can be used. At the current time there is not a single injection method agreed on since it is dependent on the injection arrangement and GDI strategy [24].

A common type of GDI fuel injector, and the type used on the novel engine, is the swirl-type fluid only injector shown in Figure 2.14. High-pressure fuel is given an angular momentum as it leaves the injector resulting in a swirling flow. The swirling flow leads to a lower SMD, and increase in cone angle, and lower spray tip penetration [21]. Spray tip penetration is important so that wall or piston wetting can be avoided. Therefore, the swirl injector can be designed for the engine application so that the fuel spray interacts with the bulk airflow to obtain proper evaporation and adequate mixing in the time provided.

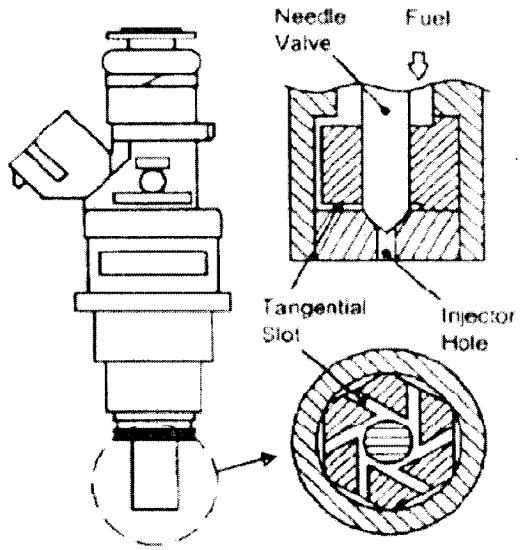

Figure 2.14: Typical GDI swirl-type fuel injector [25].

Figure 2.15 shows the characteristics of a swirl-type injector at two different swirl intensities. Two trends can be identified: greater swirl intensity and higher fuel pressure results in a lower SMD [23]. The trend also shows that pressures above 60 bar result in diminishing returns in SMD.

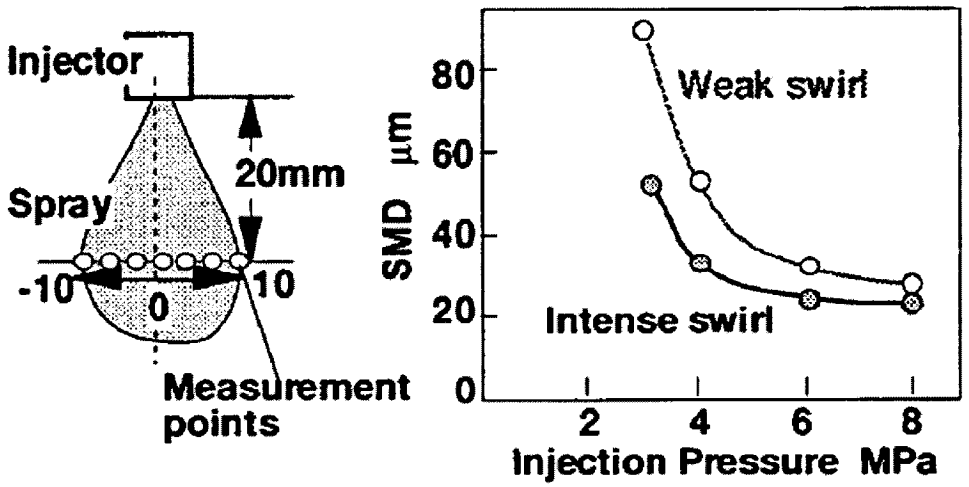

Figure 2.15: Effect of fuel pressure and swirl on SMD, from Kume et. al. [23].

The ambient back pressure refers to the pressure that the injector injects fuel into, or the pressure in the cylinder. Ambient back pressures for GDI engines can be up to 0.9 MPa [21], where typical PFI back pressures are around 0.1 MPa for a naturally aspirated engine at wide open throttle. For GDI, a longer fuel pulse width can increase the average injector ambient back pressure resulting in a change in the fuel jet divergence angle due to the increased density in the cylinder. An increase in SMD of about 6% per bar ambient back pressure is realized for a swirl-type injector. The increase is a result of the increase in droplet coalescence as the ambient density increases with the rising back pressure [21].

2.7 Gasoline Direct Injection

Traditionally, two-stroke engines mix the fuel with the air before it enters the cylinder. This leads to short-circuiting and results in unburned hydrocarbons in the exhaust. A way to eliminate short-circuiting is to directly inject the gasoline into the cylinder, e.g., GDI.

GDI is an IC engine gasoline delivery system that incorporates certain aspects of gasoline and diesel fuel systems to realize an overall advantage over these individual fuel delivery systems. GDI technology has been studied over the past twenty-five years and has the potential for reduced fuel consumption and emissions, the two main forces driving IC engine technology today. GDI systems are reported to reduce fuel consumption by 20% or more [21, 26]. Lower fuel consumption directly results in lower CO_2 production and is extremely important due to the anticipated future government regulations on greenhouse gases in North America. Increased brake torque has also been reported at wide open throttle due to the evaporative charge cooling provided by directly injecting into the cylinder [22].

Disadvantages of GDI include increased NO_x emissions at part load stratified charge (since a three way catalyst cannot be used), a requirement for more complex components, a complicated exhaust treatment system, increased computational demands on the engine control unit (ECU), and increased calibration time and expertise. Despite these drawbacks, many of the major automotive companies are considering this technology due to the many advantages listed above.

2.7.1 GDI Theory of Operation

The GDI system injects fuel under high pressure directly into the cylinder to be burned during the power stroke of the cycle. Injecting fuel directly into the cylinder allows for greater control of fuel metering, greater compression ratios, better cold start characteristics, better transient response, and the ability to operate with leaner mixtures. These advantages are relative to current optimized PFI engines. A typical GDI cylinder arrangement is shown in Figure 2.16.

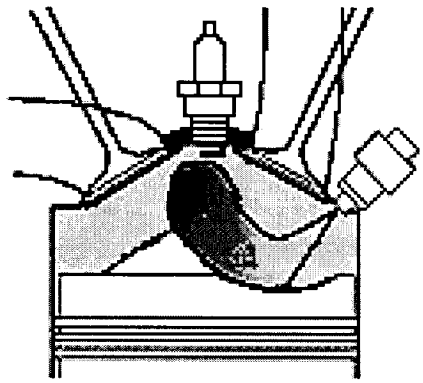

Figure 2.16: GDI arrangement, adapted from [27].

A major disadvantage of current four-stroke PFI engines is that they must be throttled to control torque. This is referred to as quantity control [26], where the quantity of charge mixture is controlled, just as the name implies. Throttling increases pumping losses and ultimately reduces the useful output of the engine. At lower engine torque and speeds where throttling losses are the greatest, GDI allows air to flow unthrottled and engine control is accomplished via quality control similar to a diesel engine. Quality control is referred to as controlling the quality of charge mixture in the cylinder [26].

Injecting directly into the cylinder allows for an increase in compression ratio due to the fuel evaporation. This evaporation causes a cooling effect, and hence allows for compression ratios as high as 12.5 [21, 26]. This effect can be maximized if the latent heat of evaporation comes from the surrounding air in the chamber and not from the wall or piston head. This rise in compression ratio results in increased thermodynamic efficiency.

GDI can operate in multiple modes, meaning that the injector can inject fuel at different times during the engine cycle. The injection mode is usually dependent on torque demands on the engine but may also be dictated by exhaust gas treatment requirements. The two main operating modes used in GDI are stratified charge mode and

homogeneous charge mode. These modes can be implemented independently or mixed during the transitional stage between fuel demands.

Stratified charge mode is used at low torque/low engine speed demands. During this mode, unthrottled airflow enters the cylinder during the intake stroke with tumble and/or swirl and is then compressed. Just before TDC, fuel is injected into the cylinder and the mixture is guided towards the spark plug. This offers a localized flammable mixture for combustion. The spark plug ignites the relatively rich mixture and the cycle continues as in a conventional PFI engine. The fundamental principle behind GDI is the ability to create a localized rich mixture right at the spark plug but maintain a global lean mixture with air-fuel ratios as high as 40-50:1 [22]. This technique is known as stratified charge and is a major feature of GDI.

Homogeneous charge mode is analogous to PFI except that the fuel is injected directly into the cylinder. This mode is used at higher torque and engine speeds where more fuel is required. As a result, earlier injection is required for evaporation and mixing. Fuel is injected during the intake stroke with four-stroke engines and during the compression stroke with two-stroke engines in an effort to create a homogeneous stoichiometric mixture throughout the cylinder. The mixture is then compressed and burnt just as in a PFI engine.

2.7.2 Operating Strategies and Mode Selection

Stratified charge can be achieved with many orientations of the fuel injector, intake valves, and spark plug. It is generally accepted that the spark plug should be located centrally to minimize flame travel distance and to decrease the potential of knock. Therefore, differences in GDI systems are mainly in their injection and airflow

arrangements. There are three major forms of charge stratification: spray-guided, wall-guided, and air-guided. The theory behind these stratified methods will be discussed below.

Spray-Guided Stratified Charge

With spray-guided systems the fuel injector is at the centre of the engine head and injects along the axis of the cylinder as shown in Figure 2.17. The spark plug is located near the injector so that the trailing edge, or boundary of the injected fuel, can be ignited. This arrangement is known as a narrow spacing arrangement. Since the spark plug is very close to the injector, the time between the injection event and the ignition event is small. This results in a shorter time for evaporation and mixing and can prevent complete combustion, which leads to an increase in hydrocarbon emissions. Conversely, there is minimal wall wetting since the fuel is injected along the axis of the cylinder, which eliminates hydrocarbon emissions associated with wall wetting. Airflow into the cylinder usually has a high amount of swirl in order to contain the fuel in the centre.

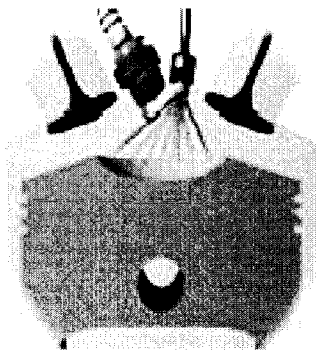

Figure 2.17: Spray-guided system [28].

Wall-Guided Stratified Charge

Wall-Guided stratified charge is a common mode of mixing the fuel and air due to its wide spacing arrangement. The injector is located at the side of the combustion chamber and the spark plug in the centre of the head as shown in Figure 2.18. The wide spacing arrangement gives a longer time for evaporation and mixing compared to the spray-guided arrangement. For wall-guided systems, the piston bowl design is especially important since it guides the fuel towards the spark plug. The air charge motion created in the cylinder also plays a role to guide the fuel towards the spark plug [24]. This side injection arrangement is better suited for cycle-to-cycle variation in injection patterns but can also have increased wall wetting. Therefore injector angle is an important variable to consider when designing a wall-guided injection system.

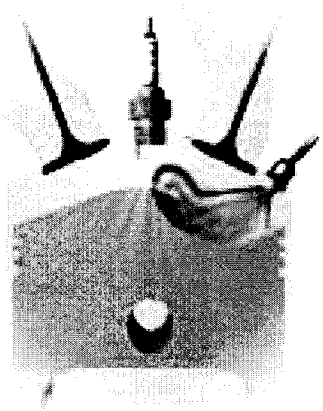

Figure 2.18: Wall-guided system [28].

Air-Guided Stratified Charge

Air-guided systems rely more on the bulk flow of the incoming air charge to guide the fuel to the spark plug. This means that the piston bowl does not have to be as aggressive as in wall-guided systems. This piston design is also more desirable for homogeneous

charge mode. This system is more sensitive to airflow and hence, the air charge flow formation is of high priority during the design stage, especially at low engine speeds. An air-guided arrangement is shown in Figure 2.19.

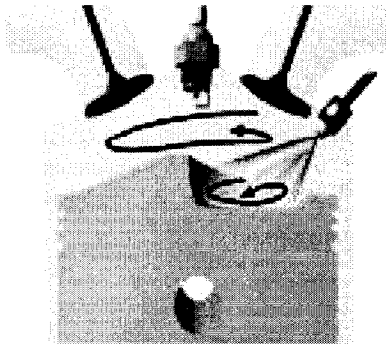

Figure 2.19: Air-guided system [28].

Homogeneous Charge

The homogeneous combustion mode, which operates with a global stoichiometric mixture, is necessary for high power requirements. Therefore, at a certain point the engine management system changes from stratified mode to homogeneous mode or visa versa. In some four-stroke engine designs, like the Bosch system [26], the incoming air will be throttled in homogeneous mode. Throttling is not desirable, but in the high torque/speed range where homogeneous mode is used, losses are relatively less than the low torque/low speed region. Larger stoichiometric charge mixtures require a longer time for the fuel to evaporate and mix; therefore, fuel is injected during the intake stroke. The bulk swirl/tumble air motion of the incoming air aids in mixing the fuel to provide a global stoichiometric mixture.

Mode Selection

The mode usually depends on the amount of fuel required by the engine to produce a specific torque level, i.e. load. Since stratified mode offers a local rich mixture to ignite, there is a limit to the amount of stratified charge that can burn. Limits include time for injection and mixing time available to get a combustible mixture. At this point the engine will change into homogeneous mode or lean homogeneous mode to provide combustible mixture. A mode map is usually entered in the ECU for the operating range of the engine. Of course this map is affected by many other variables such as engine temperature, transient response requirements, and exhaust treatment requirements.

With the increasing fuel prices and the more stringent emission regulations, GDI technology has the potential to meet future needs. GDI has the potential to lower fuel consumption by up to 25% and reduce CO_2 production accordingly. These advantages are a result of lower pumping losses, increased volumetric efficiencies, higher compression ratio, higher thermodynamic efficiencies, and lower heat loss. Challenges associated with current GDI systems include a more complicated exhaust treatment system for lean combustion, specialized fuel system, relatively higher emissions, and higher ECU and calibration requirements.

Chapter 3 Current Two-Stroke GDI Technology

The advantage of high power-to-weight and simple design makes the two-stroke engine a popular power source for small applications such as personal watercraft, snowmobiles, trimmers, blowers, and chainsaws. At the other end of the power scale, large two-stroke diesel engines are used to generate electricity, power locomotives, and power ships, taking advantage of their high brake fuel conversion efficiency that can reach 54% [12]. In the automotive sector, two-strokes have experienced some mass production in Europe during the early 20th century but to date have had very limited success in North America [29].

With recent advancements in GDI technologies, the application of direct injection to two-stroke engine field has stimulated research. The reason is that GDI not only provides benefits outlined in section 2.7, but it also eliminates the short-circuiting problem common with traditional two-strokes. The following literature review provides a discussion of current two-stroke GDI engine efforts with an emphasis on engine design and layout. For a historical review of the two-stroke engine, refer to the following references [12, 30].

In comparison to four-stroke engines, the high power-to-weight, low maintenance, and relative simplicity make two-stroke engines favourable in the personal watercraft industry. Since 2003, Bombardier has produced the Evinrude E-TEC line of outboard direct-injection two-stroke engines ranging in power from 30-186 kW (2007 models) [31]. These loop-scavenged engines inject gasoline when the exhaust port closes using a fuel only direct injection system. The piston has a small bowl in the centre to contain fuel spray so that stratified charge combustion can be used at light loads [32].

Lubrication oil that is designed to burn completely during the combustion process is injected into the incoming air stream at a controlled rate dependent on operating conditions.

Table 3.1 presents four GDI outboard marine engines and two multi-port fuel injected outboard marine engines from different manufacturers. The GDI models achieve superior power-to-displacement and power-to-weight values when compared to their four-stroke counterparts.

Table 3.1: Outboard marine engine comparison [31, 33, 34].

Engine	Type*	Power (kW)	Disp. (cm^3)	Mass (kg)	Power/disp. (kW/L)	Power/mass (kW/kg)
Evinrude E-TEC 200	V6 GDI 2S	149	2589	190	57.6	0.785
Yamaha HPDI 200	V6 GDI 2S	149	2596	216	57.5	0.691
Evinrude E-TEC 200 H.O.	V6 GDI 2S	149	3279	231	45.5	0.646
Yamaha V MAX HPDI 200	V6 GDI 2S	149	3342	245	44.6	0.609
Yamaha F200	V6 MPFI 4S	149	3352	265	44.5	0.563
Honda BF200	V6 MPFI 4S	149	3471	267	43.0	0.559

* 2S – Two stroke, 4S – Four stroke. MPFI – Multi-port fuel injection.

Power-to-weight is important for any engine used for transportation, including automobile engines. In the late 1990's the Orbital Engine Company of Australia attempted to design a two-stroke engine for automotive application. The "Genesis" engine was a crankcase-scavenged GDI engine that used the Orbital Combustion Process (OCP), an air-assisted fuel injection system [35]. The injection system uses a typical PFI fuel injector in combination with an air injector to create atomization of the fuel. The engine used loop scavenging with an exhaust port valve to provide asymmetrical port timing. Figure 3.1 shows a cutaway of the engine while Table 3.2 lists the engine specifications.

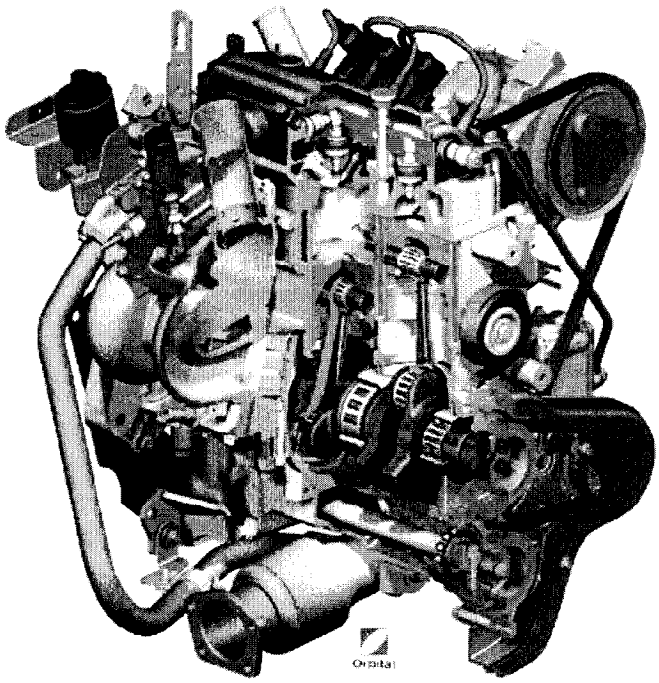

Figure 3.1: Cutaway of the Genesis engine [35].

Table 3.2: Genesis engine specifications [35].

Bore x Stroke (mm)	84 x 72
Displacement (cm^3)	1197
Compression Ratio	10.5:1

Another two-stroke automotive engine project was completed in 2003 by a group in Europe, consisting of Lotus Engineering et. al. [36]. The objective of the project called ELEVATE (European Low Emission V4 Automotive Two-Stroke Engine) was to build a 120 kW two-stroke automotive engine with a 15% reduction in fuel consumption compared to a four-stroke, as well as size and weight benefits over four-stroke diesels. The engine was also designed to meet Euro 3 emissions standards without the use of a DeNOx catalyst.

The engine used cylinder ports to control scavenging with a charge-trapping valve at the exhaust port for asymmetrical timing. An external screw compressor was used for scavenging and also offered low-volume high-pressure air to the air-assist fuel injection system. Two combustion modes were used: normal spark initiated ignition and controlled auto ignition mode (CAI) for low loads. The external compressor allowed for

wet-sump lubrication, typical of four-stroke automotive engines. Figure 3.2a shows the engine scavenging properties tested in a single cylinder testing apparatus. The Jaguar scavenging data is not discussed here but is available at [37]. The torque and fuel consumption data is presented in Figure 3.2b. In the end, the power objective was met with a peak power of 119.8 kW. However, over a simulated drive cycle, results indicated a 10% increase in fuel consumption over the best four-stroke engine available at the time.

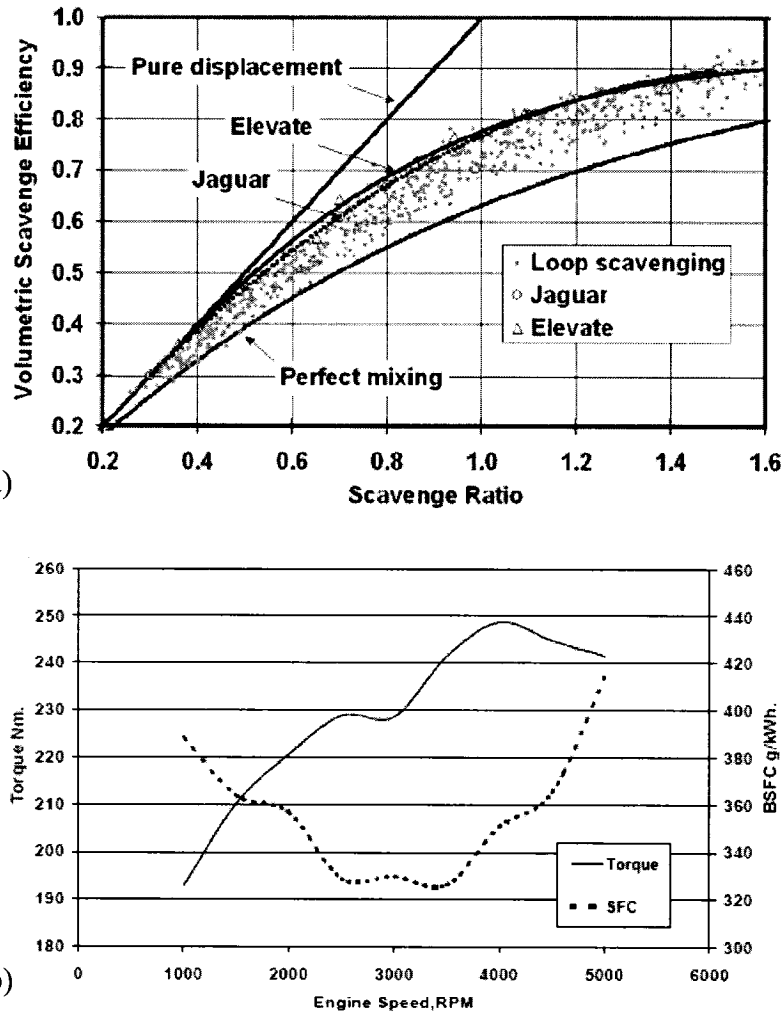

Figure 3.2: ELEVATE engine performance; a) Scavenging properties; b) Torque and fuel consumption, both graphs from [36].

In 1995 Hyundai Motor Co. reported on an experimental piston-ported GDI two-stroke engine for automotive use [38]. The study compared two Schnurle loop-scavenged designs and also compared injection techniques, air-assisted and fluid only. The engine schematic and specifications are provided in Figure 3.3 and Table 3.3 respectively. This engine also used an external supercharger for scavenging so that a wet-sump lubrication system could be used as it was thought to be required for engine durability.

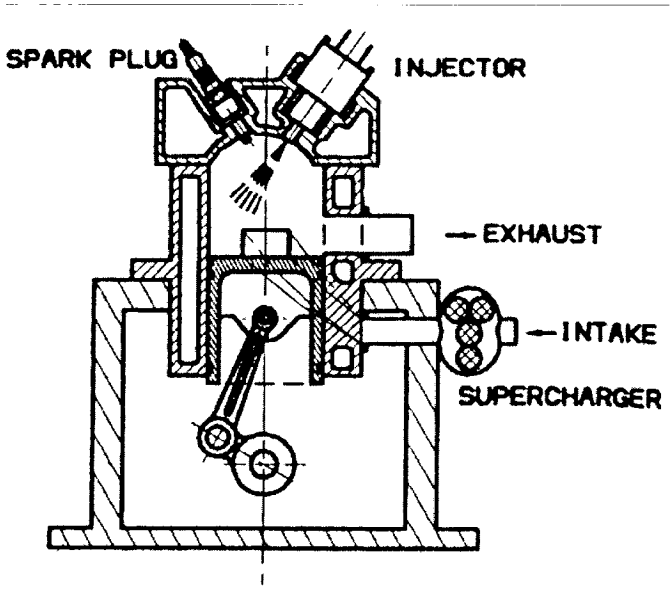

Figure 3.3: Cutaway of the Hyundai experimental engine [38].

Table 3.3: Hyundai engine specifications [38].

Bore x Stroke (mm)	82.3 x 75
Displacement (cm^3)	399
Compression Ratio (effective)	6.9:1
Intake open/close (deg. bBDC/aBDC)	67/67
Exhaust open/close (deg. bBDC/aBDC)	87/87

It was concluded that the air-assist injector performed better than the high-pressure fuel only injector. The air-assist injector provided droplets with a SMD of less than 6 μm at a fuel pressure of 7.5 bar and air pressure of 5 bar while the high pressure fuel injector gave droplets of about 6 μm SMD with a fuel pressure of 70 bar. The

Hyundai engine produced a power of 17.5 kW at 4800 rpm resulting in a power-to-displacement of about 43.9 kW/L.

In 2004 Fuji heavy industries and Chiba University published results from their research on a GDI two-stroke test engine [39]. A one-cylinder test engine was built to accommodate stratified charge mode as seen in Figure 3.4. The engine was based on a Fuji Heavy Industries personal watercraft two-stroke engine that already had direct injection but suffered from unstable combustion under light load. The study investigated stratified and homogeneous injection modes and ultimately reported on the power output and fuel consumption of the engine at low engine speed.

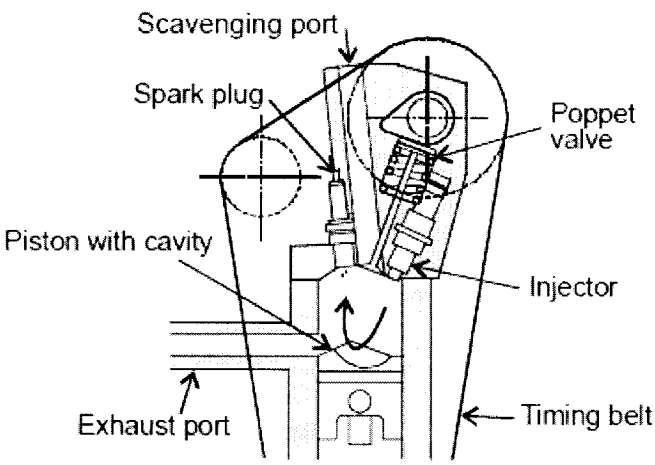

Figure 3.4: Schematic of the Fuji engine [39].

Table 3.4: Fuji engine specifications [39].

Bore x Stroke (mm)	71.3 x 65
Displacement (cm^3)	260
Compression Ratio (effective)	7.6
Intake open/close (deg. bBDC/aBDC)	40/80
Exhaust open/close (deg. bBDC/aBDC)	70/70

The test engine contained a four-stroke style cam driven poppet valve in the head to control scavenge flow. Exhaust ports where located at the bottom of the cylinder as with conventional two-stroke engines. The fuel only injector was located towards the peripheral of the cylinder head while the spark plug was located near the centre. The GDI arrangement was a wall guided system where the scavenging port guided the air

down the cylinder wall and over the piston to create reverse tumble. The engine was externally charged with a Lysholm type compressor.

Figure 3.5 shows the brake power output for this engine. It can be seen that the engine performed better than the base engine, which used conventional scavenge ports in the cylinder wall, and the latest four-stroke at the time, in all categories.

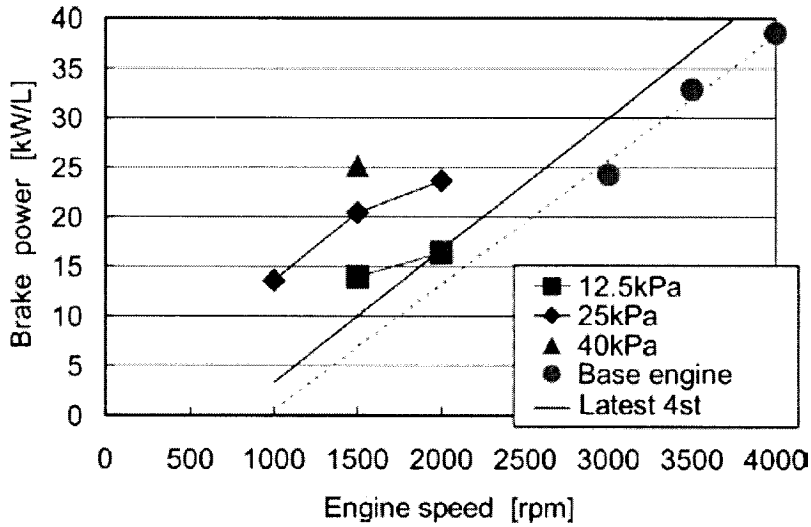

Figure 3.5: Brake power results for the Fuji Engine. Pressures represent the intake charge pressure, graph from [39].

Figure 3.6 shows the hydrocarbon emissions and brake specific fuel consumption data for the engine, including the carburetted base engine. The data shows the benefit in fuel consumption and emissions provided by GDI, mainly from eliminating fuel short-circuiting.

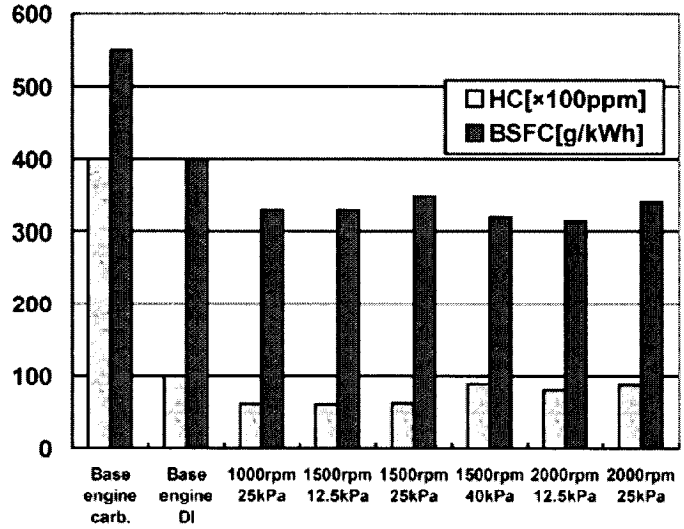

Figure 3.6: Hydrocarbon emissions and base specific fuel consumption for the Fuji engine, graph from [39].

Considering the engines discussed above, many different engine designs have been studied for two-stroke application. It does not seem that a definite charging, scavenging, and fuel delivery method is agreed upon. Table 3.5 offers a comparison of these designs.

Table 3.5: Engine design comparison [31, 35, 36, 38, 39].

Engine	Year	Config-uration	Disp-placement (cm^3)	Power /disp. (kW/L)	Charging	Scavenging	Fuel Delivery*
Evinrude**	2003	V6	2589	57.6	Crankcase	Loop	HP
Orbital	2000	L3	1197	46.8	Crankcase	Loop	AA
ELEVATE	2003	V4	N/A	N/A	Screw compressor	Loop	AA
Hyundai	1995	1	399	43.9	Supercharger	Loop	HP/AA
Fuji	2004	1	260	23.9***	Lysholm compressor	Uniflow	HP

* AA – Air-assist fuel injection, HP – High-pressure fuel only injection.
** Evinrude E-TEC 200 hp model.
*** For the 25 kPa intake pressure.

Air-assist fuel injection is the choice for three of the five engines due to its satisfactory atomization at a fraction of the fuel pressure. The fuel injector used for some

air-assist units is simply a port fuel injector that is readily available for a low cost; this may be attractive for a low cost GDI two-stroke. High-pressure fuel systems do eliminate an additional air supply to the injector, but require high cost components and present starting challenges due to the high fuel pressure required at starting.

In two of the three cases where the engine was designed for automotive use, a wet sump was chosen. The high-pressure plain bearing design is proven and provides reliability throughout a vehicle's service life. With this system an oil control ring is needed, or two as suggested by the ELEVATE group, to prevent oil from entering the cylinder wall ports.

Another feature that three of the engines had was asymmetrical scavenge port timing to let the scavenge port (or valve) remain open after the exhaust port closes. This eliminates short-circuiting and offers more for tuning versatility. In the case of the ELEVATE and Orbital engine, an exhaust port control valve closes the exhaust port early during compression so that the intake effectively remains open after the exhaust closes.

The natural evolution of the two-stroke engine is to first replace the carburetor with direct fuel injection to eliminate short-circuiting, and then improve light load regions with stratified charge. Evinrude and Fuji followed this path. At this time in two-stroke GDI development, an optimal GDI strategy, charging method, or injecting method is not clear. The novel engine discussed in this thesis offers another scavenging technique in the quest for two-stroke GDI engine optimization.

Chapter 4 Experimental Apparatus

The experimental apparatus is comprised of two major components: the engine apparatus and the data acquisition system. A diagram of the engine apparatus is shown in Figure 4.1 and a photograph of the engine apparatus is provided in Figure 4.2. The individual components will be described in this section.

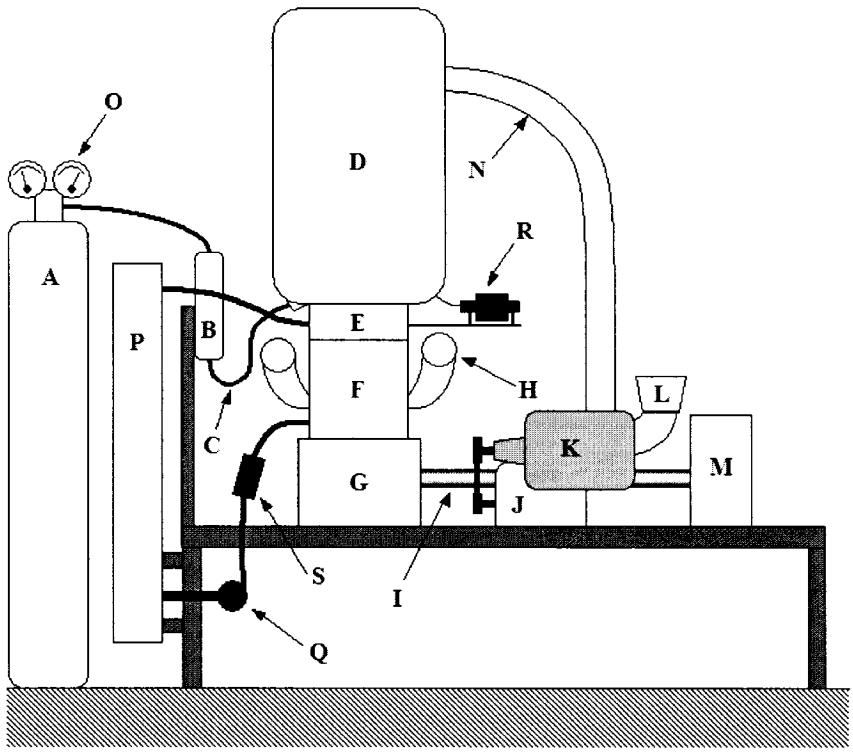

A – Nitrogen tank
B – Fuel canister
C – Fuel line
D – Intake Plenum
E – Engine head
F – Engine cylinder block
G – Crankcase
H – Exhaust header (x2)
I – Dynamometer shaft
J – AC motor
K – Roots-type supercharger
L – Airflow turbine
M – Dynamometer
N – Air transfer hose
O – Fuel pressure regulator
P – Cooling tower
Q – Water pump
R – Ignition coil
S – Water heater

Figure 4.1: Diagram of experimental engine apparatus.

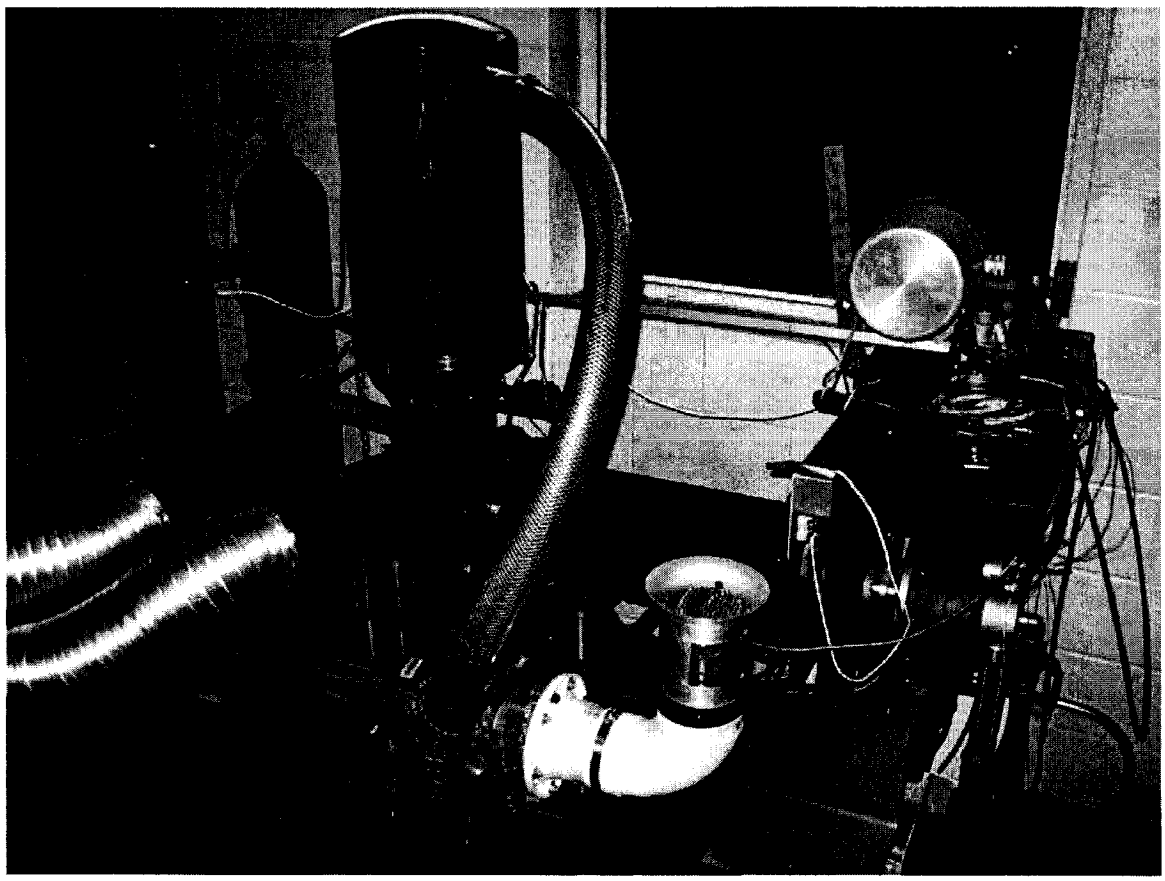

Figure 4.2: Photograph of the engine apparatus.

4.1 The Engine

The engine is a combination of parts from a 1975 Yamaha 400 cc motorbike and original parts built for the project. The engine specifications are listed in Table 4.1.

Table 4.1: Engine Specifications

Make	Modified 1975 Yamaha DT 400
Type	Water cooled, Single cylinder, Two-stroke
Scavenging	Externally scavenged, Top-down Uniflow
Fuel System	Gasoline Direct Injection
GDI mode	Homogeneous mode only
Number of Cylinders	1
Bore x Stroke (mm)	86.0 x 70.0
Displacement (cc)	407
Clearance Volume (cc)	32
Adjusted Stroke (mm) (at exhaust closed)	52.5
Trapped Displacement (cc)	305
Compression Ratio (effective)*	10.5
Intake valves open/close	Dependent on engine speed
Exhaust ports open/close	120° aTDC/120° bTDC
Ignition	DENSO Coil-over-plug
Fuel Injector	Siemens Deka Solenoid Injector, Hollow-cone fuel spray, cone angle of 40°
Fuel Injection Pressure	7.5 MPa (75 bar)
ECU	MOTEC M4

* Effective compression ratio refers to the ratio of the cylinder volume at the moment the exhaust ports close to the clearance volume.

4.1.1 Main Engine Components

A picture of the main assembly with the intake plenum removed is shown in Figure 4.3. The engine crankcase, crankshaft, connecting rod, and piston are from a 1975 Yamaha DT400 two-stroke engine.

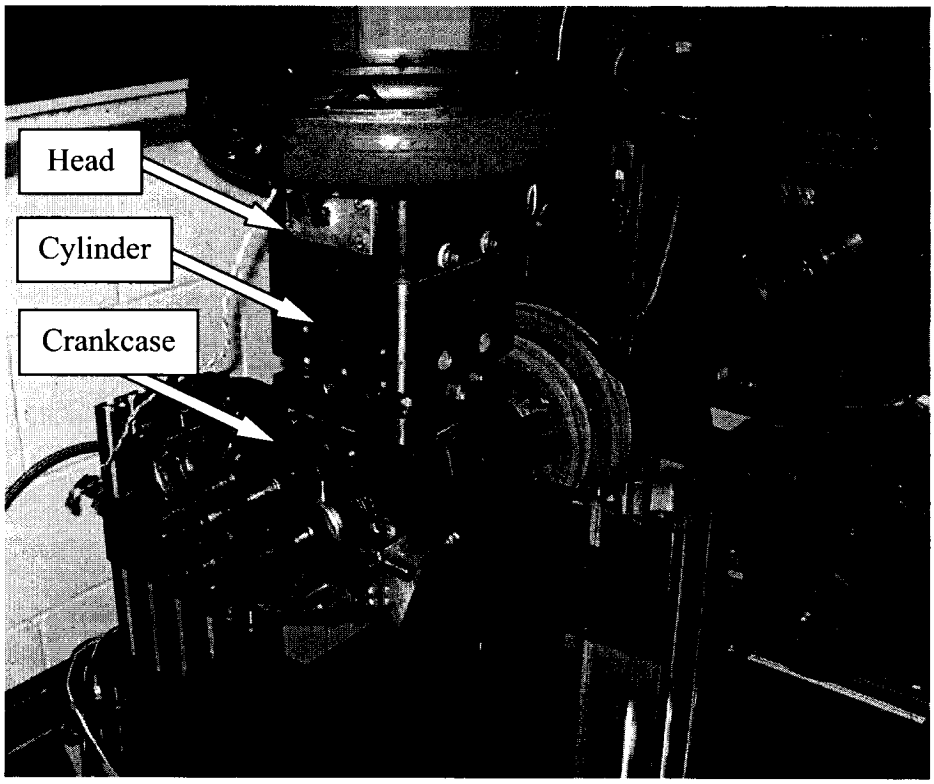

Figure 4.3: Engine photograph showing major components.

The engine head was built of steel with water jacket for cooling. It contains an array of 16 passive check valves that react to the pressure differences between the intake plenum and the cylinder. The airflow pathway is shown in Figure 4.4. Each check valve consists of a thin square steel platelet contained in a cavity by a retaining plate as shown in Figure 4.5. The retaining plate is made of stainless steel with a diameter of 90 mm and a thickness of 2 mm. It is fastened to the head by two small bolts and can be easily removed to access the platelets. The retaining plate acts as a flow obstacle for the incoming air but is a physical requirement to retain the platelets. Figure 4.6 through Figure 4.8 show the engine head and the check valve detail.

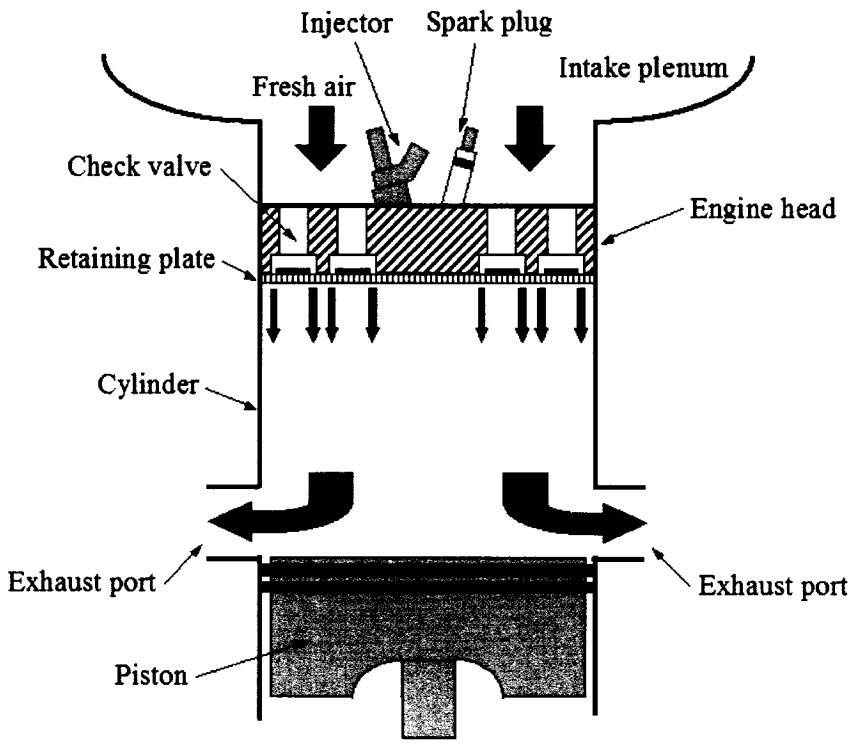

Figure 4.4: Engine airflow path showing location of components.

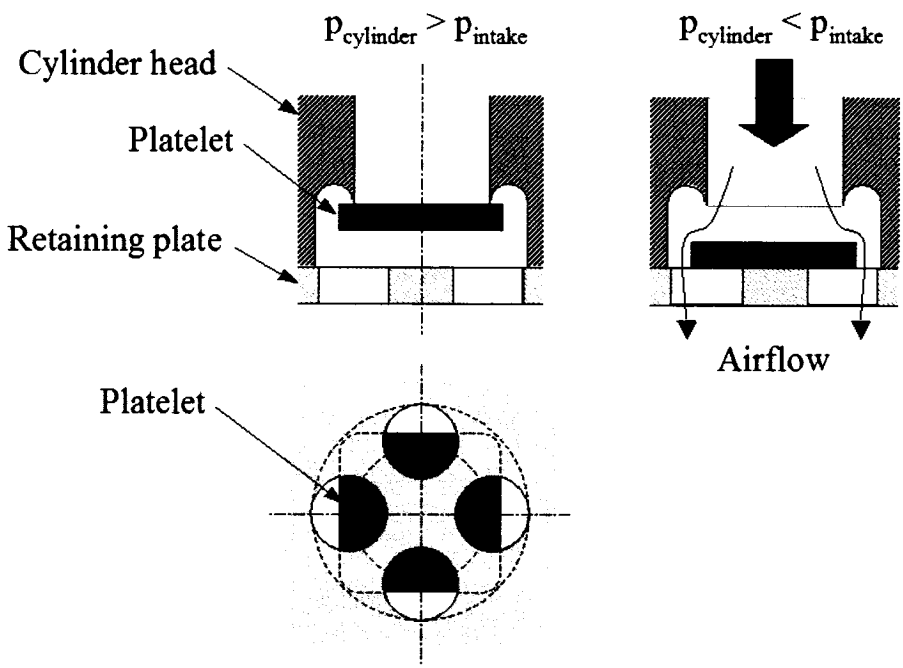

Figure 4.5: Check valve operation diagram.

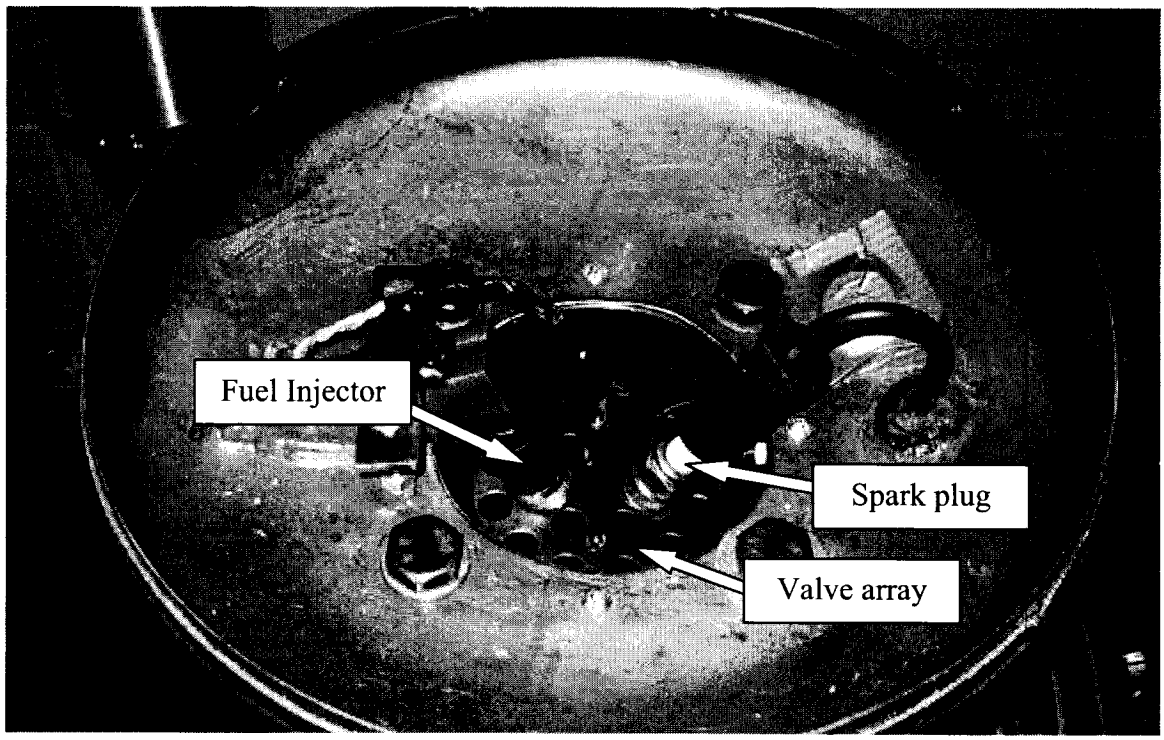

Figure 4.6: Top of cylinder head showing valve array.

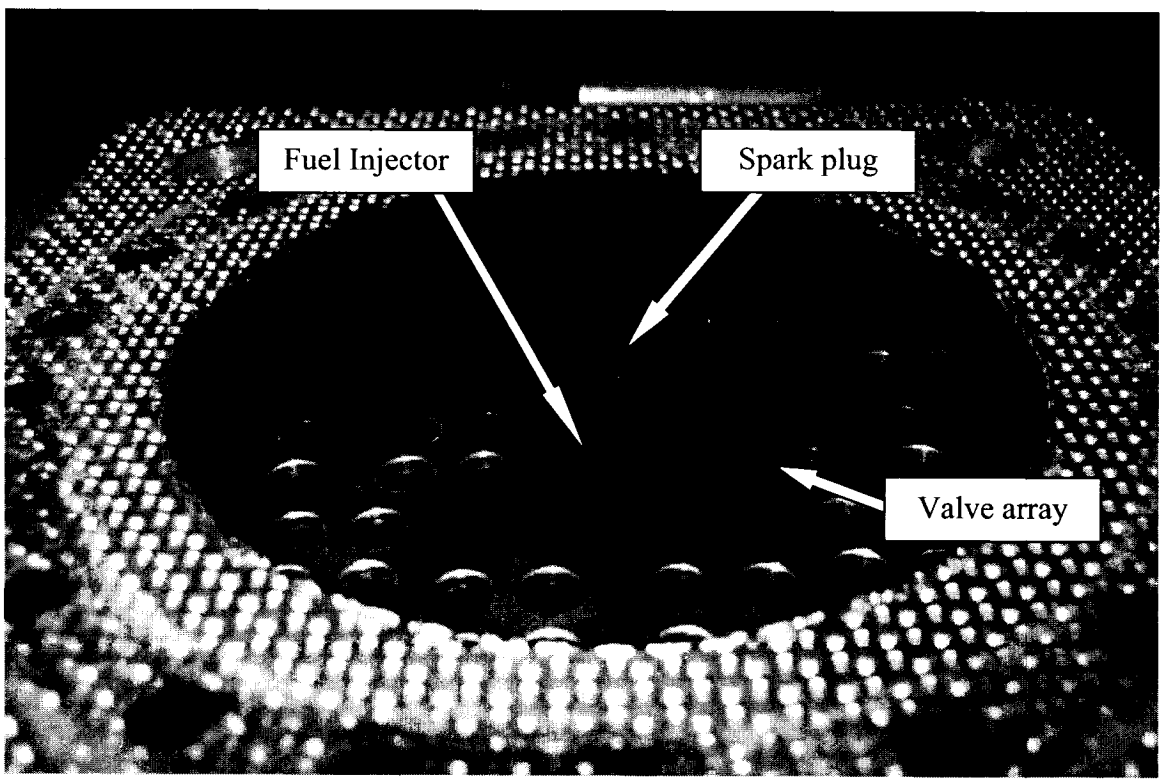

Figure 4.7: Bottom of cylinder head showing valve array.

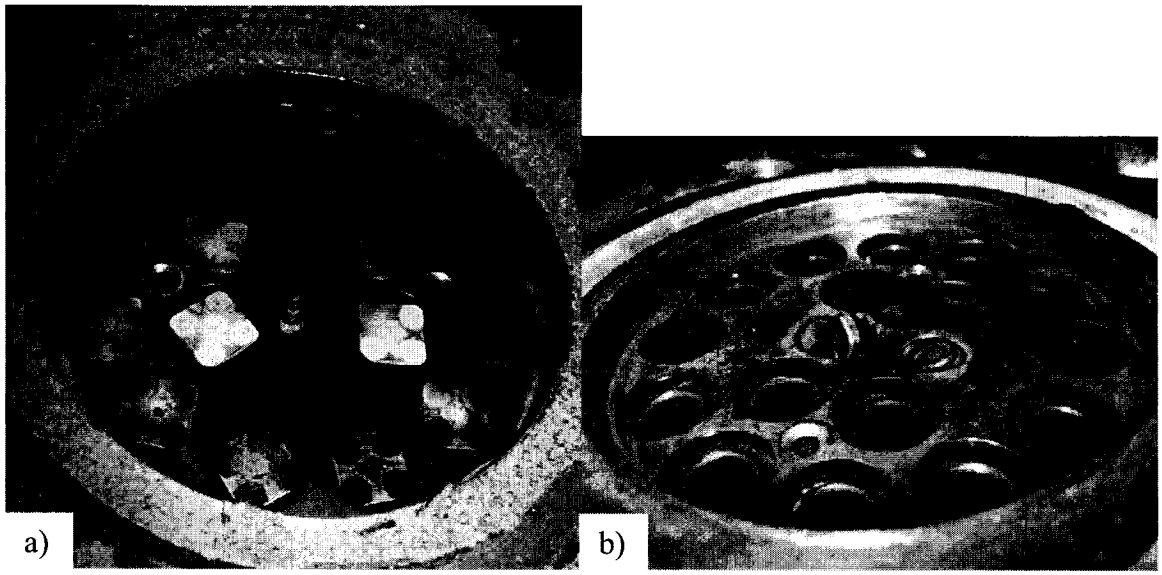

Figure 4.8: Bottom of valve array. a) Retaining plate removed exposing platelets. b) Platelets removed exposing check valve cavity.

The check valve operation differs from normal port and poppet valve performance and ultimately governs the performance of this engine. To determine valve timing it was necessary to find a way to identify when the passive valves open or close. Valve activity is difficult to measure directly because the valves are located in a confined space exposed to combustion temperatures and pressures. Also, the valves are passive, i.e. they are not driven off a predictable cam profile as with cam driven poppet valves. Therefore another means of identifying valve activity was needed. A simple way of doing this was by inspecting a cylinder pressure signal like the one shown in Figure 4.9 from a pressure transducer mounted in the engine head.

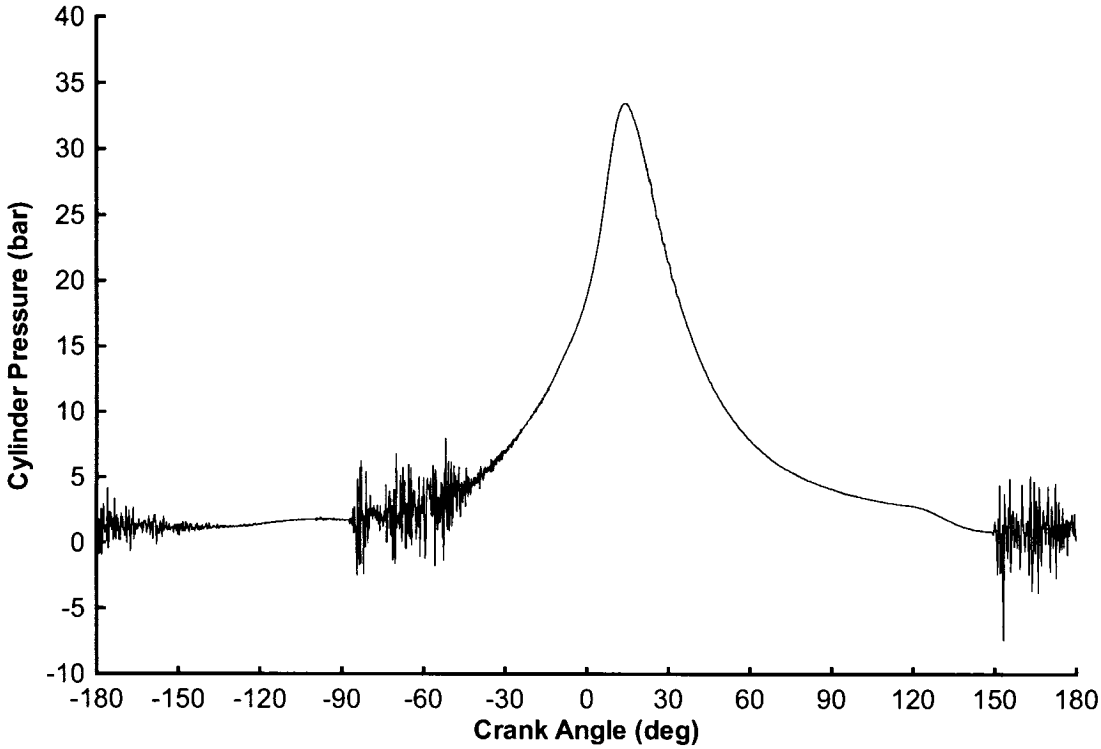

Figure 4.9: Fired engine pressure for one cycle at 2000 rpm 5.5 ms fuel pulse width. Noise in pressure signal indicated where the valves open and close. Intake closed is at 86° bTDC and intake open is at 150° aTDC.

It is evident that a clear disturbance or "noise" in the pressure signal occurs in the area where the valves should open and close. Therefore, it is logical that the noise in the signal is produced by the platelets impacting the retaining plate or the valve seat. As well, the vibration sensitive piezoelectric pressure transducer was located directly on the engine head. To test this theory, the engine was turned off, the engine head was impacted with a wrench, and the cylinder pressure was recorded. A similar noise pattern appeared in the pressure signal confirming that a vibration input does cause a disturbance in the signal.

The noise was used to identify when the platelet hits the retaining plate during opening, or the valve seat during closing. Note that this method does not identify when the valves begins to move, only when they are fully opened or closed. Some preliminary

CFD experiments performed in the Queen's combustion lab indicate that the platelets take roughly 1.3 ms to open at 2000 rpm and 50 kPa gauge intake plenum pressure. At this operating condition, the crankshaft rotates 15.6° during platelet transition.

The valve timing diagram shown in Figure 4.10 will be used to understand how the valves behave during a typical fired engine cycle. Starting at BDC, the exhaust ports are fully open as well as the intake valves, allowing for scavenging of the cylinder. As the piston moves up towards TDC, the exhaust port area decreases until the exhaust ports are completely closed at 120° bTDC. At this time the cylinder pressure rises to the plenum pressure and airflow into the cylinder stops. As the piston moves up further, it causes the cylinder pressure to increase and surpass the intake plenum pressure causing a reverse airflow. This reverse airflow and cylinder pressure forces the platelets against the valve seat, closing the cylinder at about 86° bTDC for the example in Figure 4.9. Also note that fuel injection starts at 120° bTDC and continues until 53° bTDC for this specific example. After the intake valves close the air-fuel mixture is compressed until 25° bTDC when the spark is fired to ignite the mixture. Combustion occurs and causes a peak pressure at about 14° aTDC. The piston is forced down and the pressure drops accordingly until 120° aTDC when the exhaust ports begin to open initiating blowdown, distinctly recognized by the higher rate of pressure drop. When the cylinder pressure drops below the plenum pressure at about 150° aTDC, flow starts through the check valves into the cylinder and scavenging begins. The cycle then repeats itself. Note the natural by-product of the passive check valve design is asymmetrical intake valve timing.

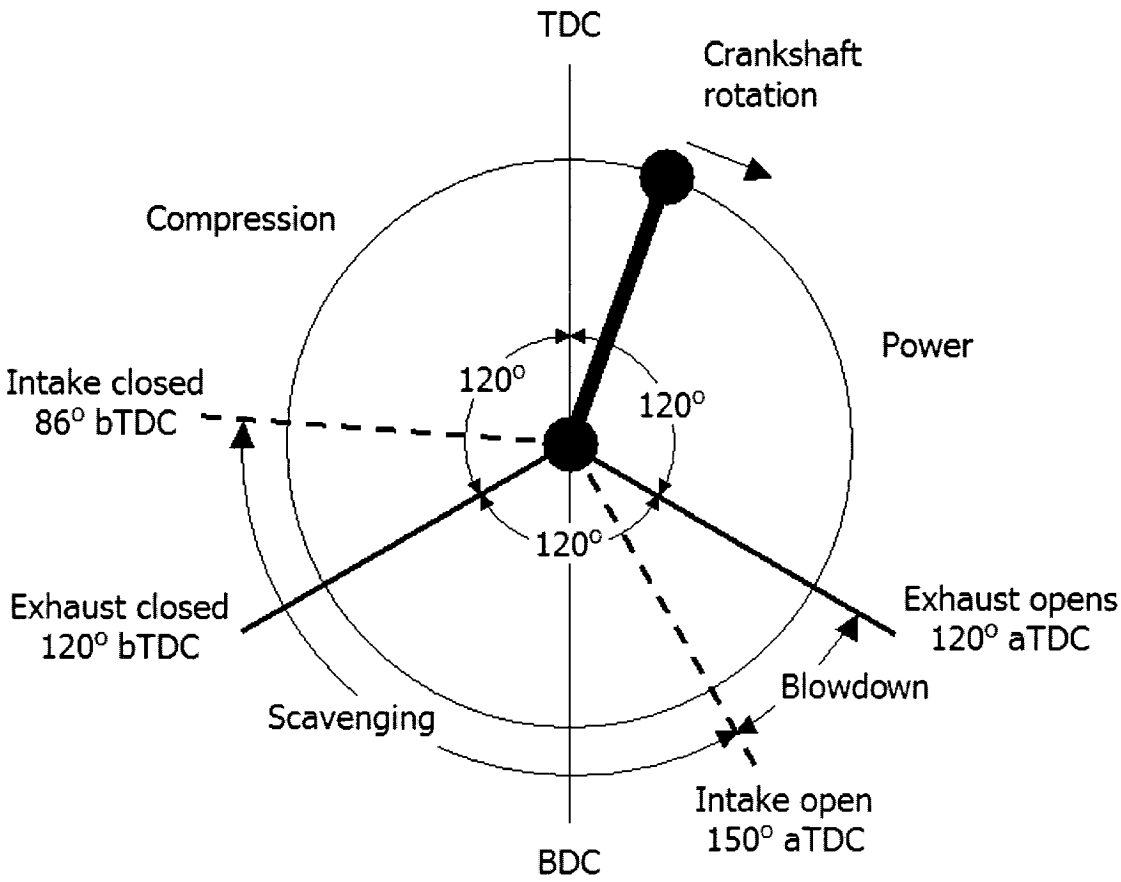

Figure 4.10: Timing diagram for novel engine at 2000 rpm.

Three different platelet set designs, set A, B, and C, were tested in the fired engine. A representative platelet from each set is shown in Figure 4.11. The platelet properties are listed in Table 4.2.

A drilled retaining plate, cross retaining plate, and perforated retaining plate were tested under motoring conditions. The three different retaining plates are shown in Figure 4.12.

The cylinder was originally machined specifically for this engine from steel to a bore of 86 mm. At the base of the cylinder there are two groups of four diametrically opposed exhaust ports as shown in Figure 4.13. The exhaust ports begin to open at 120° aTDC, are fully open at BDC, and close completely at 120° bTDC.

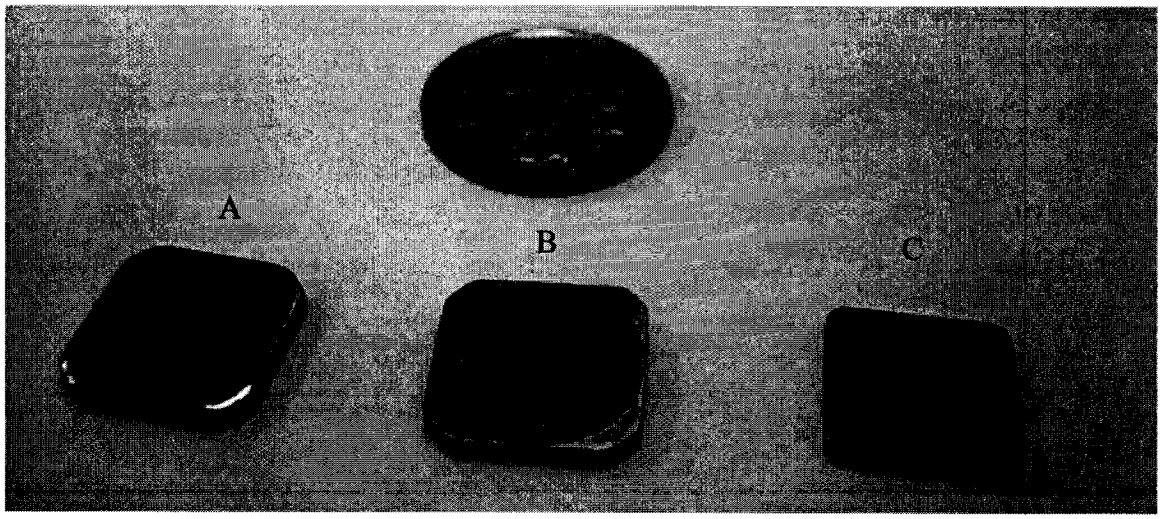

Figure 4.11: A sample platelet from each platelet set tested in the fired engine. From left to right: set A, set B, set C.

Table 4.2: Platelet properties.

Platelet Property	Set A	Set B	Set C
Material	Stainless Steel	Tool Steel	Tool Steel
Width (mm)	12.74	12.84	11.85
Length (mm)	12.74	12.84	11.85
Thickness (mm)	1.47	1.15	1.15
Mass (g)	1.77	1.36	1.23

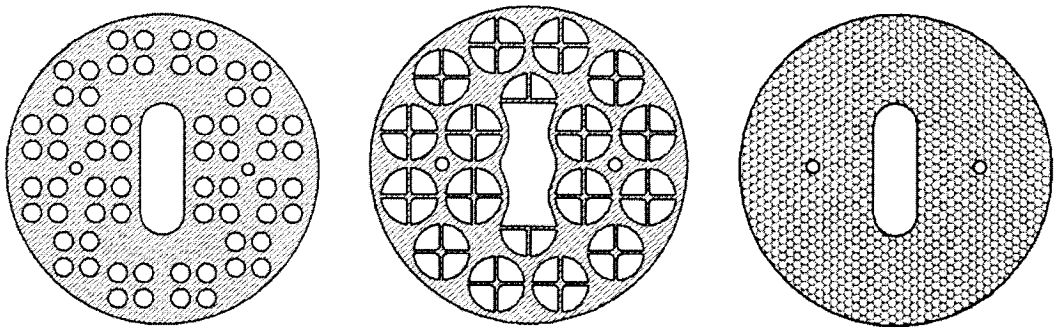

Figure 4.12: The three retaining plate designs: a) Drilled retaining plate; b) Cross retaining plate; c) Perforated retaining plate.

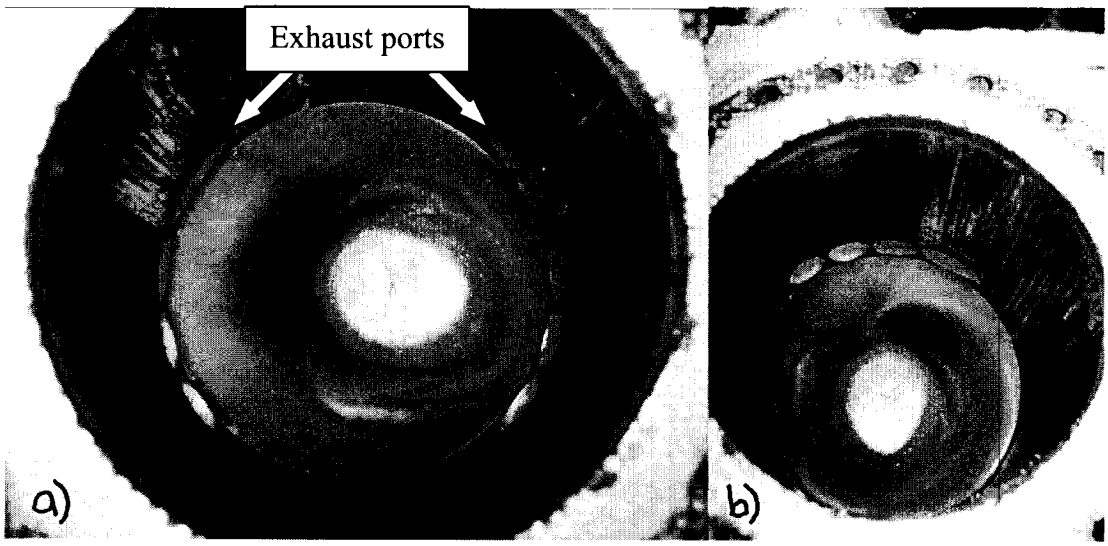

Figure 4.13: Photograph of the cylinder with the piston at BDC and the exhaust ports fully open; a) looking straight down the cylinder; b) looking down the cylinder from the side.

The cylinder block also contains a water jacket for cooling, and two lubricating holes at the bottom of the cylinder. The original engine required a fuel-oil blend to lubricate the crankcase bearings and cylinder walls. This method was not available for the engine so a small amount of oil was manually added to the crankcase through the lubricating holes before each engine test.

The piston used for the project was the original piston from the Yamaha two-stroke engine, shown in Figure 4.14. The piston was an aluminium piston with a convex crown designed for the original scavenging method and was ultimately a poor design for the new top-down uniflow scavenging system.

A flywheel and starting system typical of production engines was used for fired engine operation. Motoring tests were performed using an AC motor pulley drive system. A range of engine speeds was achieved using different pulley diameters on the crankshaft. The flywheel was machined in house out of steel and bolted on the end of the crankshaft.

Figure 4.14: Piston used in the engine; note the convex piston crown.

The starter and ring gear was an aftermarket Yamaha starter kit made for a snowmobile. The starter kit provided an engine cranking speed of about 650 rpm and worked very well for this application. Figure 4.15 shows the final starter arrangement.

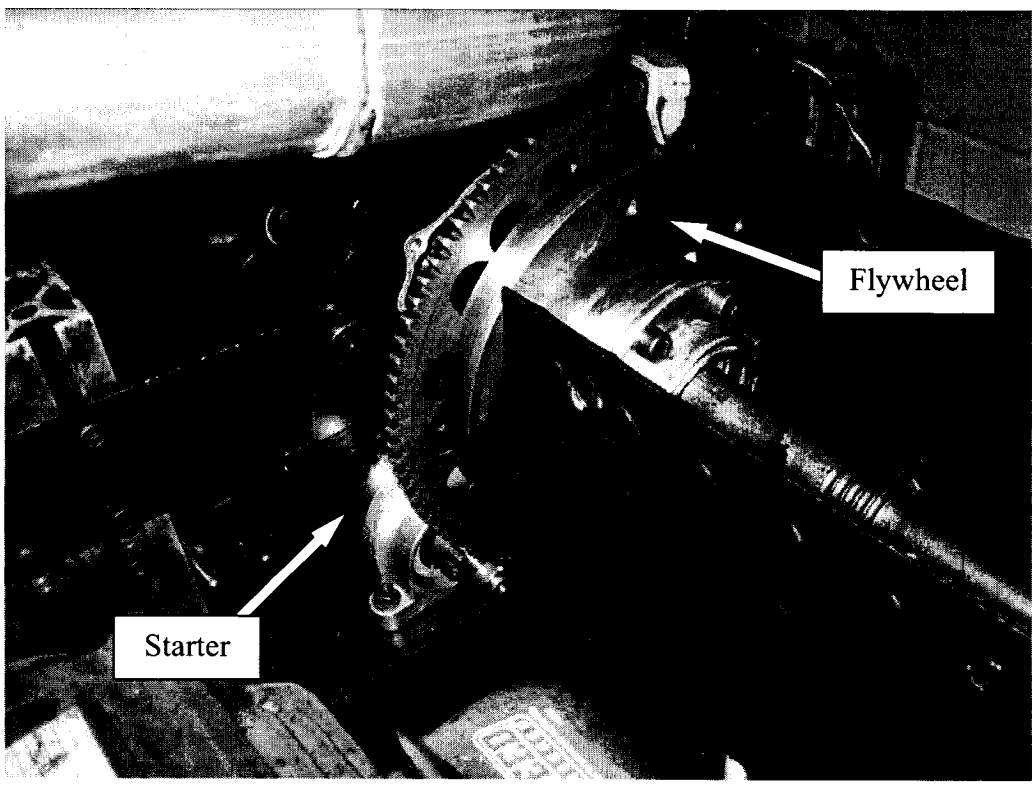

Figure 4.15: Starter and flywheel.

4.1.2 Intake System

As with all two-stroke engines, the air used to purge the cylinder must be pressurized. A Roots-type supercharger as shown in Figure 4.16 driven by an AC motor was used to raise the pressure in the intake plenum for scavenging. An 11-gallon (3785 cc) intake plenum constructed out of a portable compressed air tank was placed between the supercharger and the engine head. It was decided to build the intake plenum this large so that it removed any pressure waves before the air entered the cylinder. It has been suggested that a surge tank like this should be roughly ten times the cylinder volume [13].

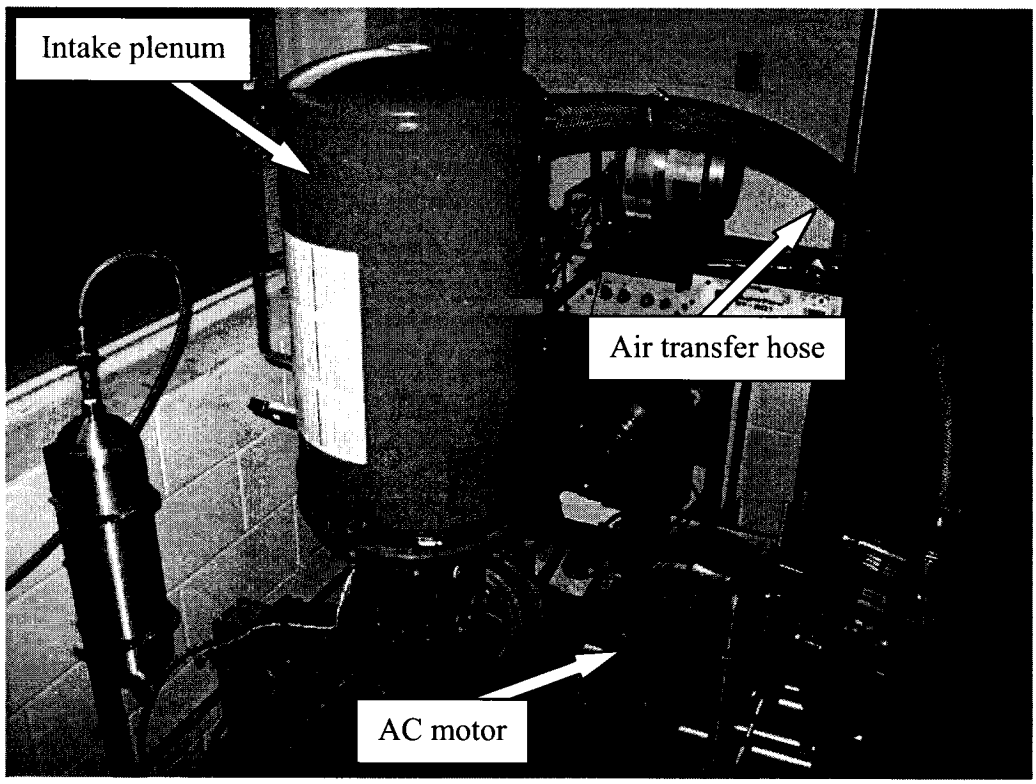

Figure 4.16: Photo of apparatus showing the motor-driven supercharger, air transfer hose and large red intake plenum used to reduce pressure waves.

An airflow measurement turbine located on the suction side of the supercharger measured volumetric airflow so that, when combined with the ambient air density, the air mass flow could be calculated. The air mass flow is needed to calculate the delivery ratio

and obtain a rough measure of the air-fuel ratio. A photograph of the supercharger and airflow turbine is shown in Figure 4.17.

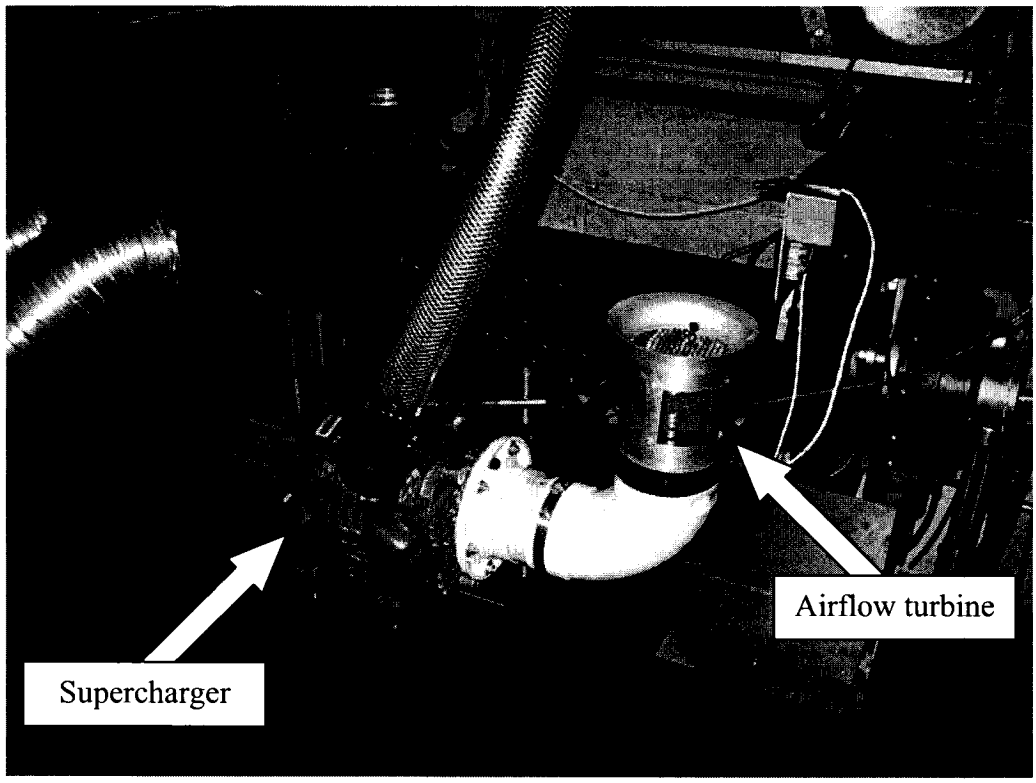

Figure 4.17: Airflow measurement turbine and Roots-type supercharger.

4.1.3 Exhaust System

Four exhaust ports are located on either side of the cylinder bore at the lower part of the cylinder. An exhaust header was used to gather the exhaust gas from each port and emit one stream of exhaust gas. Since the ports were on either side of the engine, two exhaust headers were used as shown in Figure 4.18.

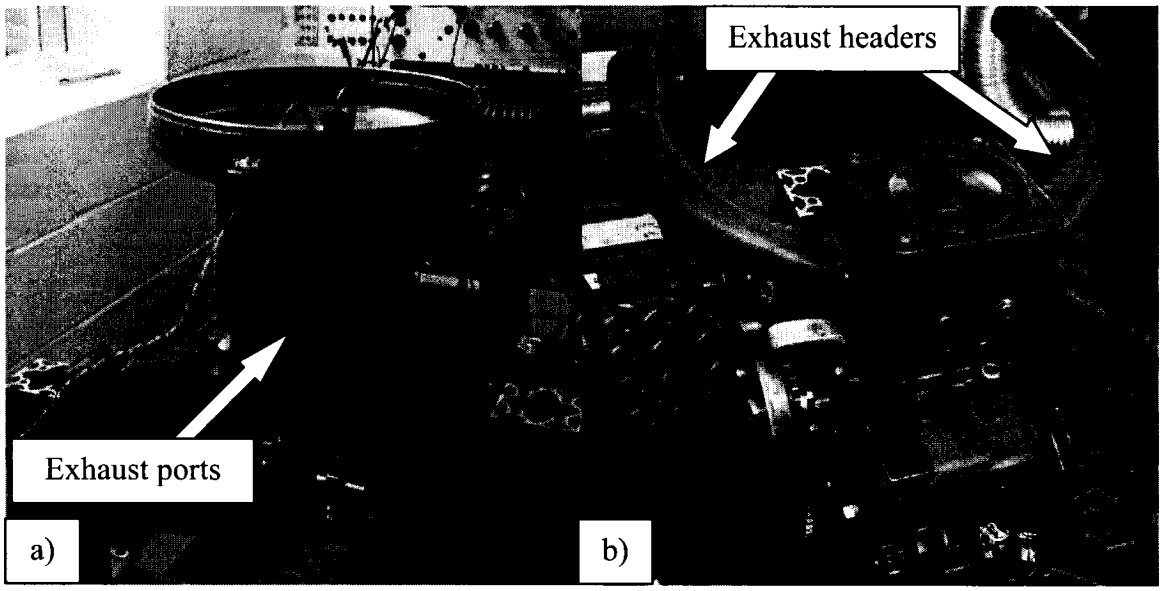

Figure 4.18: a) Exhaust ports on one side of the engine. b) Exhaust headers on either side of the engine.

The exhaust gases were vented outside of the building by an exhaust fan but the exhaust back pressure had to remain near atmospheric pressure for scavenging. The exhaust fan itself did provide some vacuum so it was decided to use two stovepipes and support them near the exhaust headers; therefore, the exhaust gas would be sucked into the stovepipe while maintaining the test cell static pressure at the exhaust header exit. A system like this also cools the exhaust with the entrained air. Figure 4.19 shows the exhaust configuration.

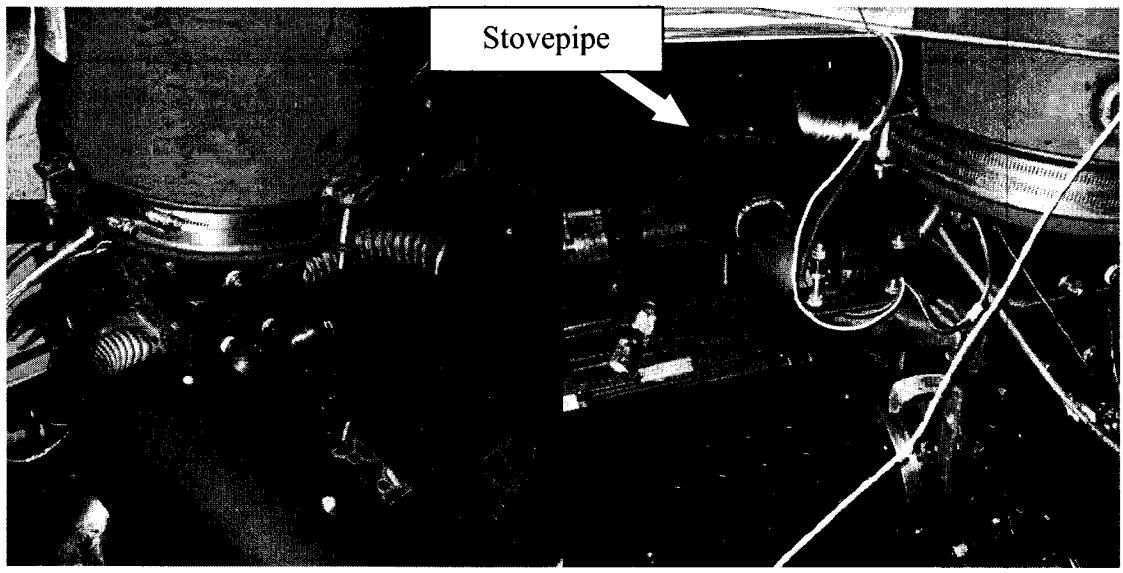

Figure 4.19: Exhaust venting.

4.1.4 Engine Control Unit

The ECU used for this project was a MOTEC M4. All events such as ignition timing, injection timing, and fuel pulse width could be adjusted as required for each test. A versatile injection system was needed so that fuel could be injected on the compression stroke as opposed to the intake stroke as with conventional four-stroke engines. A computer outside of the dynamometer cell was connected to the ECU via a serial cable for on the fly parameter adjustment. A full list of ECU specifications is located in Appendix A and a wiring diagram is located in Appendix B.

4.1.5 Fuel System

To obtain the injection pressure necessary for GDI engines, the fuel was pressurized using nitrogen gas. The fuel injection pressure was changed easily using the nitrogen tank regulator. A Swagelok two-litre canister acted as the fuel tank and stainless steel lines and fittings routed the fuel to the fuel rail, see Figure 4.20. The fuel rail was an original part machined from steel that clamped the fuel injector in place as shown in

Figure 4.21. The fuel rail and injector seat were machined to accommodate this specific injector.

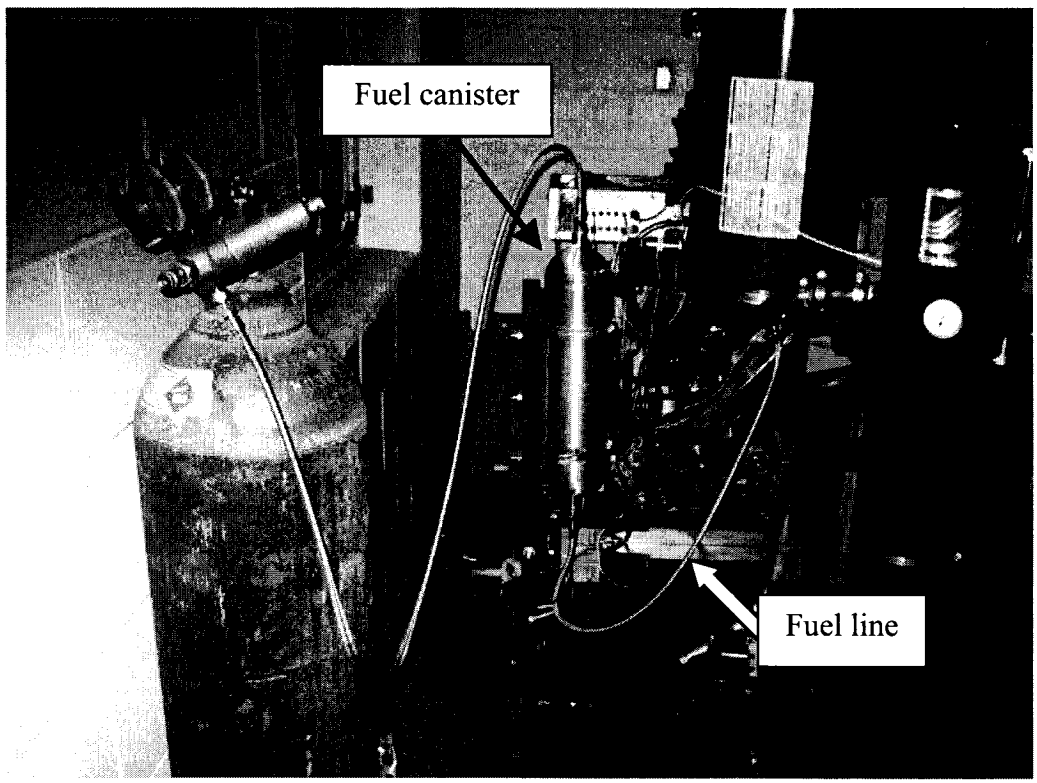

Figure 4.20: Fuel system.

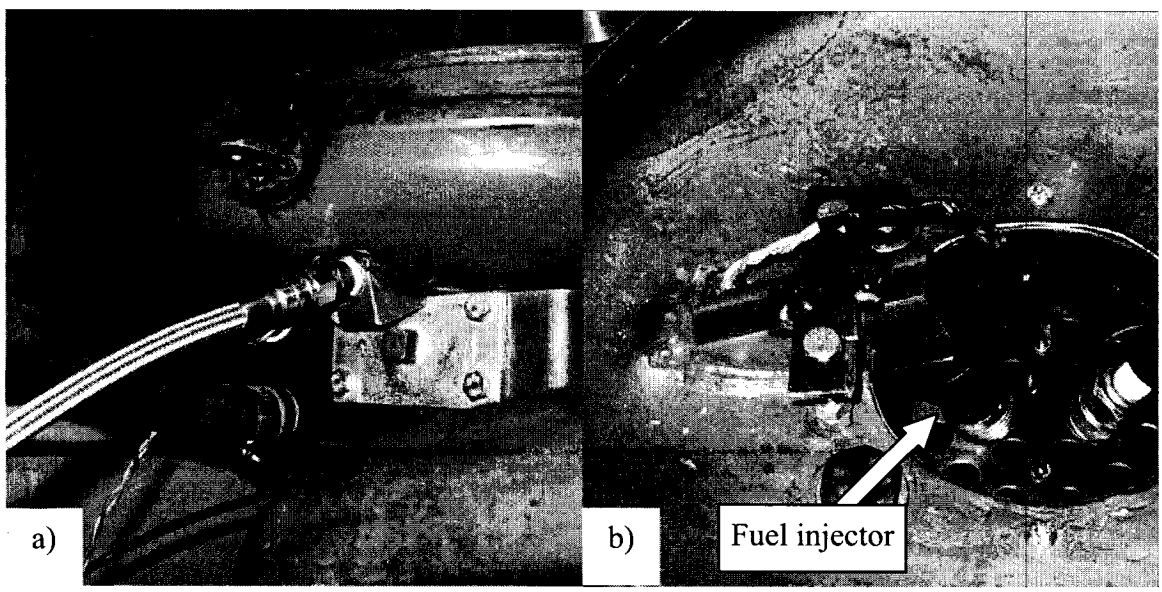

Figure 4.21: Fuel rail detail: a) fuel line connecting to the fuel rail; b) close-up of fuel rail, injector and injector seat inside the plenum.

A Siemens Deka fuel injector was used for this engine. The injector was designed for the GDI 2.0L engine used in the Renault Laguna. A picture of the injector and injector specifications are presented in Figure 4.22 and Table 4.3, respectively. A fuel injection pressure of 75 bar was used for all tests.

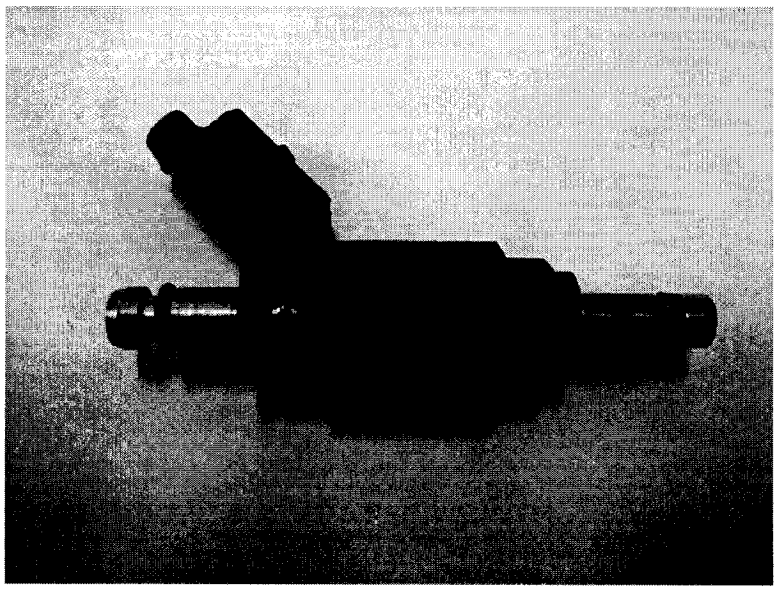

Figure 4.22: Siemens Deka GDI fuel injector.

Table 4.3: Injector specifications.

Manufacturer	Siemens
Model	Deka
Injector Type	High pressure, swirl type
Fuel Pressure Range	4-10 MPa
Spray characteristics	40° cone angle, hollow cone

The fuel used for all tests was Sunoco ULTRA 94 gasoline. This 94 octane unleaded gasoline contains 10% ethanol by volume and is available from most Sunoco gas stations. The addition of ethanol at this level can have some positive effects on engine performance [40-42]. The lower heating value is 42 MJ/kg and the stoichiometric air-fuel ratio is 14.0 [42, 43]. The reason for a high octane fuel was to prevent damage to the engine caused by knock. When the cylinder air-fuel mixture is either fuel rich or fuel

lean, slow flame speeds can result (see section 2.4). Slow flame speeds give time for the unburned end gas to spontaneously ignite as opposed to being consumed by the flame reaction zone initiated by the spark plug. The end gases ignite due to the high pressure and high temperature produced by the propagation of the flame and the expansion of the combustion products. The high pressure and temperature associated with knock can cause severe mechanical damage to the piston and cylinder surfaces.

4.1.6 Ignition

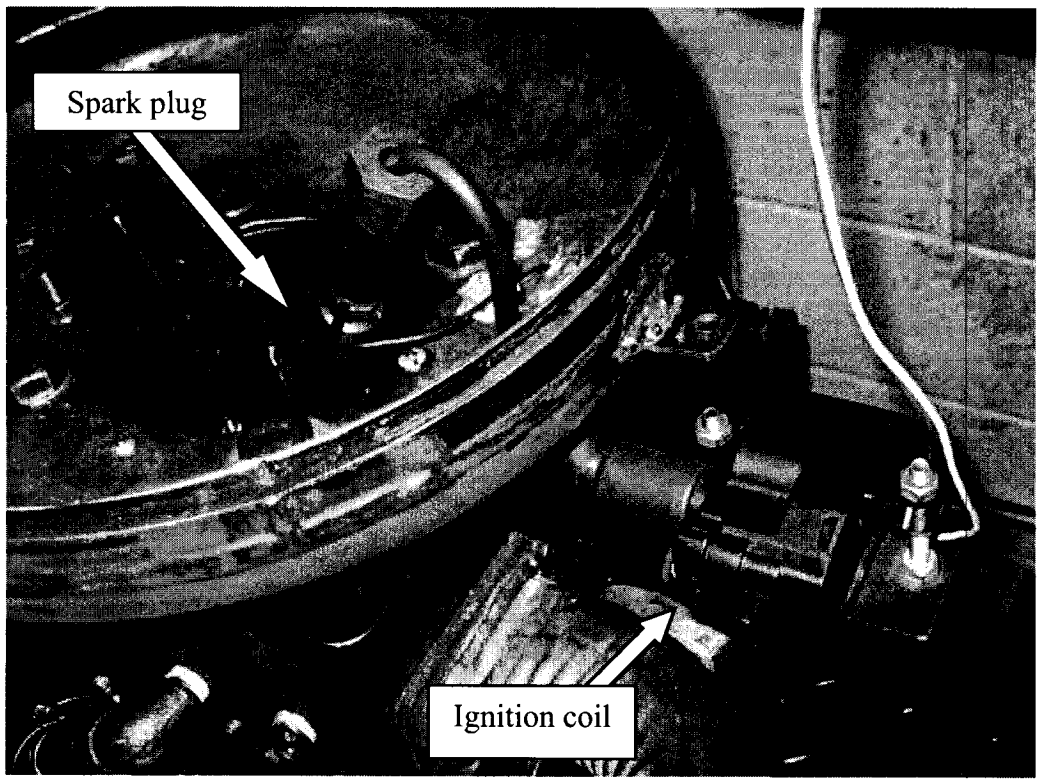

Figure 4.23: Ignition coil and spark plug.

A DENSO coil-over-plug ignition unit supplied the ignition energy to the spark plug as shown in Figure 4.23. A Kistler 6117BCD17 measuring spark plug was used for all tests. This spark plug was designed for four-stroke engines but operated reliably

during the testing without severe fouling problems. The spark plug gap was set to 0.76 mm (0.030 in) for all tests.

4.2 Data Measurement and Acquisition

Engine control and data acquisition (DAQ) were performed outside of the dynamometer cell with the set up shown in Figure 4.24. The first computer communicated with the ECU through a serial cable. It displayed real time engine operating conditions and allowed for tuning on the fly. Two other computers were used for data acquisition. One ran the LabView program that sampled the data from the National Instruments (NI) DAQ card and the other sampled data that was recorded by the SuperFlow dynamometer.

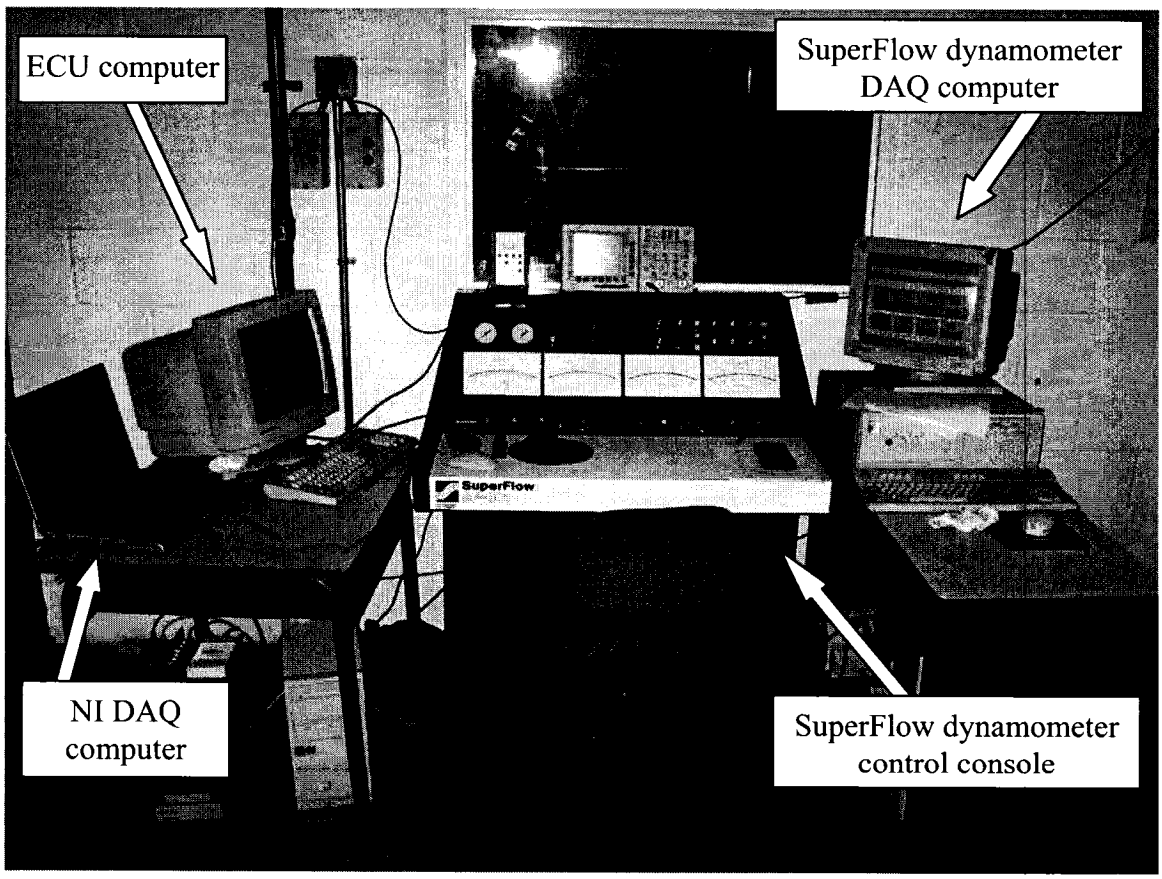

Figure 4.24: One dedicated computer controlled engine ECU parameters and displayed real time engine conditions while the other computers recorded data from the NI data acquisition and SuperFlow data acquisition. Engine loads were set using the control console.

4.2.1 SuperFlow Dynamometer

A SuperFlow 901 hydraulic dynamometer was used to load the engine. The dynamometer also measured brake torque, volumetric airflow, and ambient air temperature in the cell.

The torque range was 0-1350 N-m with an accuracy of ±0.2% full scale or ±2.7 N-m. Note that for some of the brake torque results reported, the uncertainty is larger than the difference in values measured. This is not of concern since the indicated values are of the most interest for this thesis and the main function of the dynamometer is to load the engine. The dynamometer was calibrated before the tests with a lever arm and calibration weight. The airflow meter had a range of 2-70 L/s with an accuracy of ±0.5% full scale or ±0.3 L/s. The airflow turbine was calibrated using a flowbench equipped with an orifice plate. For the airflow tests, trends were of interest more than specific values and since the test method was consistent, the uncertainty was not critical. The temperature accuracy can be estimated as ±0.5°C.

Within the power absorber shown in Figure 4.25, the engine drives a vaned rotor that interacts with a stator through the shearing or viscous forces of the water flowing through. The stator is connected to the absorber housing that is free to rotate on bearings but restricted by a strain gauge load cell. The water shearing inside the absorber causes a rotational force on the stator that is measured by the load cell. A servo valve changes the amount of water flowing through the absorber, thereby controlling the load. Load control is essential so that the required test conditions can be achieved.

With the force from the load cell and the distance at which the force is acting, the engine brake torque can be calculated. When combined, the input shaft rotation speed and the measured torque results in the brake power.

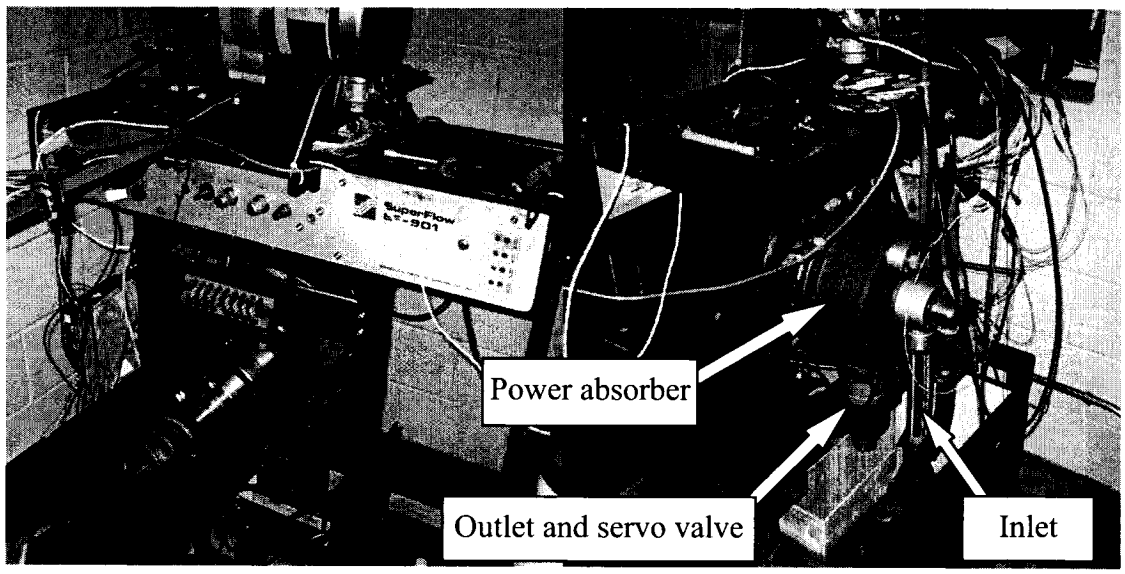

Figure 4.25: Front and back of the SuperFlow 901 dynamometer.

The dynamometer was too large for an engine of this size and as a result the engine speed range was small. Below 1000 rpm the dynamometer would lose its water prime and inconsistent loading would occur. At the maximum fuel pulse width tested, the engine only had enough power to reach about 2100 rpm with no load. At this operating condition, the power output of the engine equalled the parasitic load of the dynamometer. Therefore, the test points ranged from 1000 rpm to 2000 rpm.

The engine was connected to the dynamometer with an axle assembly from a 1985-1987 Canadian model Volkswagen Jetta, as shown in Figure 4.26. The shaft contained two constant velocity (CV) joints with a flange at one end and a splined shaft at the other. The flanged end was bolted to the engine flywheel while the splined shaft slid into the mating adaptor hub that was bolted to the dynamometer. The CV joints and

spline coupling allowed for minor misalignment. A heavy-duty guard was built to contain any parts in case of failure.

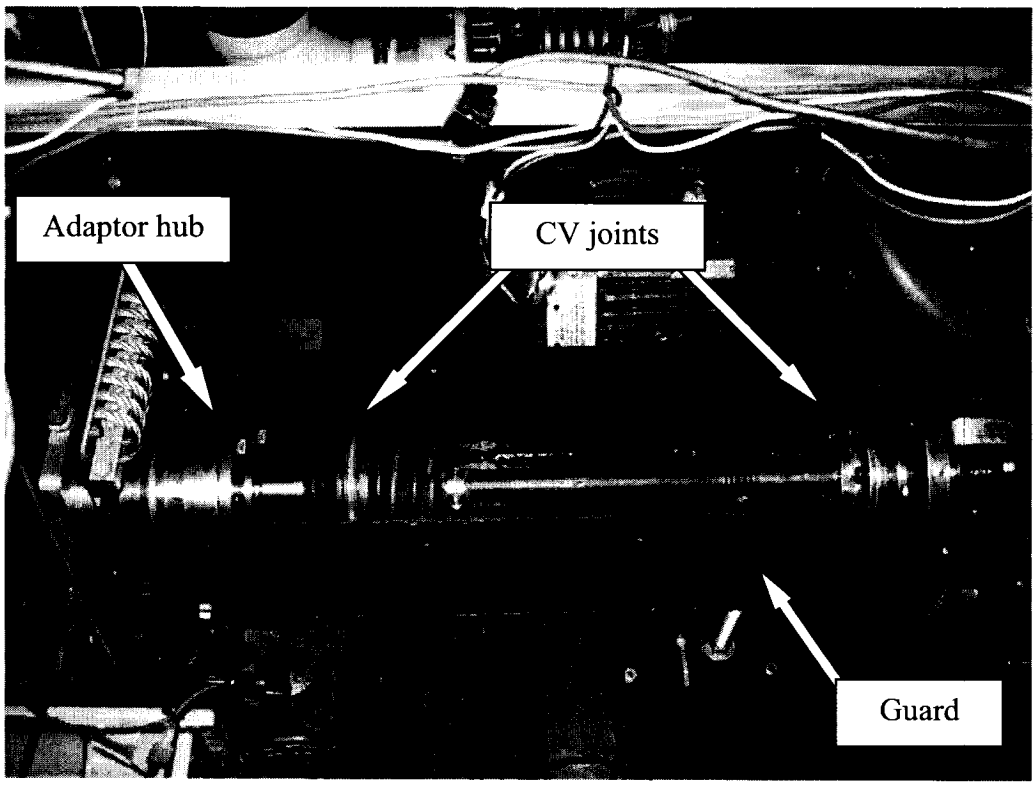

Figure 4.26: CV shaft coupling the engine to the dynamometer. Guard top is removed to show the shaft.

The dynamometer also had a cooling tower that was connected to the engine. A water pump was put in the plumbing so that water could circulate around the cylinder and head to cool the engine. The water pump was controlled with a switch on the control console. An in-line water heater was used to warm up the engine for easier starting.

4.2.2 National Instruments Data Acquisition System

A 16-Bit National Instruments USB-6210 data acquisition system was used to sample voltages from the cylinder pressure sensor, intake plenum pressure sensor, crankshaft trigger wheel sensor, and injector current transducer. The data was saved to a computer with LabView program. Each manually triggered event sampled 40,000 data points at a

sample rate of 50 kS/s. This resulted in 0.8 s of data or 16 cycles at 1250 rpm, 19 cycles at 1500 rpm, 22 cycles at 1750 rpm, and 26 cycles at 2000 rpm.

Cylinder Pressure Sensor

A Kistler 6117BCD17 spark plug pressure transducer was used to measure cylinder pressure. The piezoelectric pressure transducer incorporated into the spark plug has a pressure range of 0-200 bar and a linearity of ±0.1% full scale output. The resulting measurement uncertainty was ±0.2 bar. A Kistler 5010 charge amplifier converted the capacitance signal into a voltage signal for the data acquisition. The charge amplifier was set to 5 bar/volt for motoring tests and 10 bar/volt for fired tests. The time constant was set to "long" and the sensitivity set to 16.1 pC/bar.

"Drift" in the voltage signal required anchoring the data to a known pressure during the cycle. The pressure at the end of blowdown was used for this since it is approximately atmospheric. The final cylinder pressure, p_c, was calculated using Eq. (4.1), where x is the bar/volt value, e is the charge amplifier voltage, and the offset is the difference between the recorded pressure and atmospheric pressure at the end of blowdown.

$$p_c = xe + offset \qquad (4.1)$$

Intake Plenum Pressure Sensor

The intake plenum pressure was measured by an Omega PX219-030A5V, 0-2.1 bar absolute pressure transducer with an accuracy of ±0.25% full scale. The resulting measurement uncertainty was ±0.005 bar or ±0.5 kPa. The transducer was calibrated with two known pressures: 0 bar using a vacuum pump, and atmospheric pressure as

reported at the Kingston airport at the time of calibration. The calibration resulted in a linear equation used to relate pressure to voltage.

Crankshaft Trigger Wheel Sensor

The crankshaft position was calculated using the same trigger wheel signal used by the ECU. A 58-tooth trigger wheel with a two-tooth gap, as shown in Figure 4.27, was used to produce the signal. A gap is required to identify an index tooth so that TDC can be located.

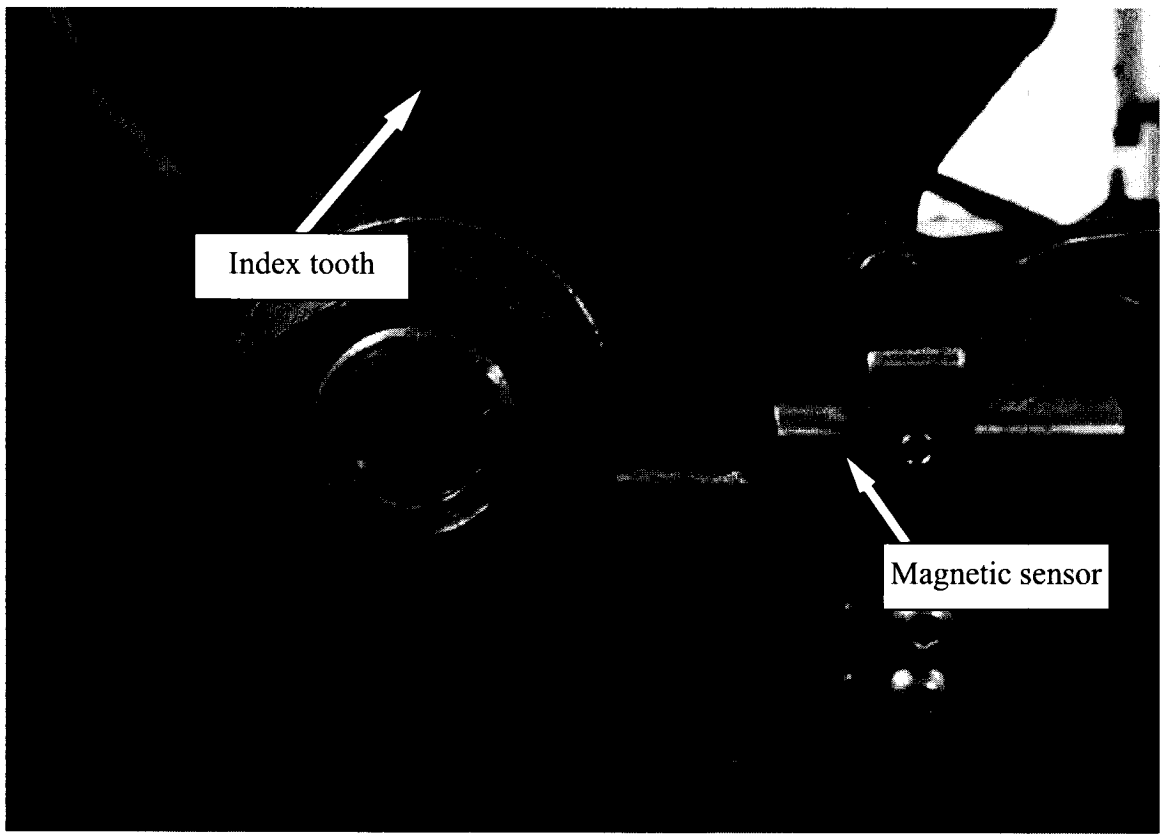

Figure 4.27: Trigger wheel located at TDC.

As the trigger wheel rotates, teeth pass by a fixed magnetic sensor and induce an alternating current in the sensor leads. The result measured by the DAQ is an alternating voltage signal across the sensor leads. For this particular wiring, the voltage drops, from

positive to negative, through zero volts when a tooth is aligned with the sensor. An example of the sensor signal is shown in Figure 4.28.

The trigger wheel resulted in a pulse every six degrees. TDC was found using a dial indicator. A TDC index angle of 266° was used to relate the index tooth (first tooth after the gap) to TDC for the calculations. An estimated uncertainty for this value is ±0.5°.

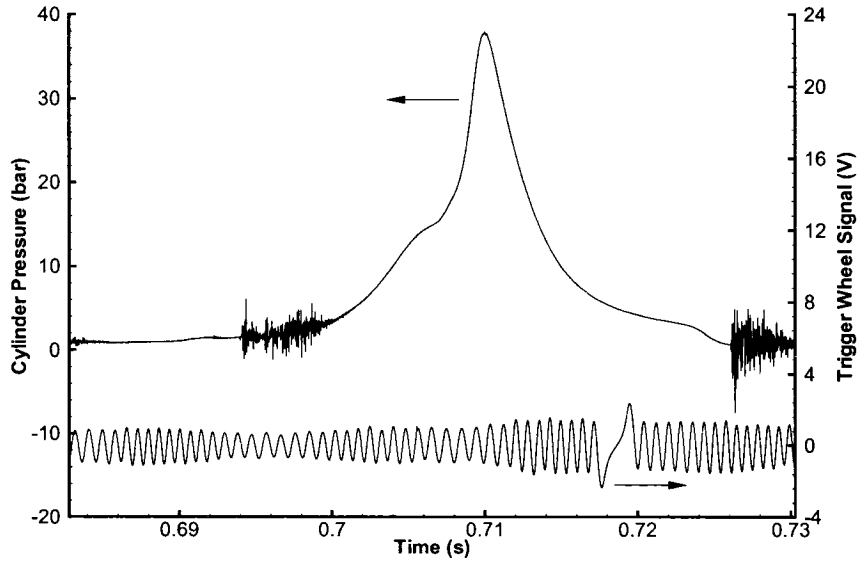

Figure 4.28: Representative trigger wheel voltage signal.

Injector Current Transducer

An AC current transducer was used to record injection timing. The jaws of the transducer were put around the fuel injector signal wire to detect fuel injection. The details of the voltage output were not important since this transducer was used only to identify the injection location and not measure the value.

Chapter 5 Experimental Results and Discussion

5.1 Engine Tests without Combustion

An engine head airflow test and motoring test were done to gather information on check valve behaviour. Check valve performance can be influenced by platelet design and retaining plate design. The tests presented in this section focus on the effects of the retaining plate design. Platelet design is investigated in section 5.2.2 with the fired engine tests.

5.1.1 Engine Airflow

Airflow is the main factor that dictates power output for a two-stroke engine because it governs how much combustion products remain in the cylinder after scavenging. This is why intake and exhaust airflow characteristics for an engine must be known and optimized for the desired operating range. The three retaining plate designs presented in section 4.1.1 were installed in the engine head and tested using a simple steady flow flowbench built in house. The flowbench provided actual airflow data as well as a pressure drop across the cylinder head. With this information the flow coefficient for each retaining plate was calculated and compared.

The flow coefficient, C_f, and discharge coefficient, C_d, are important values that reveal flow performance through an engine intake valve. The flow coefficient and discharge coefficient are defined as the ratio of the measured mass flow rate and the theoretical mass flow rate through a reference area [44]. The difference between the two coefficients is the reference area; with respect to engine poppet valves, the flow coefficient is based on the intake port area while the discharge coefficient is based on the

poppet valve curtain area. Since the check valves in this head are either fully open or fully closed, the flow coefficient was calculated using the minimum area at the check valve. The reference area is defined in more detail below.

For comparison between C_f and C_d, Figure 5.1 from Xu [44], shows typical flow values for two different engine heads tested in a flowbench. It can be seen that the C_d decreases slightly while the C_f increases with increasing valve lift. The difference is due to the reference area; the C_d area is based on the valve curtain area, which increases with valve lift, where the C_f area is based on the port throat area that remains constant at all valve lifts. The C_d can reveal more detail at low valve lift due to its reference definition [44].

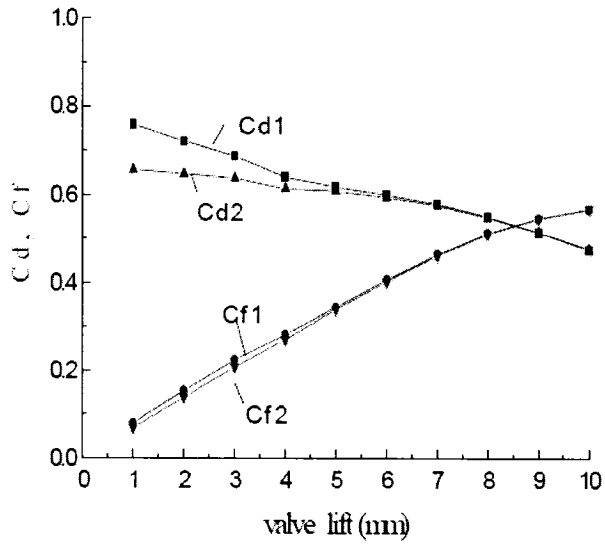

Figure 5.1: Typical flow data for two different engine heads with poppet valves, from Xu [44].

Generally, flow coefficient values can only be compared if they use the same reference area definition. Therefore, poppet valve values from Figure 5.1 cannot be directly compared to the novel engine results found below since the reference area used is

not necessarily the minimum flow area in the flow. The reference area used for the novel engine experiments is the minimum flow area.

A suction type flowbench shown in Figure 5.2 was built using a Siemens ELMO-G 2.55 kW blower to draw air through the system. Atmospheric air enters an airflow measurement turbine, flows through the engine head, through a length of 100 mm ID PVC pipe, past a control valve, and finally through the blower. The air turbine measures the actual airflow while a manometer measures the difference between the atmospheric pressure and the static pressure taken at a location downstream of the head. Figure 5.2 shows a diagram of the apparatus. The Superflow airflow measurement turbine shown in section 4.1.2 was used for these tests. The turbine was fitted with flow straighteners before and after the turbine. A control valve is located just before the blower to control the airflow rate.

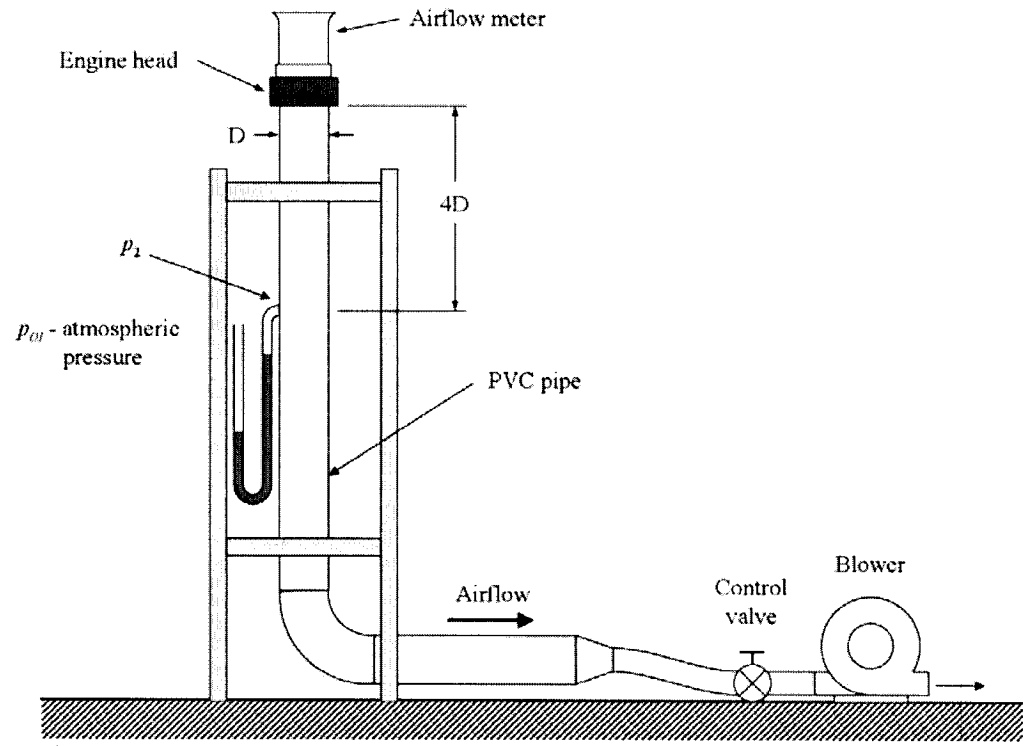

Figure 5.2: Flowbench apparatus.

The measurements from the flowbench were taken at steady flow conditions. With regard to the operating engine, even though the pressure drops recorded in this test are well below the pressure drops across the intake of the operating engine, it is accepted that steady flow tests at these lower pressures predict engine performance [44, 45].

The following method was used to calculate the ideal mass flow rate. Since the highest airflow velocities observed were well below a Mach number of 0.3, the ideal mass flow was calculated ignoring compressibility effects. Therefore, assuming incompressible flow, the following equation yields the ideal mass flow rate:

$$\dot{m}_i = A_{ref}\sqrt{2\rho(p_{01} - p_2)} \qquad (5.1)$$

For this experiment, p_{01} was the atmospheric pressure and p_2 was the static pressure downstream from the valve. Ideally the static pressure at the valve is required but since it is not easily obtained, it can be taken at some point downstream and assumed to be equal. The static pressure, p_2, for this experiment was taken at four tube diameters downstream [11, 45]. The density, ρ, was calculated based on the atmospheric conditions. The reference area, A_{ref}, for each test is taken to be the minimum flow area through the check valve. For the cross and perforated retaining plates, the minimum flow area is the cylindrical curtain area immediately above the platelet. For the drilled retaining plate the minimum flow area occurs through the retaining plate itself and not at the cylindrical curtain area as with the others, see Figure 5.3. Finally the equation for the flow coefficient can be expressed as:

$$C_f = \frac{\dot{m}}{\dot{m}_i} \qquad (5.2)$$

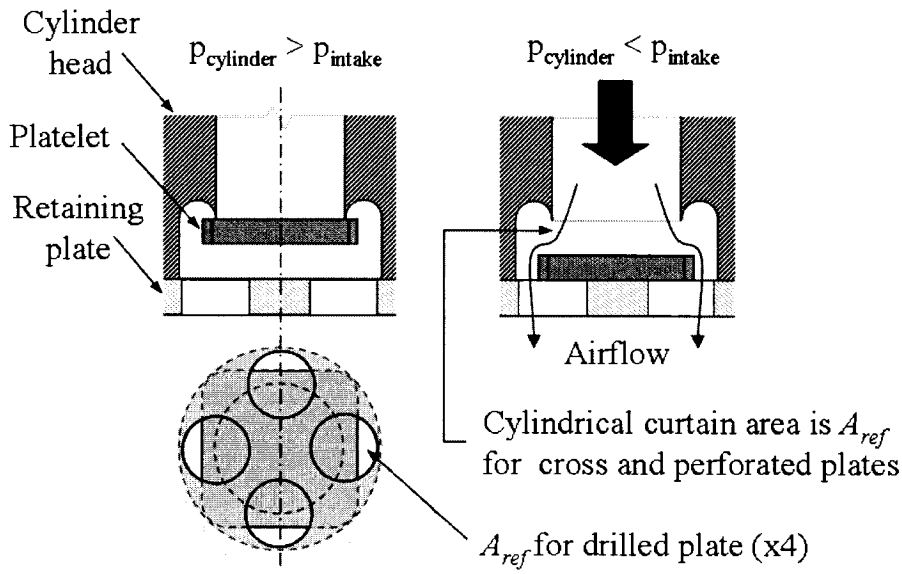

Figure 5.3: Check valve detail showing reference area.

The airflow measurements for each retaining ring are plotted in Figure 5.4. The data reveal that the air mass flow rate is highest through the perforated retaining plate for a given pressure drop across the head. From the data displayed in Figure 5.4, the C_f values at 508 mm H_20 gauge were calculated and are shown in Table 5.1. A pressure drop of 508 mm H_20 is in the range where flowbench tests are performed [44]. The results follow the same trend as the mass flow rate results, with the perforated plate giving the highest C_f and the drilled plate giving the lowest.

Based on the mass flow data and C_f data, the perforated retaining plate is the most desirable since it is closer to the ideal case where C_f is unity. It also provides the highest mass flow. Unfortunately, the perforated plate and the cross retaining plate are the most fragile and may not provide the most robust design. These two plates have small cross sections at some points and would likely fail under combustion conditions. The motoring results in the next section show some desirable results for the drilled retaining plate that supported the decision to use it for the fired engine tests.

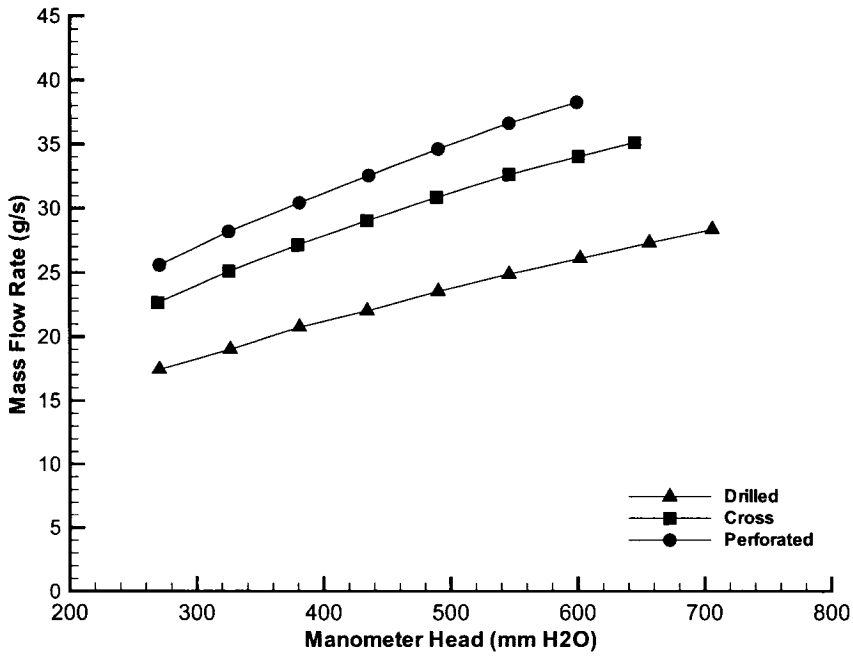

Figure 5.4: Air mass flow rate through each retaining plate.

Table 5.1: Flow Coefficient Results at 508mm H_2O.

Retaining plate	C_f
Drilled	0.55
Cross	0.72
Perforated	0.81

5.1.2 Engine Motoring

The following section provides experimental results showing cylinder pressure behaviour and valve timing for motored conditions. The tests considered here led to the retaining plate selection for the fired engine tests. Engine motoring refers to turning the crankshaft by an external source without firing. In this case an AC motor was used to drive the engine at various speeds using different pulley ratios.

Figure 5.5 shows the measured cylinder pressure for a representative motoring cycle for the final configuration of the engine containing the drilled retaining plate and the lighter platelets, set C. A description of the valve activity throughout motoring cycle will now be presented.

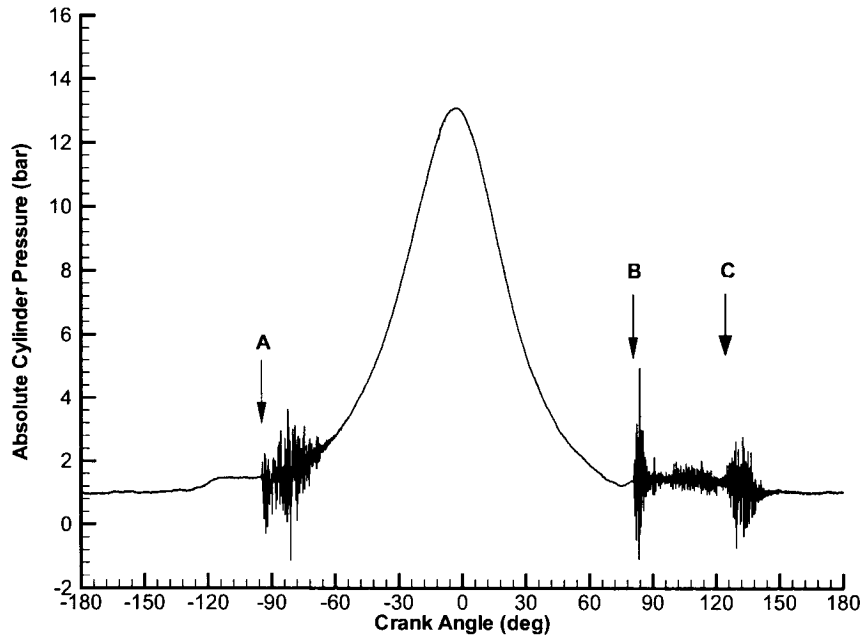

Figure 5.5: Motoring at 675 rpm with an absolute plenum pressure of 141kPa.

Starting at BDC, or –180° in Figure 5.5, the pressure in the cylinder is effectively atmospheric and the piston starts moving towards TDC. At 120° bTDC the piston completely covers the exhaust ports and the cylinder pressure rises to the plenum

pressure. The airflow into the cylinder stops shortly thereafter. As the piston moves up, it causes the cylinder pressure to increase and surpass the intake plenum pressure causing a reverse airflow. This reverse airflow and cylinder pressure lifts the platelets and forces the platelets against the valve seat, sealing the cylinder. The noise starting at point "A" indicates when the platelets hit the valve seat. After this there is a pressure rise in the cylinder until just before TDC when it starts to decline. The peak pressure occurs before TDC, opposed to TDC for the isentropic case, as a result of heat transfer and leakage past the piston and possibly through the valves [46]. As the piston moves down towards BDC, the cylinder pressure drops just below plenum pressure at about 75° aTDC causing the valves to react at 80° aTDC. From this point until 120° aTDC where the exhaust ports begin to open, the valves seem to be in a "neutral state," either open or closed as indicated by the noise. Over this neutral state region between points "B" and "C" the platelets may be affected by the pressure waves within the cylinder since the average pressure difference across them is very small. At 120° aTDC the exhaust port begins to open and the cylinder pressure drops. This prompts the platelets to impact the retaining plate at point "C" and the valve opens.

Motoring tests were done to determine valve closing times and peak compression pressure within the cylinder. Three different retaining plates (see section 4.1.1) were tested at four different motoring speeds. The pressure in the plenum was 134 kPa and platelet set B was used. Figure 5.6 shows the cylinder pressure over one crankshaft revolution for four different engine speeds using the drilled retaining plate.

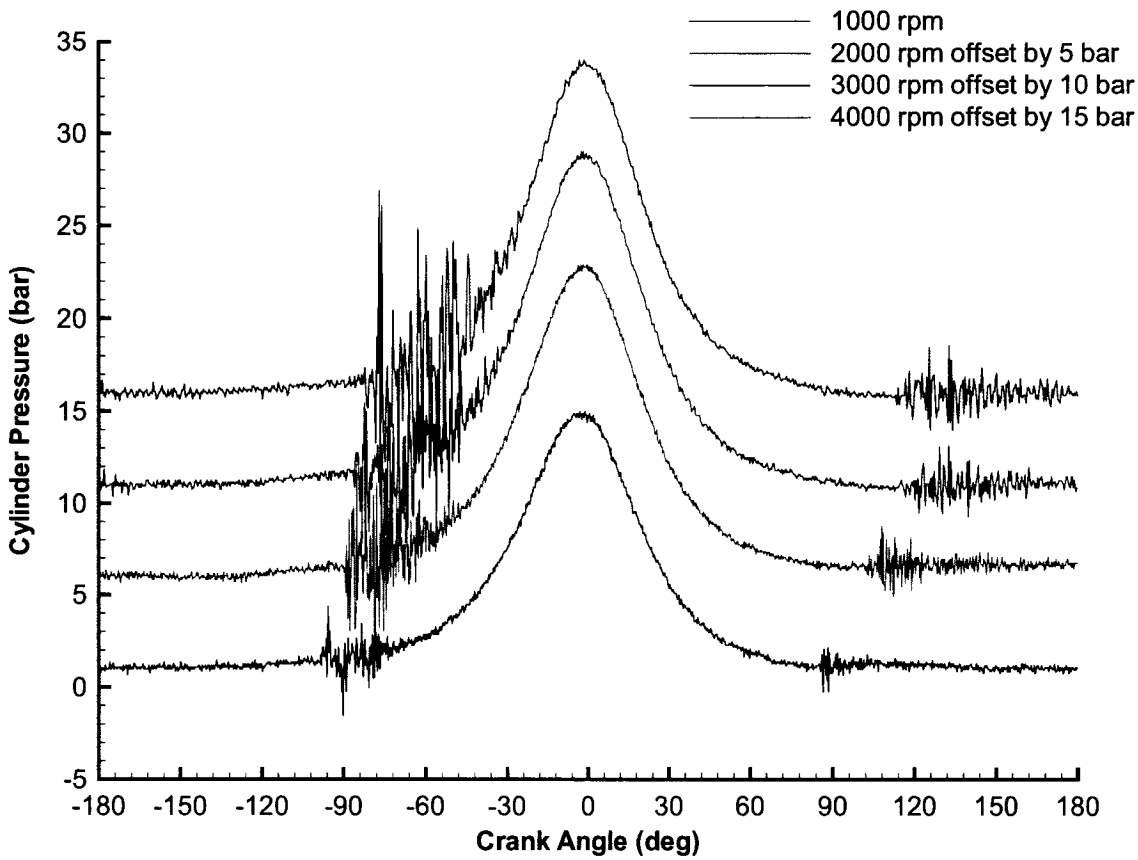

Figure 5.6: Absolute cylinder pressure for motored engine with drilled retaining plate, platelet set B, and absolute plenum pressure of 134 kPa. Pressures are absolute with the following offset: 1000 rpm offset by 0 bar, 2000 rpm offset by 5 bar, 3000 rpm offset by 10 bar, 3600 rpm offset by 15 bar.

As the motoring speed increases, the noise starts closer to TDC indicating that the platelets close later in the cycle. This reveals that the platelets have a finite reaction time and therefore take some time to start moving when forced upon by the pressure differential across them. The data also reveal that the platelets open later due to higher compression pressure. The cross and perforated retaining plates were tested and showed trends similar to the drilled retaining plate shown in Figure 5.6. All peak pressures and intake closing times are shown in Figure 5.7.

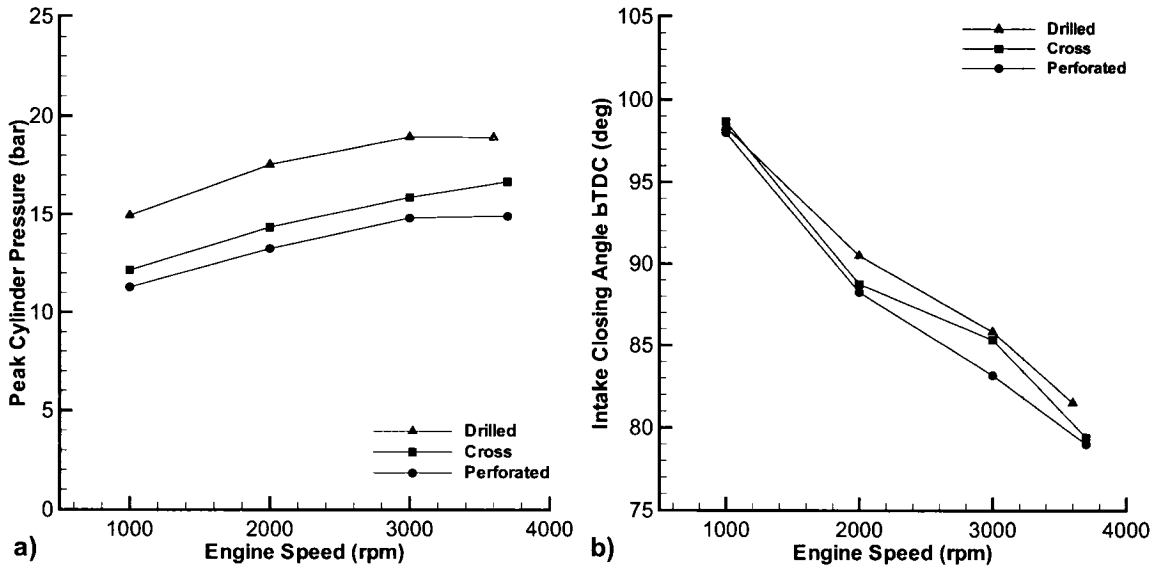

Figure 5.7: a) Peak motored absolute cylinder pressure for each retaining plate. b) Intake valve closing angle for each retaining plate.

It can be seen that the highest peak cylinder pressures are realized with the drilled retaining plate, see Figure 5.7a. The check valves also close earlier for the drilled plate at the three higher engine speeds, see Figure 5.7b. At 1000 rpm, the difference in valve closing time for each retaining plate is trivial. Further valve testing and instrumentation would be needed to understand why the peak pressure for the drilled retaining plate is the highest at 1000 rpm despite the fact that the intake closing times are similar. The airflow tests may offer some insight into this phenomenon. Based on the airflow studies, the drilled retaining plate has the lowest flow coefficient for flow from the plenum to the cylinder. If this were the same for the reverse flow, the lower mass flow would translate into more trapped mass in the cylinder for compression. A higher compression pressure is of course advantageous for both starting and normal firing operation.

The higher compression pressures, earlier closing times and robust design led to the selection of the drilled retaining plate for the fired engine tests despite the weaker airflow performance, i.e. lower flow coefficient. The drilled retaining plate was the only

retaining plate used for fired engine tests. It was decided to focus on tests with one retaining plate as test time was limited and refining the drilled retaining plate was challenging enough.

Proper valve design requires that enough flow area is provided so that the average air velocity through the valves is less than the sonic velocity to prevent choking [13]. It would seem appropriate then that a design study for this engine be done using the valve area, such as the area used for the C_f calculation, so that any onset of choking is identified. Unfortunately this analysis may not serve well since after further experimental investigation, it was determined that the platelets rotated in the cavity and aligned themselves in an undesired orientation during engine motoring and potentially during engine operation. It can be seen in Figure 5.8 that the platelets can rotate and align in an orientation that blocks airflow, e.g. worst-case orientation is shown in Figure 5.8b.

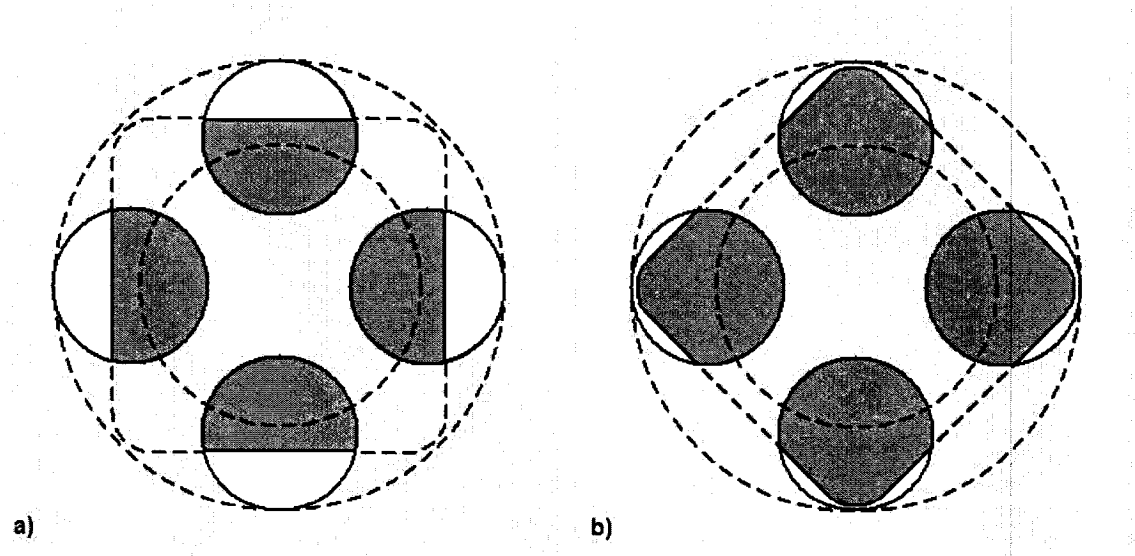

Figure 5.8: Illustration of check valve looking up at the retaining plate; a) Platelet in the optimum orientation for airflow; b) Platelet rotated 45° resulting in a poor orientation for airflow.

A simple test was performed to investigate this by aligning the platelets in the optimal angular orientation to maximize airflow before motoring, see Figure 5.8a. A line was drawn on the platelet parallel to its edge so that the orientation could be seen looking down into the head as shown in Figure 5.9. The blower was then switched on with the piston at BDC and the mass flow was recorded at 37.8 g/s. Then the starter switch was pushed and the engine was motored. After the starter switch was released and the engine stopped cranking, the mass airflow resulted in 33.6 g/s with the piston at BDC. This value was lower than the original value indicating a higher flow restriction. Upon removal of the intake plenum, all of the platelets had rotated 45° and aligned themselves in the undesirable orientation as shown in Figure 5.8b. Figure 5.9 shows a photograph of the platelet orientation before and after motoring. Soot circles on the platelets, see Figure 4.8a, and retaining plate wear patterns that were made during engine firing are further evidence of undesirable orientation.

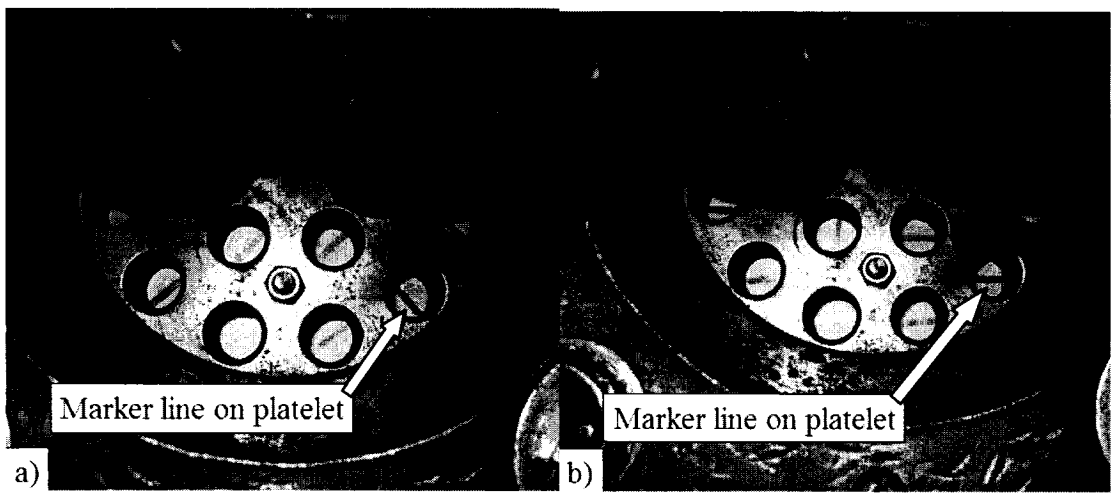

Figure 5.9: Looking down at the engine head; a) Platelets aligned for optimal airflow before motoring; b) Platelets rotated 45° after motoring.

It seems that when the platelets move up against the valve seat, the airflow aligns them in this way. This also presents the question: how is air getting into the cylinder if

the platelets align in a way to block off the airflow? It may suggest that the air enters the engine during platelet transition, from closed to open, by flowing around the platelet or that enough airflow gets through regardless of this undesired alignment. The fact that the engine runs indicates that there is enough air for some scavenging. A more detailed study on platelet behaviour independent of this thesis is required to better understand this phenomenon.

5.2 Engine Tests with Combustion

The following tests reveal, for the first time, the engine performance at low speed for this novel engine. The first study presents the brake torque vs. engine speed at three different fuel pulse width settings. This was one of the initial tests done on the engine with only brake values recorded. With a lack of cylinder pressure data, limited analysis can be done but it was decided that the data should be included as a reference for any future brake torque testing. The second study in this section identifies how the physical platelet properties effect engine performance and reveal a distinct trend favouring the platelet with the lowest mass. The third study looks at the effect of start of injection (SOI) and end of injection (EOI) on engine performance in an effort to learn about the air-fuel mixing properties within the cylinder for this engine. The fourth test looks into the indicated specific fuel consumption at various operating conditions so that evaporation and air-fuel mixing characteristics are revealed. Finally, the results that provided the best performance are presented, discussed, and compared with some production engines and experimental engines.

The engine performance is characterized by indicated values obtained from the cylinder pressure time history. The integration technique along with a sample calculation

for each result is presented in Appendix C. Some pressure traces presented in the results have been filtered, i.e. have had the platelet "noise" removed. This filtering method is also provided in Appendix C. A discussion regarding the uncertainty in the results is located in Appendix F.

An "engine test" will represent a test where data was acquired for a unique engine operating condition at steady state. The operating condition is defined by ECU settings, atmospheric conditions, and physical engine component configuration. Further, a "test session" will represent a series of engine tests separated by engine shut down. The reason the engine had to be shut down in between tests is that for some ECU calibrations, the ECU had to be restarted. It also allowed time to record subjective comments and confirm results.

The operating procedure for each engine test session was as follows. The fuel system was depressurized and about 2 L of fuel was poured into the canister. A syringe was used to inject oil into the lubrication holes while rotating the crankshaft by hand. This would make the piston spread the oil up and down the cylinder walls and provide some lubrication to the crankcase. After fuelling and oiling, the block heater was plugged in to heat the engine coolant up to about 60°C where the engine could easily start.

The ECU parameters such as spark timing, SOI timing, and finally initial fuel pulse width was set. Usually a "cold" engine requires a larger than normal injection of fuel, or starting enrichment, to aid in initial combustion. This is due to the reduced fuel evaporation at cold engine temperatures. A fuel pulse width of about 6-7 ms was usually selected and then quickly reduced when the engine first fired. With the ECU set, the

scavenging blower was turned on and the engine was cranked using the starter. An initial warm-up period was needed to obtain an operating temperature of about 95°C. This is high compared to the operating temperatures of traditional engines, which is around 80°C. However, it was thought that a higher temperature would promote fuel evaporation since a significant amount of piston and wall wetting was present. After the engine was at operating temperature, a load was applied on the engine by the dynamometer to bring it to the desired engine speed. Once a steady state engine speed was obtained, the NI data acquisition was triggered followed immediately by the dynamometer data acquisition. After the test, the engine was turned off and allowed to cool. Component failure was always a concern so engine-running time was kept to a minimum. Each test session had an objective so that the conditions were consistent. For example, all specific fuel consumption tests were done in one session. When data was compared from different days, an effort was made to match engine conditions.

The engine was tuned for maximum brake torque (MBT) timing. This means that the ignition timing was set to give maximum brake torque at a particular engine speed and load setting. The procedure for finding MBT timing is as follows. The engine would be set to a desired fuel pulse width, engine speed and mildly advanced ignition timing while recording brake torque. The ignition timing was then advanced and the brake torque recorded again. This was done for an array of ignition timing and the timing that produced the maximum torque was used for the performance tests.

As the timing is advanced from TDC, the engine produces more torque until a maximum, and then the torque starts dropping off. The torque drops off because combustion starts too early and counteracts the piston on the compression stroke,

decreasing the engine brake torque. Figure 5.10 shows a timing test for 1250 rpm and 4.5 ms pulse width. The MBT timing is 13° bTDC in this case. A finer degree increment is usually done when tuning production engines but this experimental engine was not robust enough to do extensive testing.

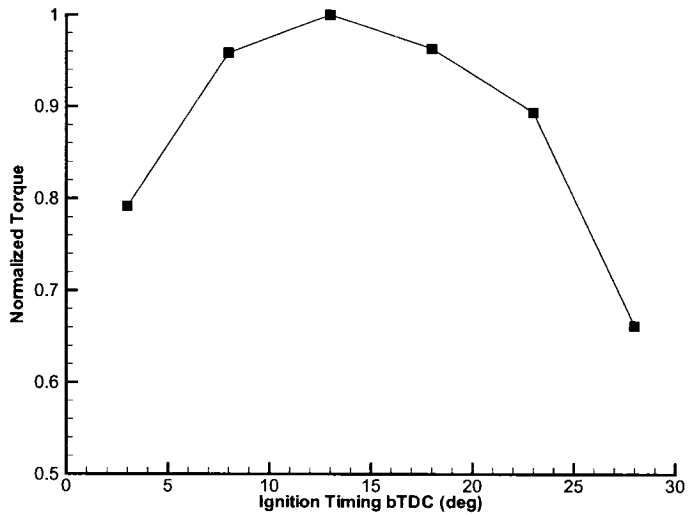

Figure 5.10: Relative change in torque with ignition timing.

5.2.1 Initial Tests

The initial engine tests were done without the NI data acquisition system and therefore only brake torque and engine speed from the dynamometer was available. Despite this, it is beneficial to present this data as it indicates torque output trends for this engine and is a reference for future testing. As described in the apparatus section, the engine uses an external Roots-type blower driven by an electric motor to scavenge the cylinder. As a result, the brake values given do not reflect the blower power and thus are higher than would be the case if the blower were driven off the crankshaft.

All initial tests used platelet set B, the drilled retaining plate and a SOI set to 113° bTDC. Table 5.2 summarizes the test conditions and results and Figure 5.11 shows the torque trends. The nominal engine speeds tested were 1250, 1500, 1750, and 2000 rpm.

Table 5.2: Initial engine test conditions and results.

Load (fuel pulse width)	**4.5 ms**				**5.5 ms**			
Engine Speed (rpm)	1270	1502	1777	2054	1249	1497	1776	2049
Ignition Timing (bTDC)	13	23	23	33	8	18	18	28
Brake Torque (N-m)*	29.3	28.1	25.6	20.5	31.6	31.2	28.1	23.5
Brake Power (kW)*	3.9	4.4	4.8	4.4	4.1	4.9	5.2	5.0
Load (fuel pulse width)	**6.5 ms**							
Engine Speed (rpm)	1281	1511	1782	2042				
Ignition Timing (bTDC)	13	23	23	28				
Brake Torque (N-m)*	25.1	23.6	22.0	14.9				
Brake Power (kW)*	6.1	6.8	7.5	5.8				

* This torque and power does not account for the external supercharger power.

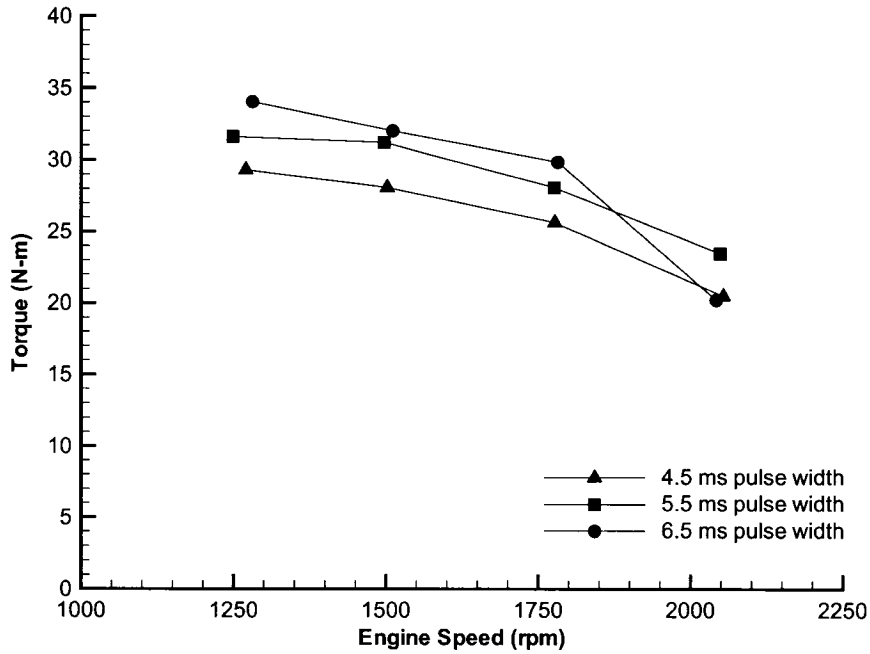

Figure 5.11: Engine torque for different pulse widths.

Figure 5.11 shows a consistent drop in torque as engine speed increases for all loads. A drastic drop in torque is revealed for 6.5 ms at 2000 rpm and deviates from the trend seen in the lower fuel pulse widths. This may be an anomaly since test data from other days showed a more consistent torque of around 25.8 N-m for the same test

conditions and MBT timing. This lower torque value is presented for consistency purposes since it was taken in the same test session as the other tests at 6.5 ms.

The reason for the increased torque at low engine speed is increased time for scavenging, fuel evaporation, and air-fuel mixing. Low engine speed provides longer cycle times with more time for scavenging, resulting in more air through the head and less residual gas in the cylinder. Similarly, the longer cycles provide more time for fuel evaporation and air-fuel mixing. At higher engine speeds less time for fuel evaporation and increased residual gas both lead to a slower flame speed.

Traditional two-stroke engines have a "convex" torque curve throughout their engine speed range [14]. Torque builds with an increase in engine speed to a maximum mid rpm range due to tuning and charging efficiency and then drops towards the upper engine speed limit. In the tests above, the novel engine has its highest torque at the lowest engine speed with torque decreasing as engine speed increases. This is a result of insufficient scavenging, evaporation, and air-fuel mixing. Better airflow mechanisms to promote scavenging and air-fuel mixing along with better injection techniques should be implemented in future designs.

In the current state of novel engine, it can be seen that increasing the fuel pulse width results in an increase in torque. As discussed later in section 5.2.4, the engine is running fuel rich with fuel pulse widths greater than 2.9 ms. Therefore, increasing the fuel just increases the amount of fuel participating in combustion. The data presented here identify how changing the fuel pulse width effects engine torque and, more importantly, at what conditions the engine makes the highest torque.

5.2.2 Platelet Response

This study compares the performance of three different sets of check valve platelets installed in the engine. The platelet properties are presented in section 4.1.1. Platelet set B was the original set used for the motoring tests and all original efforts to get the engine to run. Throughout testing the platelets were cracking and failing so new platelets had to be made. Set A was made from stainless steel. It was thought that the good high temperature properties of stainless steel would be desirable for this application. The stainless did hold up well for the limited testing done. The thinner platelets, set C, were available to the engine from the start but it was thought that they would be less robust than the others. As shown in Table 5.3, platelet set C performed the best out of the three different tests and proved to be as reliable as the others during the limited testing.

Table 5.3: Platelet comparison test conditions and results.

Property	Test 1	Test 2	Test 3
Test No.	143	67	118
Retaining Plate	Drilled	Drilled	Drilled
Platelet Set (mass in grams)	A (1.77)	B (1.36)	C (1.23)
Head Coolant Temp (°C)	95	97	95
Ambient Temp (°C)	21.0	16.6	20.4
Atmospheric Pressure (kPa abs.)	100.1	102.4	101.0
Intake Plenum Temp (°C)	59	49	42
Intake Plenum Pressure (kPa gauge)	61.1	48.0	51.4
Air Mass Flow (g/s)	24.0	31.2	30.5
Engine Speed (rpm)	1223	1245	1285
Fuel Pulse Width (ms)	5.5	5.5	5.5
Ignition Timing (bTDC)	15	15	15
Injection Timing (SOI bTDC)	120	120	120
IMEP (kPa)	252	390	549
COV in IMEP (%)	11.4	7.3	2.8

It can be seen that the lighter platelets, set C, resulted in the highest IMEP and the lowest COV in IMEP. Platelet set B followed and platelet set A produced the worse results. It was also noted at the time of the test that the heavy platelets did not perform well at any fuel setting ranging from 3.0 ms to 5.5 ms. The operation was unstable as indicated with the high COV in IMEP. Two reasons for the low IMEP are: mass of the platelet and increased dimensions of the platelet. The mass of the platelet would result in slower response time and later closing; therefore, less fresh air was retained in the cylinder and lower compression pressures resulted. This results in poor combustion and lower power output as seen in the IMEP results above. The second reason for the low IMEP could be the reduced curtain area in the check valve where the air flows into the cylinder. Since the platelets are thicker, the curtain area above the platelet decreases. The increased width and length of the platelet also reduces airflow area. Results show that platelet set A yields a reduction in airflow and an increase in intake pressure in comparison to the other platelet sets, likely due to the reduced curtain area and increased dimensions.

Figure 5.12 shows representative pressure traces for each platelet. It can be seen that for platelet set C, the intake valve noise starts earlier than the others indicating that the valves close earlier. This leads to higher compression pressures and better combustion. Also, notice that the noise ends earlier in the cycle for the light platelets. This either reflects that the lighter platelets produce less vibration or that the platelet requires less time to seat itself.

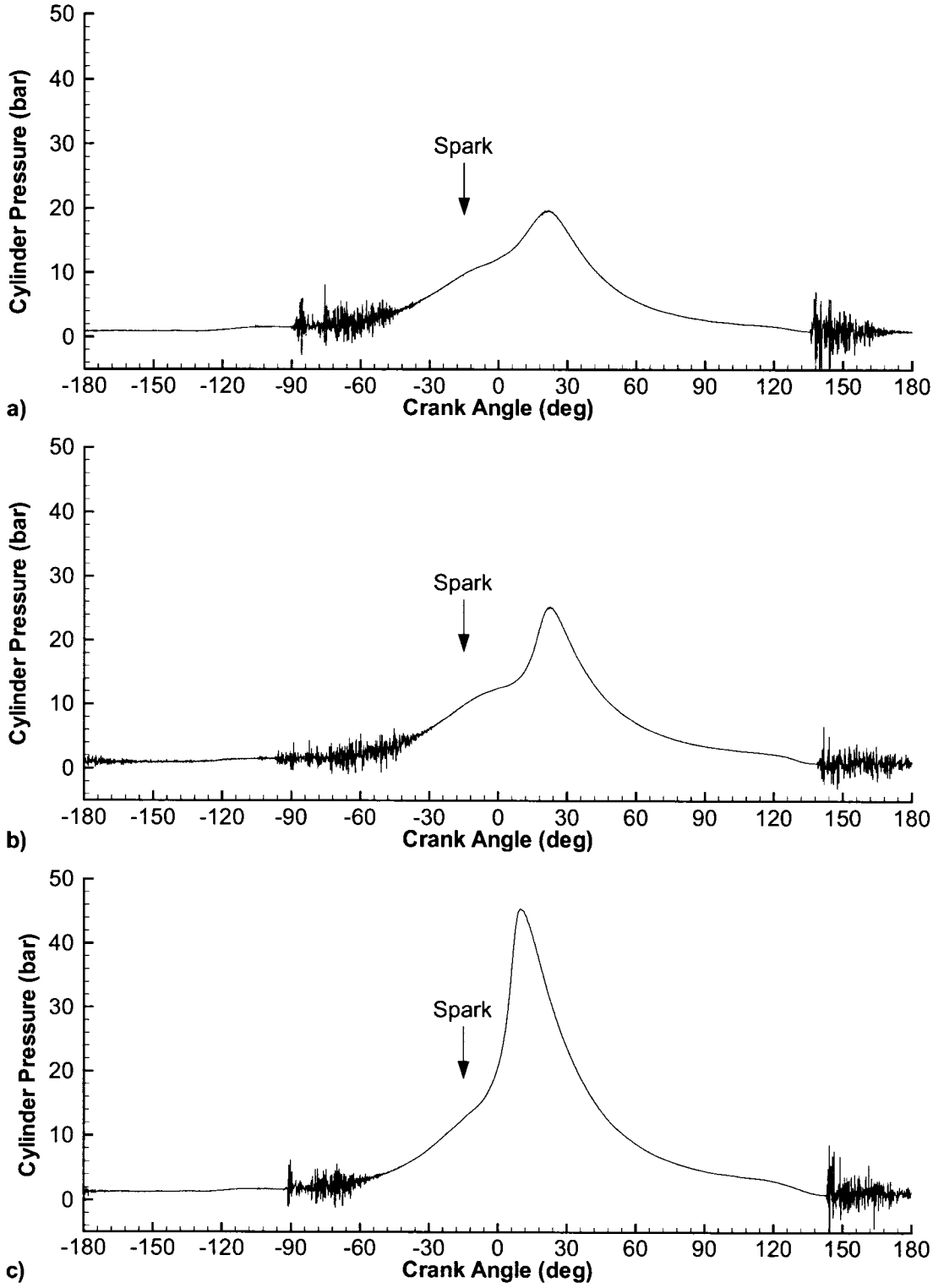

Figure 5.12: Representative cylinder pressure for each platelet set at 1250 rpm, 5.5 ms fuel pulse width, and ignition timing of 15° bTDC. a) Set A. b) Set B. c) Set C.

Figure 5.13 shows indicator diagrams for 15 cycles using platelet set A, the heavy platelets, and platelet set C, the light platelets. The differences in area contained within the pV curves show the COV in IMEP. It is clear that the lighter platelets provide a more repeatable combustion cycle and hence provide better performance.

The pressure peak location also indicates characteristics of the combustion event. Figure 5.14 shows that the pressure peaks for platelet set A are delayed in comparison to platelet set C. The delayed peaks are a result of slow flame speed caused by a high

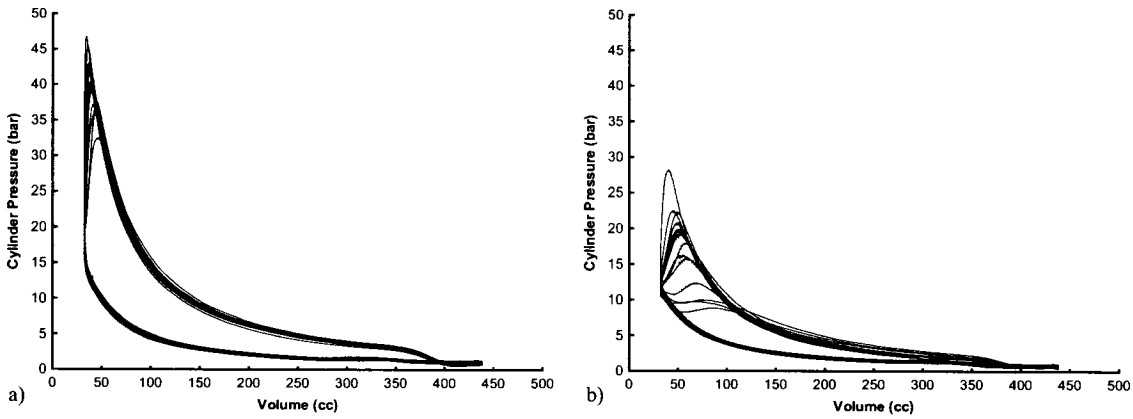

Figure 5.13: Indicator diagrams for 15 cycles at 1250 rpm and 5.5 ms fuel pulse width. a) Platelet set C with a COV in IMEP of 2.8%. b) Platelet set A with and COV in IMEP of 11.4%.

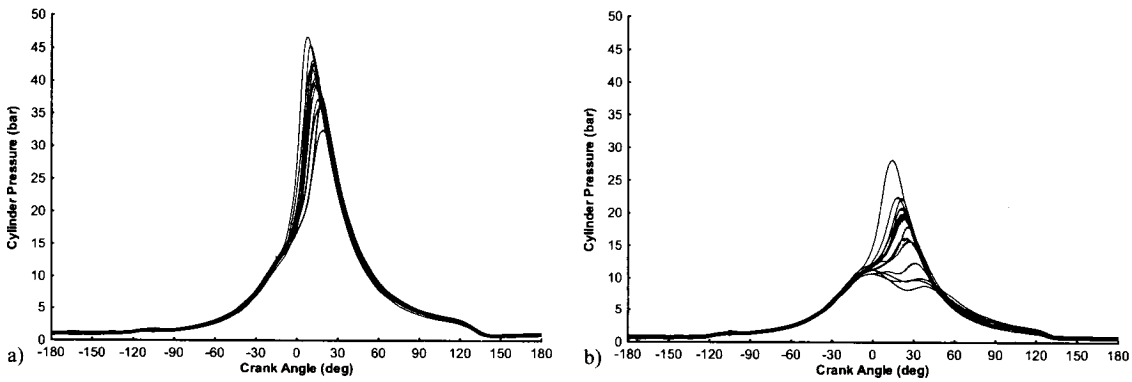

Figure 5.14: Pressure traces for 15 cycles 1250 rpm and 5.5 ms fuel pulse width. a) Platelet set C. b) Platelet set A.

amount of residual gas. This leads to partial burning, where the mixture still burns as the exhaust port opens. Clearly the heavy platelets result in poor scavenging and poor IMEP values. The light platelets, set C, provided a low COV in IMEP and increased IMEP indicating that a light robust platelet is required for optimal performance. The low COV does indicate that there is ample scavenging in the cylinder to cause a consistent cycle-to-cycle combustion.

5.2.3 Fuel Injection Timing

Fuel injection timing has a major impact on fuel evaporation, air-fuel mixing, and charge cooling. For the following data set, fuel injection timing was adjusted and the corresponding engine performance was recorded. It was decided to set the SOI at 120° bTDC, where the exhaust ports are fully closed, to eliminate the possibility of fuel short-circuiting. There was a hesitation to start the injection that early because the intake valves had not closed yet. Any reverse airflow through the valves might have taken some fuel into the intake causing backfiring in the intake. This did not prove to be a problem but for safety, the blower was left on for a short time after shut down to clear any fuel that might have entered the intake. For GDI it is desirable to inject fuel during the time when the intake valves are open so that the charge cooling effect by the evaporation of the fuel can take place and allow more air mass into the cylinder.

Injection timing was set at 120° bTDC initially and increased in 10° steps until the power dropped off. The engine operating conditions and results are presented in Table 5.4 while Figure 5.15 graphically shows the resulting engine performance for each SOI.

Table 5.4: Fuel injection timing test conditions and results.

Property	Test 1	Test 2	Test 3	Test 4
Test No.	67	68	69	71
Retaining Plate	Drilled	Drilled	Drilled	Drilled
Platelet Set	B	B	B	B
Head Coolant Temp (°C)	97	96	97	97
Ambient Temperature (°C)	16.6	16.0	16.6	16.0
Atmospheric Pressure (kPa abs.)	102.4	102.4	102.4	102.4
Intake Plenum Temp (°C)	49	48	49	48
Intake Plenum Pressure (kPa gauge)	48.0	47.6	47.3	47.3
Engine Speed (rpm)	1245	1292	1239	1295
Fuel Pulse Width (ms)	5.5	5.5	5.5	5.5
Ignition Timing (bTDC)	15	15	15	15
Start of Injection (bTDC)	120	110	100	90
End of Injection (bTDC)	79	67	59	47
Mass Air Flow (g/s)	31.3	31.5	31.4	31.6
IMEP (kPa)	390	383	372	288
COV in IMEP (%)	7.3	9.9	5.5	47.7

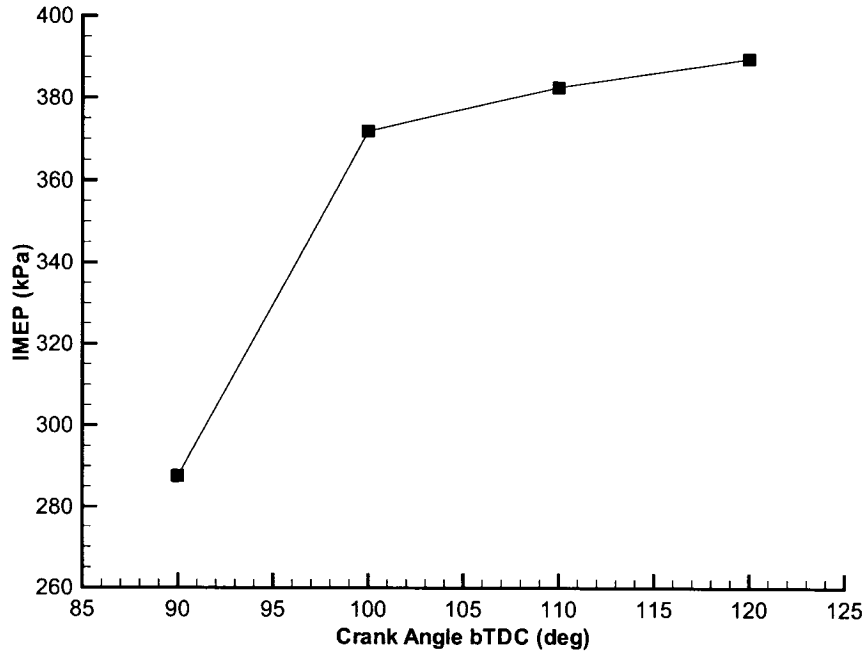

Figure 5.15: Effect of Start of Injection on IMEP.

All four tests were performed at a constant engine speed so that the scavenging was consistent for each test. It can be seen that the IMEP drops significantly between 100° and 90° bTDC indicating that there is insufficient fuel evaporation and air-fuel mixing below 100°. It is interesting to note that the IMEP only drops 5% from 120° to 100° and then falls by 26% from 120° to 90° injection timing. The data indicates that the injection timing only becomes sensitive below a SOI of 100° bTDC, or more importantly at an EOI of 59° bTDC. For interest sake, the critical evaporation and mixing times are as follows: at a SOI of 100° there is 11.3 ms until ignition and at EOI there is 5.8 ms. As a visual guide, Figure 5.16 and Figure 5.17 are presented to compare the injection timing for one cycle at a SOI of 120° bTDC and 90° bTDC respectively.

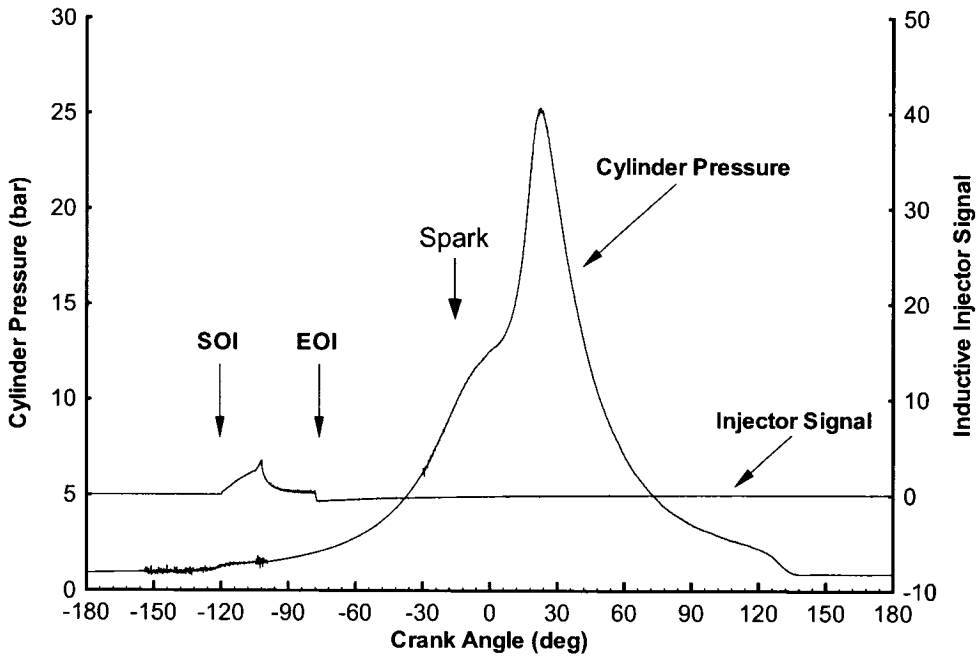

Figure 5.16: Injector signal and filtered cylinder pressure for one cycle with a SOI of 120° bTDC.

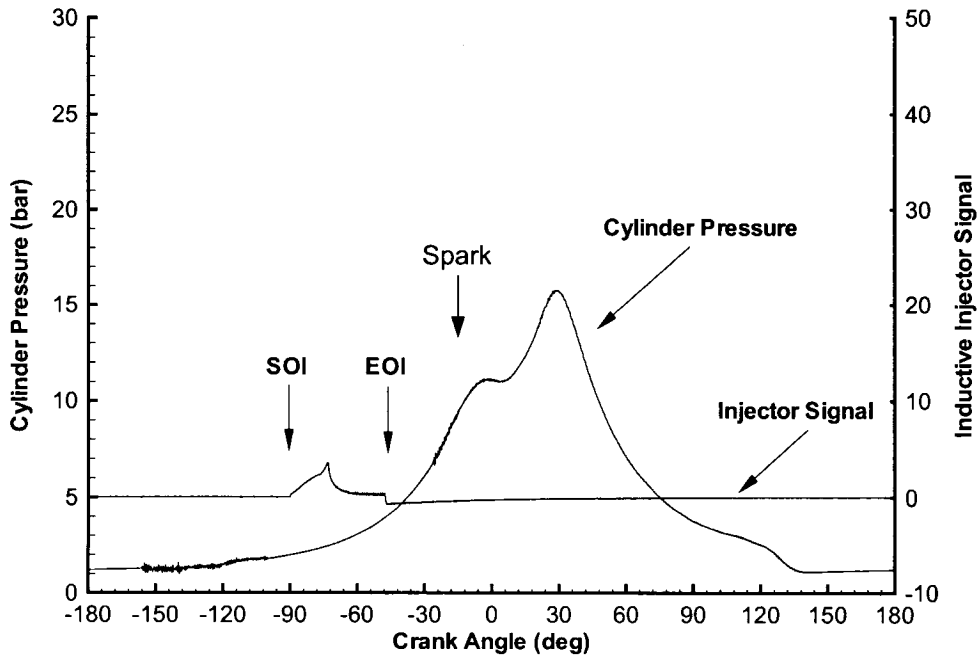

Figure 5.17: Injector signal and filtered cylinder pressure for one cycle with a SOI of 90° bTDC.

Location of the injection, i.e. SOI and EOI, can affect the following important air-fuel mixing parameters: time available for mixing, spray formation, spray impingement on the piston or cylinder walls, and charge cooling effect. All of these parameters change when the injection timing changes and either promotes evaporation and mixing or inhibits it. Another important aspect of setting the injection timing is phasing it properly with the air movement in the cylinder. For the engine under study, the air enters the top and flows down towards the exhaust ports during scavenging and then stops when the piston covers the exhaust ports. At this point, where injection begins for the earliest case, it is unknown as to the nature of the flow field and turbulence inside the cylinder. A discussion regarding some of these parameters is presented below in an effort to understand the results presented above and to provide some recommendations for improving performance.

Assuming a constant fuel pulse width like in these tests, start of injection determines the time that the fuel has to mix with the air. A later SOI results in less time between EOI and ignition, and the opposite for an earlier SOI. Based on this simple fact, it seems that earlier injection times are favoured so that the fuel has a longer time to fully evaporate and mix with the air in order to provide a homogeneous mixture. Other factors come in to play that make this not so obvious.

Changing the SOI, and with it EOI, can also affect the back pressure on the injector and hence affect the spray pattern. It can be seen in Figure 5.16 that at SOI the pressure is 1.2 bar while at EOI the cylinder pressure is about 2 bar giving an average ambient back pressure of about 1.6 bar. In comparison, in Figure 5.17 the injection starts when the cylinder pressure is at about 2 bar and EOI is at about 4 bar yielding an average ambient back pressure of about 3 bar. Generally, ambient back pressure will increase under these circumstances: moving SOI closer to TDC for a constant pulse width, increasing fuel pulse width with a constant SOI, and increasing engine speed. This is because the injector is open longer into the compression stroke. As discussed in the literature review, a difference in ambient back pressure can alter injection characteristics and spray pattern by narrowing the spray cone. A positive effect from increased back pressure is that as the charge is compressed, an associated temperature rise occurs that can increase the evaporation rate [21].

Another parameter related to injection timing is spray impingement on the piston, or piston wetting. In normal GDI four-stroke engines an effort is made so that the injection occurs to minimize piston wetting; injections are usually between 90^{o} and 180^{o} aTDC on the intake stroke so that the fuel spray closely follows the piston down to BDC

without hitting it. This cannot happen for two-stroke engines as the piston is on its way up during injection.

After disassembly of the test engine, it was clear that high levels of fuel impingement on the piston had occurred as shown in Figure 5.18. The piston was clean in the trajectory of the injection spray and a carbon film was present around it. It appeared as if the fuel spray had been impacting the piston directly as a high speed jet. This leads to wetting of the piston and creates a fuel film that provides rich mixture close to the piston decaying the homogeneity of the mixture. In fact, the fuel film can burn as a "pool fire" as opposed to the desired premixed flame if the conditions are right [21]. Some evaporation does occur when fuel hits the hot piston, but with extreme piston wetting, as is the case here, it is detrimental to engine performance. Therefore, special care should be taken so that piston wetting is minimized.

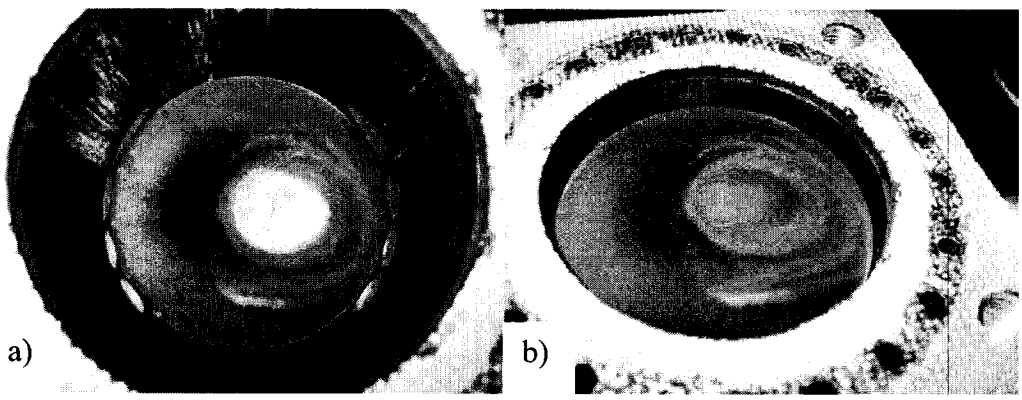

Figure 5.18: Piston within cylinder after dissasembly; a) Shiny part indicates where the injector spray impacts the piston as a high force jet; b) Another view showing the carbon deposits.

As discussed in section 2.7, charge cooling can be achieved if injection occurs when the intake valves are open. From the example above, injection timing is set at 120° bTDC and intake valve closing is at 97° bTDC. Therefore, there is some charge cooling effect since the intake valves are open for about 20° of the injection duration.

For this engine, the data indicates that 120° bTDC is a good choice for injection timing since it results in the highest IMEP and, since the fuel pulse width is constant, ISFC as well.

5.2.4 Fuel Consumption

It is desirable to have low indicated specific fuel consumption as it relates the fuel burned to the power output of the engine. The intent for this study was to see how fuel pulse width affected ISFC. Maintaining a constant engine speed will fix the scavenging properties so that the ISFC is a result of the evaporation and air-fuel mixing properties at each fuel pulse width.

Table 5.5 summarizes the operating conditions for the test session. The engine speed was set to 1500 rpm since lower fuel pulse widths were obtainable at that engine speed. The fuel pulse width was then slowly decreased to establish a working range. The lowest pulse width was 3.0 ms and anything less would cause the engine to stall. The upper range was capped at 5.5 ms since it was predicted that lower fuel pulse widths was of more interest at this time.

Figure 5.19 shows the ISFC consumption results from Table 5.5 where the engine speed was held at 1500 rpm. The lowest ISFC is 651 g/kW-h and occurs at a fuel pulse width of 3.0 ms. The ISFC trend is generally increasing with increasing fuel pulse width at a fixed engine speed.

Table 5.5: Fuel consumption test conditions and results.

Property	Test 1	Test 2	Test 3	Test 4
Test No.	167	174	161	160
Retaining Plate	Drilled	Drilled	Drilled	Drilled
Platelet Set	C	C	C	C
Head Coolant Temp (°C)	98	98	95	95
Ambient Temp (°C)	20.4	19.9	19.9	19.9
Atmospheric Pressure (kPa abs.)	102.2	102.2	102.2	102.2
Intake Plenum Temp (°C)	50	49	42	41
Intake Plenum Pressure (kPa gauge)	48.9	48.0	50.2	50.4
Engine Speed (rpm)	1515	1484	1521	1510
Fuel Pulse Width (ms)	3.0	3.5	4.5	5.5
Ignition Timing (bTDC)	30	30	20	20
Injection Timing (SOI bTDC)	120	120	120	120
Mass Air Flow (g/s)	31.1	31.4	30.8	30.8
Delivery Ratio	2.55	2.58	2.49	2.51
Equivalence Ratio	1.08	1.25	1.57	1.92
IMEP (kPa)	370	376	502	523
COV in IMEP (%)	8.2	3.3	2.7	4.5
ISFC (g/kW-h)	651	744	716	840

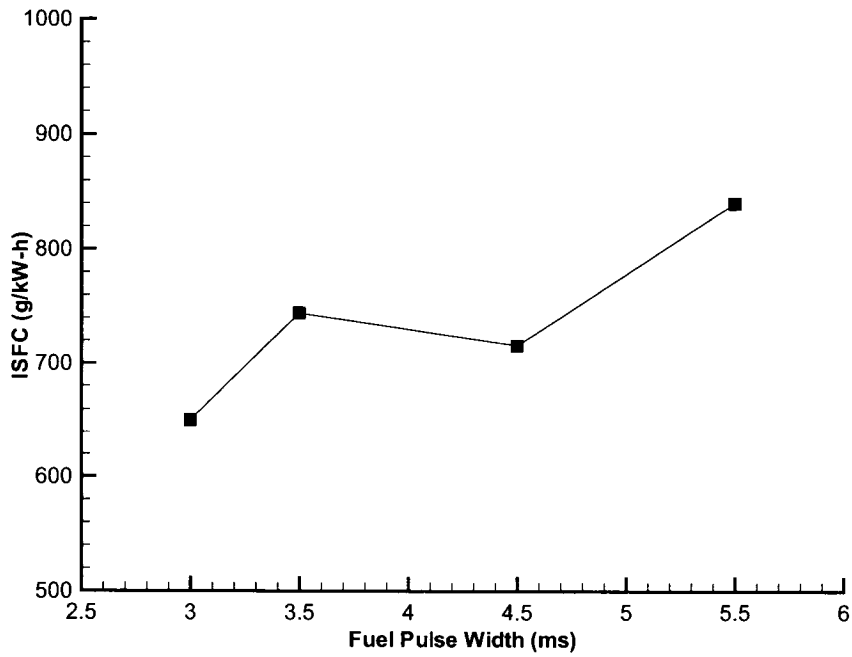

Figure 5.19: ISFC as a function of fuel pulse width at 1500 rpm.

The data clearly indicate that for the additional fuel added there is a marginal return in power. This is expected since the fuel injected far exceeds the stoichiometric requirements for a fully scavenged cylinder volume. Increasing the fuel injected just "floods" the cylinder. Smoke in the exhaust and soot deposits on the exhaust pipes indicated that the engine was running rich. The resulting data just indicates how rich the engine was running. If fuel evaporation and air-fuel mixing was improved, the trend indicates that better ISFC values could be obtained at lower fuel pulse widths.

For all tests presented here, the effort was to fully scavenge the cylinder and maximize power. For the ideal case where the engine scavenges the trapped cylinder of 337 cc of air, the fuel pulse width required for a stoichiometric air-fuel mixture is about 2.9 ms. This is calculated using the intake temperature and cylinder pressure when the exhaust ports close. It also assumes a homogeneous mixture with a stoichiometric air-fuel ratio. In reality the required fuel pulse width will be lower since there is always some residual gas. The fact that the engine stalls at fuel pulse widths lower than 3.0 ms indicates that air-fuel mixture preparation improvements are required.

Piston wetting is an issue with this engine as shown in section 5.2.3. This prevents all of the fuel injected from evaporating and taking part in combustion, leading to higher ISFC. A proper fuel spray design that avoids piston wetting would have enough time to fully evaporate at these engine speeds and injection pressures. Poor scavenging could also cause high ISFC since an increase in residual gas results in less power. An inconsistent air-fuel mixture throughout the cylinder could lead to a slow flame speed that reduces power and increases ISFC.

The minimum ISFC value from this novel engine in the current state is well above engines of similar size. Typical BSFC values for small-bore carbureted SI two-stroke engines range from 240-400 g/kW-h and by approximating a mechanical efficiency of 0.75, that converts to an ISFC range of 180-300 g/kW-h. With a minimum ISFC for the novel engine of 651 g/kW-h, this is about double the ISFC for typical engines. A direct comparison is hard since operating conditions are different, but these high initial values indicate that improvements to scavenging, fuel evaporation and air-fuel mixing must be made.

5.2.5 Engine Performance

This final results section presents data from the test session that gave the best performance. The operating conditions and results are summarized in Table 5.6. Higher fuel pulse widths would produce higher torque and power outputs as predicted in section 5.2.1, however, it was decided to use 5.5 ms since any additional fuel would be wasteful, see the ISFC trend in section 5.2.4.

The pressure traces from the four tests described in Table 5.6 are shown in Figure 5.20 through Figure 5.23. Each graph consists of 15 pressure traces from consecutive cycles. It can be seen that the pressure peaks all occur in the range of 10° aTDC to 27° aTDC. The location of peak pressure indicates how the mixture is burning; improper ignition timing or slow flame speed can cause late peaks. From Table 5.6, the average peak pressure occurs at 16° aTDC for all tests except for the 1250 rpm test, where the peak occurs at 21° aTDC. For typical SI engines, peak cylinder pressure occurs at about 16° aTDC with optimum timing [11]. Three out of the four tests agree with this. The late

peak recorded for the 1250 rpm test indicates that the spark timing could be advanced more.

Table 5.6: Results from best performing test session.

Property	Test 1	Test 2	Test 3	Test 4
Test No.	117	125	133	130
Retaining Plate	Drilled	Drilled	Drilled	Drilled
Platelet Set	C	C	C	C
Head Coolant Temp (°C)	97	96	98	98
Ambient Temperature (°C)	21.0	21.6	21.6	21.0
Atmospheric Pressure (kPa)	101.0	101.0	101.0	101.0
Intake Plenum Temp (°C)	42	44	50	51
Intake Plenum Pressure (kPa gauge)	52.5	51.7	52.0	53.8
Engine Speed (rpm)	1267	1528	1755	2039
Fuel Pulse Width (ms)	5.5	5.5	5.5	5.5
Ignition Timing (bTDC)	10	20	20	25
Injection Timing (SOI bTDC)	120	120	120	120
Air Mass Flow (g/s)	30.5	30.6	30.9	30.6
Delivery Ratio	2.96	2.48	2.18	1.86
Brake Torque (N-m)*	34.4	31.3	32.0	28.7
Brake Power (kW)*	4.5	5.0	5.9	6.1
Indicated Torque (N-m)	36.9	33.0	33.1	30.3
Indicated Power (kW)	4.9	5.3	6.1	6.5
Indicated Power density (kW/L)	12.1	13.0	15.0	16.0
IMEP (kPa)	570	510	511	469
ISFC (g/kW-h)	771	861	859	940
COV in IMEP (%)	2.9	2.7	2.9	5.9
Indicated Fuel Conversion Efficiency (%)	11	10	10	9
Average peak pressure location (deg aTDC)	21	16	16	16
Intake valve closed (deg bTDC)	92	89	89	87
Intake valve open (deg aTDC)	144	148	148	148

* Brake torque and power were not corrected for humidity as done within the automotive industry according to SAE standard SAE J1349.

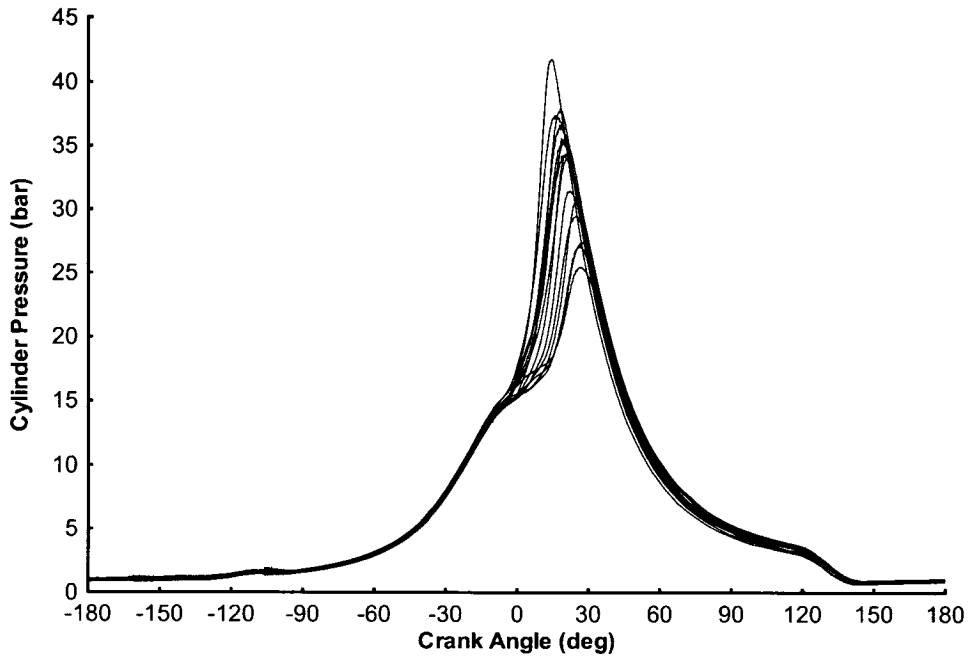

Figure 5.20: Pressure trace for 15 cycles at 1250 rpm and 5.5 ms fuel pulse width.

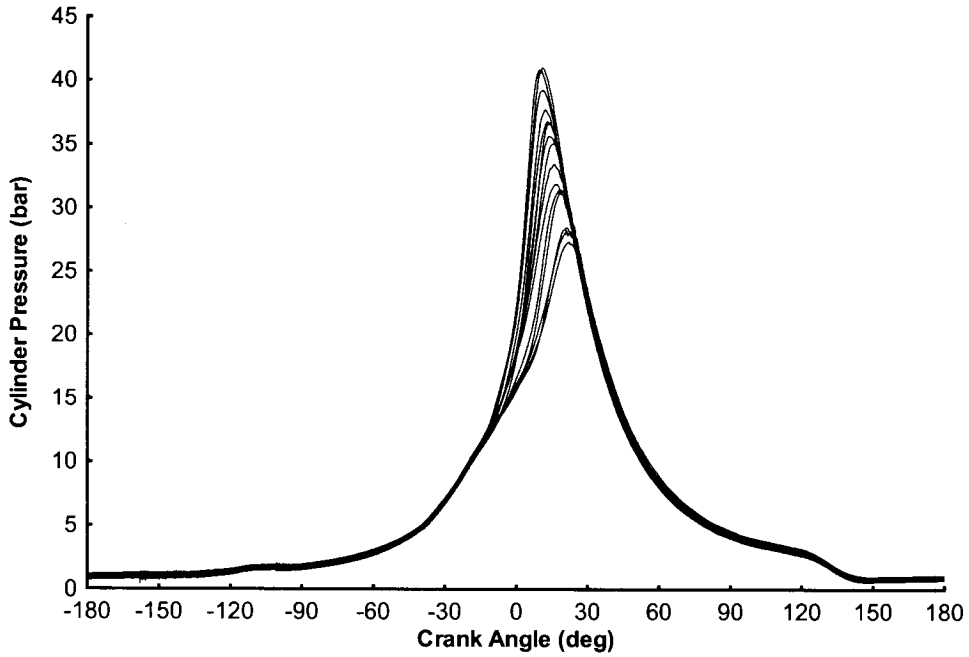

Figure 5.21: Pressure trace for 15 cycles at 1500 rpm and 5.5 ms fuel pulse width.

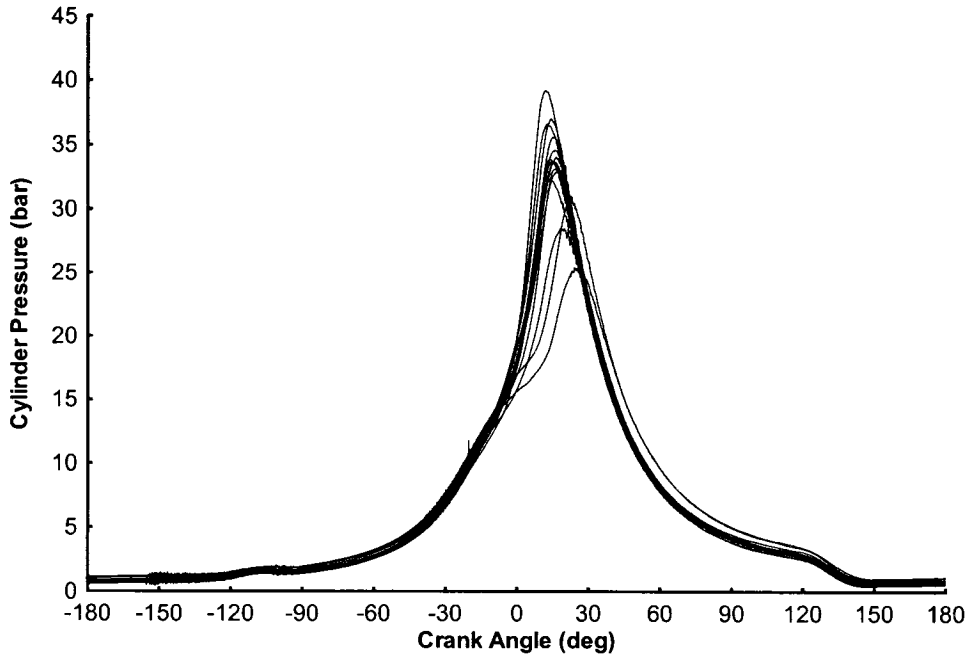

Figure 5.22: Pressure trace for 15 cycles at 1750 rpm and 5.5 ms fuel pulse width.

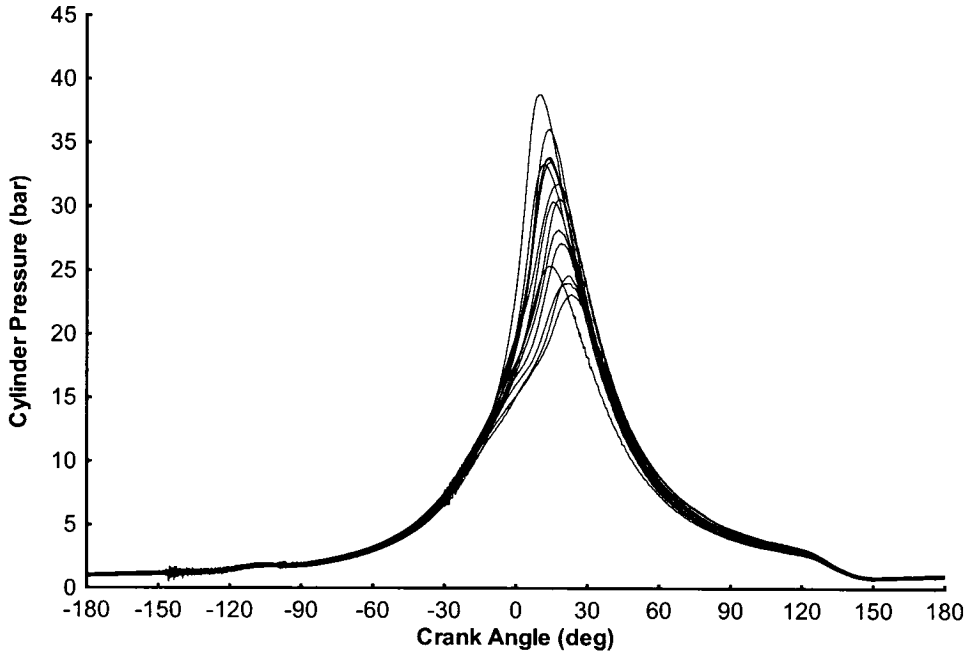

Figure 5.23: Pressure trace for 15 cycles at 2000 rpm and 5.5 ms fuel pulse width.

The indicated torque and power as a function of engine speed are shown in Figure 5.24. At a constant fuel pulse width of 5.5 ms, the maximum indicated torque is 36.9 N-

m at 1270 rpm while the maximum power is 6.5 kW at 2040 rpm. These values were obtained using the lighter platelets, set C, and the drilled retaining plate. The indicated torque decreases with increasing engine speed while the indicated power increases with increasing engine speed.

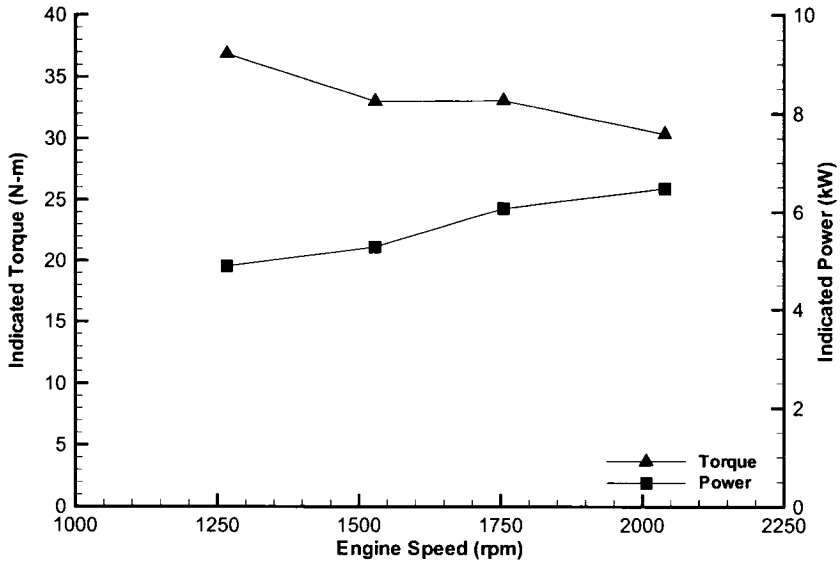

Figure 5.24: Indicated Torque and Power versus engine speed at 5.5ms pulse width.

The IMEP and ISFC results are shown in Figure 5.25. Naturally, the IMEP follows the same trend as the indicated torque. A maximum IMEP of 570 kPa was achieved at 1270 rpm. A minimum ISFC of 771 g/kW-h was obtained at 1270 rpm for this test session. Note that better ISFC values were reported in section 5.2.4.

The ISFC increases with increasing engine speed at a fixed fuel pulse width of 5.5 ms. This means that the returns in power for the fuel added are diminishing. This test differs with the ISFC test presented in section 5.2.4 since the engine speed is increasing while the fuel pulse width is held constant at 5.5 ms. Now scavenging has an affect on the results since it is dependent on engine speed. The data do not follow the typical two-stroke engine ISFC trends. ISFC usually decreases with increasing engine speed since

there is more time for heat transfer to the cylinder walls at lower engine speed. The increase in ISFC with engine speed for the novel engine is a result of decreasing torque with increasing engine speed.

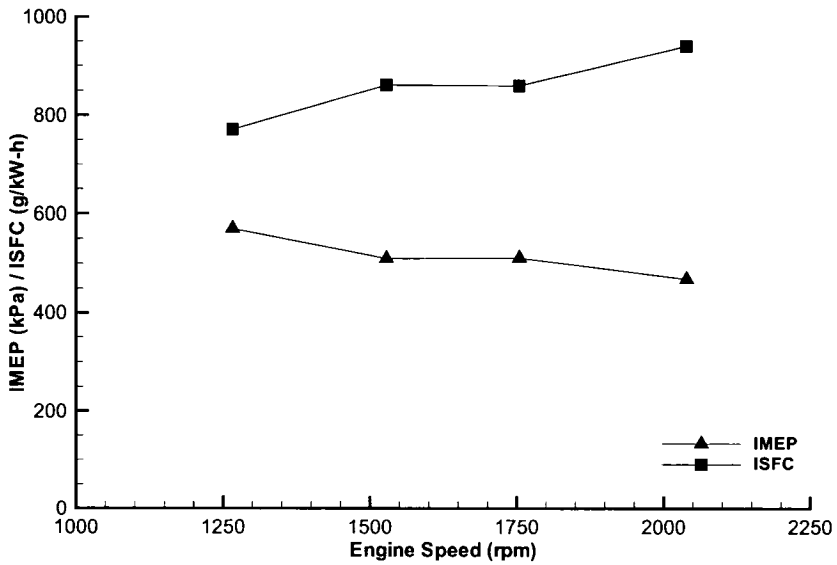

Figure 5.25: IMEP and ISFC in verses engine speed at 5.5 ms pulse width.

The trend seen for the current test is the result of individual factors that affect the work produced per cycle. As such, it is difficult to quantify the contribution from each factor. The following list describes each individual factor relating to the trend:

- Higher engine speeds reduce scavenging time and lead to higher amounts of residual gas in the mixture. The delivery ratio trend reflects this as less air is delivered to the engine with increasing engine speed. Despite the fact that the delivery ratio is greater than unity, some of this air could short-circuit through the exhaust ports without removing the combustion products. Higher amounts of residual gas mean there is less air to mix with the fuel and less torque is produced. Increased residual gas also reduces flame speed leading to slow combustion and reduced torque.

- Platelets close later in the cycle with increasing engine speed. For example, the platelets close at 92° bTDC at 1250 rpm and 87° bTDC at 2000 rpm. This could allow more reverse flow through the check valves and reduced charge volume.
- Increasing engine speed will reduce the time available for evaporation and air-fuel mixing. Therefore less combustible air-fuel mixture is available at ignition resulting in lower torque.
- Any adverse mixing effects caused by the relatively longer injection event, due to an increase in engine speed, may also affect evaporation, e.g. injection ends at 79° bTDC at 1250 rpm and 54° bTDC at 2000 rpm. Piston wetting may increase since the piston is closer to TDC at the end of injection for higher engine speeds. Higher ambient pressure could increase evaporation due to higher temperatures but it could also cause an increase in SMD leading to a reduction in evaporation.
- Turbulence in the cylinder increases as a function of piston speed. Therefore, increasing engine speed may increase air-fuel mixing and flame speed somewhat.

5.2.6 Engine Comparison

The mean effective pressure for different engines can be compared since it is independent of displacement. Usually the BMEP at peak torque is reported for an engine because it reflects the maximum work available at the crankshaft, opposed to the IMEP that only reflects the available work due to combustion. Unfortunately for this investigation only the IMEP can be used and compared since the brake values do not reflect the power required by the compressor. Despite this, an attempt to compare the novel engine IMEP values with other engines can be done using the BMEP and mechanical efficiency. A discussion regarding the required compressor power is given in Appendix E.

The Orbital 1.2 litre forced induction direct injection two-stroke engine, an engine similar to the engine discussed in chapter Chapter 3, is one of the most advanced two-stroke engines with a maximum BMEP of 785kPa [12]. If a typical mechanical efficiency of 0.75 is assumed, the resulting IMEP is about 1050 kPa. Some typical production small-bore carburetted two-stroke engines have BMEP in the 660 kPa range and assuming the same mechanical efficiency as above, this results in an IMEP of about 880 kPa. Both of these engines produce a higher IMEP compared to the IMEP of 570 kPa found for the novel engine. In fact the IMEP of the Orbital engine is almost 84% higher than the experimental engine while typical carburetted engines are about 54% higher.

The indicated fuel conversion efficiencies are reported in Table 5.6. The fuel conversion efficiency considers all of the energy available from the fuel, when in reality only a certain percentage of the fuel energy was released during combustion. The indicated thermal efficiency takes this fact into consideration but is not presented here since the combustion efficiency was not measured.

Some SI indicated thermal efficiencies can be around 50-60% [17]. Combining a combustion efficiency of 95% results in a fuel conversion efficiency of about 52%. The values for the novel engine average at about 10%, which is a fraction of some SI engine values. Based on the calculations in section 5.2.4, the novel engine was operating with excess fuel. A certain percentage of this fuel does not evaporate and burn due to piston wetting. This is the main cause for the low fuel conversion efficiencies. If there is a fuel rich mixture in the cylinder, combustion efficiency drops significantly as shown in

section 2.4. This would also lead to low fuel conversion efficiencies. Unfortunately excess fuel is needed to operate the engine at low engine speeds with the current set up.

Chapter 6 Conclusions and Recommendations

The objective of this project was met as the performance characteristics of this engine in its current state have been measured and reported. The novel head design does work and provides the two-stroke engine with an asymmetrical intake valve timing that is advantageous. The engine in its current state is considered a first prototype tested to prove that the novel passive scavenging method works. With a specific stratified and/or homogeneous GDI strategy, this engine has the potential to produce results better than reported here.

The following conclusions can be made based on the results:

- Platelets close later in the cycle with increasing engine speed, indicating that the platelets have a finite closing time. This limits the engine speed range.
- It is clear that reducing the mass and dimensions of the platelet increases engine performance. There is a limit to this finding since the platelet must be robust enough for the high pressure and high temperature combustion environment it is directly exposed to.
- The engine performed better with earlier fuel injection timing. This increased the time available for fuel evaporation and air-fuel mixing.
- At 1500 rpm the engine would not run at a pulse width lower than 3.0 ms. The stoichiometric fuel pulse width is roughly 2.9 ms, assuming a fully scavenged cylinder, an air-fuel ratio of 14, and an air density in the cylinder based on conditions when the exhaust ports are closed. This indicates that the engine is running fuel rich for all tests.

- The minimum ISFC obtained was 651 g/kW-h at 3.0 ms fuel pulse width and 1515 rpm. ISFC increases for increasing fuel pulse width, from 3.0 ms to 5.5 ms, at a constant engine speed of 1500 rpm.
- For a fuel pulse width of 5.5 ms, the maximum IMEP was 570 kPa at 1270 rpm, the maximum indicated torque was 36.9 N-m at 1270 rpm, and the maximum indicated power was 6.5 kW at 2040 rpm. The nominal engine speeds tested were 1250, 1500, 1750, and 2000 rpm.

All of the values calculated in the results are dependent on the work produced per cycle. The relatively poor performance results are a result of poor scavenging, fuel evaporation, fuel air-fuel mixing. To improve performance, design changes are required. From inspection of the valve layout, piston, and combustion chamber design, an absence of swirl, tumble, and squish within the cylinder during scavenging and compression prevented proper mixture preparation. As discussed in the literature review, swirl, squish, and tumble lead to increased turbulence during compression that increases evaporation, air-fuel mixing, and flame speed. Any air-fuel mixing results from residual airflow from the scavenging stage, piston induced turbulence, and the fuel jet itself. A poor combustion chamber exists in the current engine since the piston crown is convex. Any inherent squish would force the mixture away from the spark plug. Piston wetting also increases fuel consumption and must be minimized. The results indicate that there is in fact some mechanism for evaporation and mixing due to the simple fact that the engine runs.

The objective of this project was to run the engine in homogeneous mode since the cylinder was not suited to prepare a stratified mixture. For future designs catered to a

variable load engine, a wall guided, spray guided, or air guided stratified charge GDI system should be used, as described in section 2.7. The strategy will dictate the injector type, airflow regime, and piston design. The use of different platelets and directed valves could induce a specific flow field catering to one of the three GDI strategies.

With the results indicating better performance at lower speeds, and the platelet closing taking less crank angle at lower speeds, the head design may be suitable for a low speed diesel engine. Diesel engines can achieve higher thermal efficiencies and better specific fuel consumption than gasoline engines. The design challenge for this type of engine lies in the robustness of the platelets, since diesel peak cylinder pressures are considerably higher than gasoline engines.

References

[1] H.-A. Ohlmann, "Air and Exhaust Management System for a Two Cycle Internal Combustion Engine," U.S. Patent No. 6170444, 1998.

[2] D. Rival and G. Ciccarelli, "Numerical Investigation into Scavenging Efficiency of a Prototypical Two-Stroke Engine," presented at The Combustion Institute Canadian Section: Spring Technical Meeting, 2005.

[3] D. Ohlmann and G. Ciccarelli, "Development of a Novel Uniflow-Scavenged Two-Stroke GDI Engine," presented at The Combustion Institute Canadian Section: Spring Technical Meeting, 2005.

[4] D. Rival and G. Ciccarelli, "Evaluation of Scavenging Performance in a Novel Two-Stroke GDI Engine," SAE Paper 2006-01-0446, 2006

[5] D. Ohlmann, S. Reynolds, and G. Ciccarelli, "Development of a Novel Uniflow-Scavenged Two-Stroke GDI Engine," SAE Paper 2006-01-0187, 2006

[6] S. Reynolds and G. Ciccarelli, "Investigation of Intake Airflow for a Novel Uniflow-Scavenged Two-Stroke GDI Engine," presented at The Combustion Institute Canadian Section: Spring Technical Meeting, 2006.

[7] P. Oliver, "Numerical Investigation of a Scavenging Flow in a Uniflow-Scavenged Two-Stroke Engine," presented at The Combustion Institute Canadian Section: Spring Technical Meeting, 2006.

[8] D. Rival, "Numerical and Experimental Investigation of the Scavenging Flow in a Novel Two-Stroke Engine," M.Sc. thesis, Queen's University, Kingston, December 2005.

[9] D. Ohlmann, "Development of a Novel Uniflow-Scavenged Two-Stroke GDI Engine," M.Sc. thesis, Queen's University, Kingston, December 2006.

[10] Bosch, *Gasoline-Engine Management*, First ed. Stuttgart: Robert Bosch GmbH, 1999.

[11] J. B. Heywood, *Internal Combustion Engine Fundamentals*. New York: McGraw-Hill, 1988.

[12] J. B. Heywood and E. Sher, *The Two-Stroke Cycle Engine: Its Development, Operation, and Design*. Warrendale: SAE, 1999.

[13] C. R. Ferguson and A. T. Kirkpatrick, *Internal Combustion Engines*, Second ed. New Jersey: John Wiley & Sons, Inc., 2001.

[14] E. Sher, "Scavenging the Two-Stroke Engine," *Progress in Energy and Combustion Science*, vol. 16, pp. 95-124, 1990.

[15] GM, *Three, Four, and Six Cylinder Series 71 Two-Cycle Diesel Engines Maintenance Manual Revised.* Detroit: Detroit Diesel Engine Division of General Motors Corporation, 1947.

[16] H. R. Ricardo and J. G. G. Hempson, *The High-Speed Internal-Combustion Engine*, Fifth ed. London: Blackie & Son Limited, 1968.

[17] W. W. Pulkrabek, *Engineering Fundamentals of the Internal Combustion Engine.* New Jersey: Prentice-Hall, 1997.

[18] M. Metghalchi and J. C. Keck, "Laminar Burning Velocity of Propane-Air Mixtures at High Temperature and Pressure," *Combustion and Flame*, vol. 38, pp. 143-154, 1980.

[19] M. Metghalchi and J. C. Keck, "Burning Velocities of Mixtures of Air with Methanol, Iso-octane, and Indolene at High Pressure and Temperature," *Combustion and Flame*, vol. 48, pp. 191-210, 1982.

[20] D. B. Rhodes and J. C. Keck, "Laminar Burning Speed Measurements of Indolene-Air-Diluent Mixtures at High Pressures and Temperature," SAE Paper 850047, 1985

[21] F. Zhao, D. L. Harrington, and M. C. Lai, *Automotive Gasoline Direct-Injection Engines*. Warrendale: SAE, 2002.

[22] Y. Takagi, T. Itoh, A. Iiyama, and S. Muranaka, "Combustion Chracteristics of a Direct-Injection Stratafied Charge S.I. Engine," *JSAE Review*, vol. 19, pp. 217-222, 1998.

[23] T. Kume, Y. Iwamoto, K. Iida, M. Murakami, K. Akishino, and H. Ando, "Combustion Control Technologies for Direct Injection SI Engine," SAE Paper 960600, 1996

[24] A. M. Lippert, S. H. El Tahry, M. S. Huebler, S. E. Parrish, H. Inoue, K. Noyori, K. Nakama, and T. Abe, "Development and Optimization of a Small-Displacement Spark-Ignition Direct-Injection Engine - Stratified Operation," SAE Paper 2004-01-0033, 2004

[25] X. Wang, J. Gao, D. Jiang, Z. Huang, and W. Chen, "Spray Characteristics of High-Pressure Swirl Injector Fueled with Methanol and Ethanol," *Energy & Fuels*, vol. 19, pp. 2394-2401, 2005.

[26] Bosch, "Gasoline Direct Injection," Information CD ROM, 2001.

[27] "Technology - Gasoline Direct Injection Engine," http://www.mitsubishi-motors.co.jp/inter/technology/GDI/page1.html, Accessed April 4, 2005.

[28] "Direct Injection - Gasoline, Improving Fuel Economy through Lean Combustion," www.gmpowertrain.com, Accessed April 4, 2005.

[29] F. A. Wyczalek, "Two-Stroke Engine Technology in the 1990's," SAE Paper 910663, 1991

[30] H. R. Ricardo, *The Internal Combustion Engine: Volume 1, Slow-Speed Engines*, vol. 1: Blackie & Son Limited, 1922.

[31] "Evinrude E-TEC Specifications," http://www.evinrude.com/en-US/, Accessed April 12, 2007.

[32] S. Strauss, Y. Zeng, and D. T. Montgomery, "Optimization of E-TEC™ Combustion System for Direct-Injected Two-Stroke Engines Toward 3-Star Emissions," SAE Paper 2003-32-0007, 2003

[33] "Yamaha Outboards," http://www.yamaha-motor.com/outboard/products/lifestylehome/home.aspx, Accessed April 12, 2007.

[34] "Honda Marine BF200 Specifications," http://www.honda-marine.com/modelDetail.aspx?modelGroup=BF200, Accessed April 12, 2007.

[35] D. Shawcross, C. Pumphrey, and D. Arnall, "A Five-million Kilometre, 100-Vehicle Fleet Trial, of an Air-Assist Direct Fuel Injected, Automotive 2-Stroke Engine," SAE Paper 2000-01-0898, 2000

[36] D. Blundell, J. Turner, P. Duret, J. Lavy, J. Oscarsson, G. Emanuelsson, J. Bengtsson, T. Hammarstrom, M. Perotti, R. Kenny, and G. Cunningham, "Design and Evaluation of the ELEVATE Two-Stroke Automotive Engine," SAE Paper 2003-01-0403, 2003

[37] D. Thornhill and R. Fleck, "Design of a Blower Scavenged, Piston-ported, V6, Two-Stroke Automotive Engine," SAE Paper 930980, 1993

[38] K. J. Yoon, W. T. Kim, H. S. Shim, and G. W. Moon, "An Experimental Comparison Between Air-Assisted Injection System and High Pressure Injection System at 2-Stroke Engine," SAE Paper 950270, 1995

[39] Y. Moriyoshi, M. Arai, J. Katsuta, and K. Morikawa, "Performance Tests of Reverse Uniflow-Type Two-Stroke Gasoline DI Engine," SAE Paper 2004-32-0040, 2004

[40] M. Al-Hasan, "Effect of ethanol-unleaded gasoline blends on engine performance and exhaust emissions," *Energy Conversion and Management*, vol. 44, pp. 1547-1561, 2003.

[41] H. Bayraktar, "Experimental and theoretical investigation of using gasoline-ethanol blends in spark-ignition engines," *Renewable Energy*, vol. 30, pp. 1733-1747, 2005.

[42] A. A. Al-Farayedhi, A. M. Dawood, and P. Gandhidasan, "Experimental Investigation os SI Engine Performance Using Oxygenated Fuel," *Journal of Engineering for Gas Turbines and Power*, vol. 126, pp. 178-191, 2004.

[43] H. S. Yucesu, T. Topgul, C. Cinar, and M. Okur, "Effect of ethanol-gasoline blends on engine performance and exhaust emissions in different compression ratios," *Applied Thermal Engineering*, vol. 26, pp. 2272-2278, 2006.

[44] H. Xu, "Some Critical Technical Issues on the Steady Flow Testing of Cylinder Heads," SAE Paper 2001-01-1308, 2001

[45] B. J. Fleck, R. Fleck, R. J. Kee, and D. J. Thornhill, "The Evaluation of Discharge Coefficients in the Cylinders of High Performance Two-Stroke Engines," SAE Paper 2003-32-0029, 2003

[46] M. Tazerout, O. Le Corre, and S. Rousseau, "TDC Determination in IC Engines Based on the Thermodynamic Analysis of the Temperature-Entropy Diagram," SAE Paper 1999-01-1489, 1999

[47] T. G. Beckwith, R. D. Marangoni, and J. H. Lienhard V, *Mechnical Measurements*, Fifth ed. Reading: Addison-Wesley, 1995.

Appendices

Appendix A: ECU Specifications

General

Microprocessor 32 Bit 33 MHz with time Co-processor, Quality Standard ISO 9001, Manufacturing Standard IPC-S-815-A Class 3 High Reliability, Warranty 1 year Parts and Labor, Burn In -50 to 70 degrees for 32 hours, ECU Control Software stored in updateable FLASH memory, High RFI Immunity, Low heat generation, Battery transient protection, Environmentally sealed electronics, Waterproof connector with gold plated contacts, Case size 120 x 100 x 36 mm (4.7 x 3.9 x 1.4 inches), Weight 0.4 kg (14 oz), Cylinders 1,2,3,4,6,8,12, Engines 2 stroke, 4 stroke, Rotary (1-4), Odd or Even fire, Maximum RPM > 15,000 RPM.

Injection

4 group sequential, User programmable injector current 0.5-12 Amps peak, Battery Comp to suit any injector.

Fuel Calibration

Accuracy 0.00001 seconds, All RPM & Load sites are user programmable, Main Table (3D) 40 RPM sites x 21 Load sites (840 points), End of Injection (3D) 20 RPM sites x 11 Load sites, Overall Trim + 99%, Individual Cylinder Trim + 99%, Individual Cylinder Tables (3D) 20 RPM sites x 11 Load sites, Hi/Lo Injector Balance (3D) 20 RPM sites x 11 Load sites, Hi/Lo End of Injection (3D) 20 RPM sites x 11 Load sites, Engine Temperature and Air Temperature compensations, Two Auxiliary compensations, Injector Dead Time compensation, Accel Clamp, Decay and Sensitivity, Decel Clamp, Decay and Sensitivity, Cold Start.

Ignition Outputs

Up to 4 Ignition Outputs, One output may drive up to 8 coils using the MoTeC Ignition Expander, Versatile Ignition Interface allows connection to most OEM ignition systems including: Nissan Multi Coil modules, GM EST DFI systems, Ford EDIS DFI systems, Mazda Rotary DFI modules, Many Others.

Ignition Calibration

Accuracy 0.25 degrees, All RPM & Load sites are user programmable
Main Table (3D) 40 RPM sites x 21 Load sites (840 points), Overall Trim + 99%

Individual Cylinder Trim + 99%, Individual Cylinder Tables (3D) 20 RPM sites x 11 Load sites, Engine Temperature and Air Temperature compensations
MAP compensation, Two Auxiliary compensations, Dwell Time 20 RPM x 11 Battery sites, Odd fire engine capability Each Top Dead Center may be specified. Resolution 0.5 degree.

Boost Control Calibration

Main Table (3D) 20 RPM sites x 10 Throttle sites or 10 Gear sites, Overall Trim
Engine Temperature and Air Temperature compensations, One Auxiliary compensation.

Trigger Sensors

Directly compatible with most OEM trigger systems including: HALL, Magnetic and Optical types, Multi Tooth (e.g. Mazda and Toyota), 1 or 2 Missing Teeth (e.g. Porsche), Many other special types (e.g. Ford Narrow Tooth, Nissan/Mitsubishi Optical, Harley Davidson, Honda, GM Opti-Spark, BMW, Subaru).

Air Fuel Ratio Sensor

High Accuracy Temperature Compensated Wide Band Air Fuel Ratio Sensor Input (Optional), Range 0.75 to 1.20 Lambda, Resolution 0.01 Lambda, Accuracy 1.5% (below 1.05 La).

Other Sensors

Throttle Position, Manifold Pressure, Engine Temperature and Air Temperature, 2 Auxiliary Sensor Inputs, 2 Digital/Speed Inputs.

Data Logging

Optional Logging memory allows logging of all ECU parameters, Memory Size 512 Kbytes, Logging Rate 1-20 sets/second, Logging Time 38 minutes at 5 sets /sec (28 Parameters + Diagnostics), PC Software is available for analysis of the logged data.

Special Functions

Traction Control & Launch Control (2 wheel speed sensors) (or 4 sensors using the Traction Control Multiplexer), Gear Change Ignition Cut, Wide Band or Narrow Band Air Fuel Ratio Control (3D mapped), Over Run Boost Enhancement
Warning Alarms (Sensor Hi/Lo), Gear Detection, Ground Speed Limiting, Dual RPM Limit, Nitrous Oxide Enrich/Retard, Air Conditioner Request, Over Run Fuel Cut, Sensor Calibration Tables, RPM Limit Hard or Soft Cut Fuel and/or Ignition Cut.

Auxiliary Outputs

Four general purpose outputs (3 shared with ignition outputs), The outputs may be used for: Turbo Wastegate Control, Idle Speed Control, Fuel Used Pulse, Tachometer Output, Shift Light (Gear Dependant), Driver Warning Alarm, RPM/Load dependant device, User Defined Table (20 x 11) with definable axis parameters, Slip Warning, Fuel Pump Relay, Thermatic Fan, Air Conditioner Fan or Clutch.

Diagnostics

Injectors Open Circuit, Short Circuit, Peak Current Not Reached, Sensors Open & Short Circuit, Operating Errors RPM Limit Exceeded, Injector Overduty, Over Boost, Low Battery, Reference Error etc.

Calibration

PC Software is available for calibration.

Telemetry Link

Optional Telemetry Link allows real time monitoring and data logging.

Operating Conditions

Internal Temperature Range -10 to 85 degrees C, Ambient Temperature -10 to 70 degrees C (Depending on load and ventilation), Operating Voltage 6 - 22 V DC, Operating Current 0.4 A max, Reverse Battery External Fuse.
The MOTEC M4 ECU specifications listed here are from www.motec.com.

Appendix B: ECU Wiring Diagram

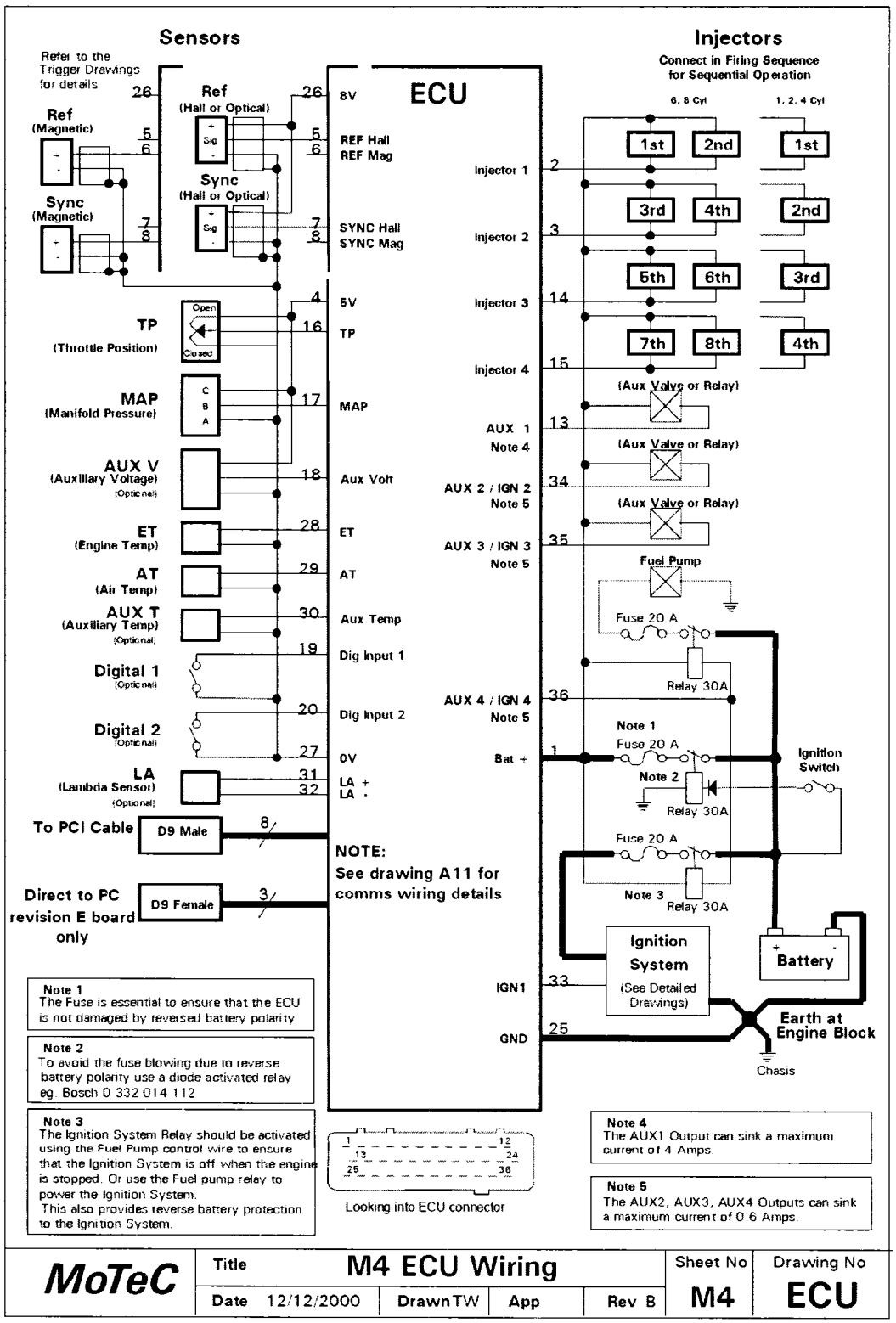

Appendix C: Sample Calculation

The following method was used to calculate the fired engine test results. The cylinder pressure transducer voltage, trigger wheel signal voltage, intake pressure sensor voltage, and injector voltage were recorded to a text file by the NI data acquisition. The intake plenum pressure signal and injector signal were post processed in MS Excel. MATLAB was used to post process the trigger wheel signal and cylinder pressure data.

The text file was imported into the MATLAB program where the cylinder pressure voltages were converted into pressures, as described in section 4.2.2. To obtain the crankshaft angle associated with the pressure data, the program calculated a crank angle based on the trigger wheel voltage signal. To do this, the program first identified the missing teeth in the trigger wheel signal (see section 4.2.2) and established an index tooth. This data point was set relative to the TDC index angle. From that point on, every time the trigger wheel voltage fell through zero volts, the crank angle incremented six degrees. For the data between points passing through zero, interpolated values were inserted. With the crank angle values known, the program calculated the cylinder volume corresponding to each pressure point using Eq. 2.4 (see section 2.1.3).

Before the pressure and volume data could be integrated, the vibration noise in the pressure signal shown in Figure C.1 was removed since it was unrelated to the cylinder pressure. The following filtering method was performed. The "intake closing" noise was fit with a curve representing an isotropic compression process. The initial pressure, p_i, and volume, V_i, are taken to be at the start of the noise and the polytropic exponent, n, is chosen to give the best fit. Eq. C.1 was used to plot the curve where the curve fit pressure, p, is a function of the cylinder volume, V.

$$p = p_i\left(\frac{V_i}{V}\right)^n \qquad (C.1)$$

The "intake opening" was fit with a line with slope, m, current crank angle, θ, and the intercept, z, as shown in Eq. C.2. In reality, z itself was a function of the initial pressure, p_i, just before the noise starts, the slope, m, and the initial crank angle, θ_i, just before the noise starts. The slope was adjusted manually to find a desirable fit.

$$p = m\theta + z \qquad (C.2)$$

During these two manual procedures, the start angle and stop crank angle for each filtered section and controlling variables, n, m, and z where recorded for each cycle. All of this data was entered in a control file that was associated with an engine test file. MATLAB called on the control file when doing each engine test calculation.

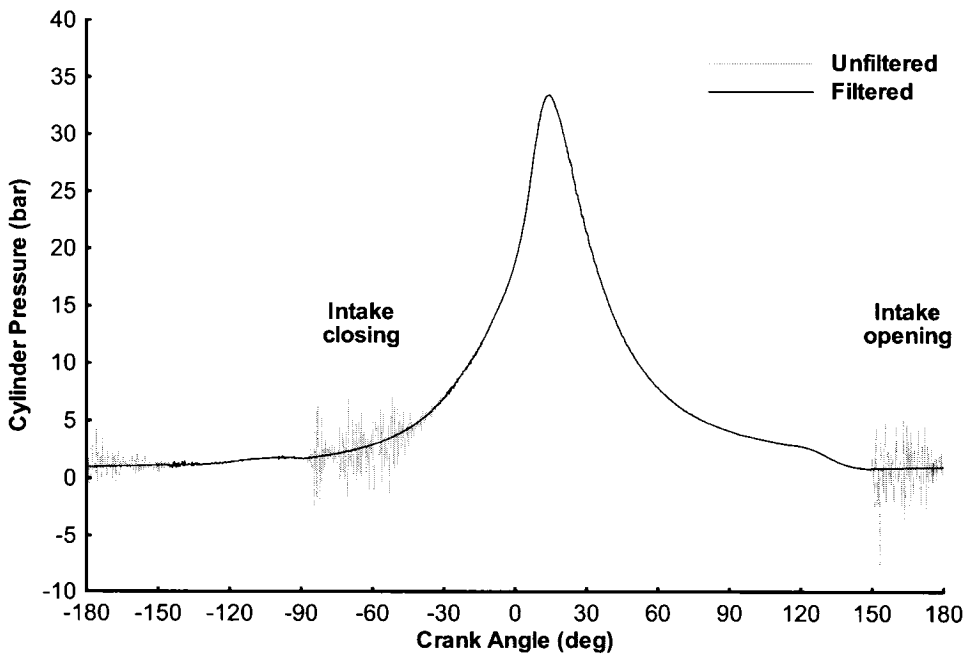

Figure C.1: Pressure trace showing the original data and the filtered data.

With the filtered pressure trace, the algorithm integrated the pV curve using a trapezoidal integration method. An acquisition sample rate of 50 kS/s resulted in 1500 intervals per cycle at 2000 rpm. The number of intervals increased as the engine speed decreased. An engine specifications file was created for the algorithm, and variables such as the fuel pulse width, fuel rate, fuel heating value, brake power, and Kistler pressure transducer offset were included in the control file.

Each single steady-state test contained multiple cycles, roughly 16 cycles for a test done at 1250 rpm, 19 cycles at 1500 rpm, 22 cycles at 1750 rpm, and 26 cycles at 2000 rpm. The MATLAB algorithm calculated the performance results for each individual cycle as demonstrated below, and then averaged them. The indicated results presented for each fired engine test is therefore an average value based on multiple cycles sampled for each steady-state test. The MATLAB code is provided in Appendix D. Not all of the values calculated in the code were used in this thesis.

An example calculation will be developed for one cycle, cycle 11, from test 130 at 2000 rpm and a 5.5 ms fuel pulse width. The averaged results for test 130 are located in Table 5.6. The work per cycle was found using the MATLAB algorithm above. The resulting work per cycle was 189.91 J/cycle. The engine speed was calculated using the trigger wheel signal and the associated time. The resulting average engine speed over the cycle was 2035.3 rpm. The indicated torque, indicated power, power density, and IMEP are calculated below.

$$T_i = \frac{W_i}{2\pi} = \frac{189.91}{2\pi} = 30.24 \text{ N-m}$$

$$P_i = \frac{W_i N}{n_R 60} = \frac{189.91 \cdot 2035.3}{1 \cdot 60} = 6442 \text{ W} = 6.44 \text{ kW}$$

$$V_d = \frac{\pi b^2}{4} s = \frac{\pi 0.086^2}{4} 0.070 = 0.0004066 \text{ m}^3 = 0.4066 \text{ L}$$

$$P_{density} = \frac{P_i}{V_d} = \frac{6.44}{0.4066} = 15.8 \text{ kW/L}$$

$$IMEP = \frac{W_i}{V_d} = \frac{189.91}{0.0004066} = 467068.4 \text{ Pa} = 467.1 \text{ kPa}$$

The ISFC was calculated next. The fuel mass flow rate was calculated using Eq. C.3 where *PW* was the fuel pulse width and *FR* was the injector flow rate. Injectors have a linear relation between the fuel pulse width and the amount of fuel injected. The injector fuel flow rate at 75 bar was 9.0 mg/ms.

$$\dot{m}_f = \frac{PW \cdot FR \cdot N\,60}{1000 n_R} \quad \text{(C.3)}$$

$$ISFC = \frac{\dot{m}_f}{P_i} = \frac{PW \cdot FR \cdot N \cdot 60}{P_i \cdot 1000 \cdot n_R} = \frac{5.5 \cdot 9.0 \cdot 2035.3 \cdot 60}{6.44 \cdot 1000 \cdot 1} = 938.6 \text{ g/kW-h}$$

The fuel conversion efficiency was calculated with the average ISFC:

$$\eta_f = \frac{P_i}{\dot{m}_f Q_{HV}} = \frac{1}{ISFC \cdot Q_{HV}} = \frac{3600}{938.6 \cdot 42} = 0.091 = 9.1\%$$

The mass airflow through the engine was calculated from the volumetric airflow measured by the dynamometer multiplied by the ambient air density in the dynamometer cell. The density was calculated with the dynamometer cell temperature and pressure using the ideal gas law.

$$\rho = \frac{p}{RT} = \frac{101.0}{0.287 \cdot 294} = 1.197 \text{ kg/m}^3$$

The air turbine was calibrated using a flowbench. The uncorrected air mass flow rate, $\dot{m}_{au}$, is corrected using the following equation:

$$\dot{m}_a = 1.0761 \cdot \dot{m}_{au} + 0.000133$$

The corrected air mass flow is then:

$$\dot{m}_{au} = Q_a \rho = 0.02365 \cdot 1.197 = 0.02831 \text{ kg/s}$$

$$\dot{m}_a = 0.02831 \cdot 1.0761 + 0.000133 = 0.0306 \text{ kg/s} = 30.6 \text{ g/s}$$

The delivery ratio was calculated using the resulting air mass flow rates:

$$\Lambda = \frac{\text{mass of fresh charge delivered}}{\text{displaced volume} \times \text{ambient density}}$$

$$\Lambda = \frac{\dot{m}_a \cdot 60}{V_d \cdot N \cdot \rho} = \frac{0.0306 \cdot 60}{0.0004066 \cdot 2035.3 \cdot 1.197} = 1.85$$

Appendix D: MATLAB Program

```
clc;
clear all;
% This program calculates the imep and other values for the given cycle data
%----------------------- input data files ---------------------------
datafile1 = input('Enter data txt filename: ','s');
data = importdata(datafile1);%read in text file
datafile2 = input('Enter curvefit txt filename: ','s');
curvefit=importdata(datafile2);

dataamount  = input('Enter the number of data points: '); %input the amount of data to
write
%dataamount = 40000;
%input crank index from MOTEC
%crankindex = input('Enter the Crank Index (criP): ');
crankindex = 266;
%----------------------- initial loop for zero reference -------------
m=0;
%find the first tooth
endloop = 0;
while endloop == 0;
   m=m+1;
   if data(m,2) >0 & data(m+1,2)<=0
      t1= data(m,1);
      endloop = 1;
   end
end
%find second tooth to get a delta
endloop = 0;
while endloop == 0;
   m=m+1;
   if data(m,2) >0 & data(m+1,2)<=0
      t2= data(m,1);
      endloop = 1;
   end
end
%find index tooth
%needed the first two while loops to find delta
delta = abs(t2-t1);
while abs(t2-t1) <= 2*delta
   %falling
   delta=abs(t2-t1);
   m=m+1;
   if data(m,2) >0 & data(m+1,2)<=0
      t1=t2;
```

```
      t2 = data(m,1);
   end
end
%----------------- angle assignment loop --------------------------
%column identification
timecolumn=1;
%crankcolumn=2
%intakecolumn=3
cylindercolumn=4;
%injector/sparkcolumn=5
cyclecolumn=6;
rpmcolumn=7;
anglecolumn=8;
cyclenumbercolumn=9;
volumecolumn=10;
cylinderpressurecolumn=11;
correctedpressurecolumn=12;
workcolumn=13;

crankangle=0;
cyclecount=0;

offset=360-crankindex;
sampleperiod = data(2,1) - data(1,1);
n1=m+1;

for n=m:dataamount-1
   data(n,cyclecolumn)=cyclecount+1;
   if data(n,2) >0 & data(n+1,2)<=0
      data(n,anglecolumn) = crankangle+offset;
      if n>m % this condition is set so that t2-t1 isn't 0 as it would be in the first loop
         t1=t2;
      end
      t2 = data(n,1);
      if crankangle -(cyclecount*360)<=342
         degreerate = 6/(t2-t1);
      end
      if crankangle -(cyclecount*360)==360
         degreerate = 18/(t2-t1);
      end
      degreestep = degreerate*sampleperiod;
      if crankangle >= 6;
         if crankangle-(cyclecount*360)<=342;
            crank2 = crankangle - 6;
         end
         if crankangle-(cyclecount*360)==360;
```

```
            crank2=crankangle-18;
            cyclecount = cyclecount+1;
          end
          data(n,rpmcolumn) = degreerate/6;
          for l=n1:n-1;
            crank2 = crank2 + degreestep;
            data(l,anglecolumn) = crank2+offset;
            data(l,rpmcolumn) = degreerate/6;
          end
        end
        n1=n+1;
        if crankangle-(cyclecount*360) <342
          crankangle = crankangle + 6;
        else crankangle = crankangle + 18;
        end
    end %end of main loops
end
end
%------------------------- build a column to indicate actual cycle ----------------------
%max_cycle=0;
for p=m:dataamount-1
    if data(p,anglecolumn)>=180
        cyclenumber=fix((data(p,anglecolumn)-180)/360)+1;
        data(p,cyclenumbercolumn)=cyclenumber;
    else
        data(p,cyclenumbercolumn)=0;
    end
end
max_cycle=cyclenumber;
%------------------ establish Pressure curve for numerical integration
% establish volume based on crank angle
enginespecs=importdata('enginespecs.txt');
vc=enginespecs(1,1); %vc in cc
b=enginespecs(2,1)/10; %b in cm
s=enginespecs(3,1)/10; %s in cm
l=enginespecs(4,1)/10; %l in cm
a=s/2;

calvalue=10; %Kistler calibration number
pressureoffset=curvefit(1,17);

for n=m:dataamount-1
    angle=data(n,anglecolumn);
    data(n,volumecolumn)=vc+pi*((b^2)/4)*(l+a-(a*cos(angle*pi/180)+(l^2-
a^2*(sin(angle*pi/180))^2)^(1/2)));
end
```

```
cyc=0;
for n=m:dataamount-1
   pressure=data(n,cylindercolumn)*calvalue+pressureoffset;
   data(n,cylinderpressurecolumn)=pressure;
   data(n,correctedpressurecolumn)=pressure;
   cycle = data(n,cyclenumbercolumn);
   %intake fit
   if data(n,anglecolumn)>180 & cycle < max_cycle;
      if data(n,anglecolumn)>= curvefit(cycle,2) & data(n,anglecolumn)<
curvefit(cycle,3)
         if cyc ~= cycle;
            cyc=cycle;
            initialpressure = data(n,cylinderpressurecolumn);
            initialvolume = data(n,volumecolumn);
         end
         correctedpressure =
initialpressure*(initialvolume/data(n,volumecolumn))^(curvefit(cycle,4));
         data(n,correctedpressurecolumn)=correctedpressure;
      end
      % linear exhaust fit 1
      if data(n,anglecolumn)>= curvefit(cycle,5) & data(n,anglecolumn)<
curvefit(cycle,6)

data(n,correctedpressurecolumn)=curvefit(cycle,7)*data(n,anglecolumn)+curvefit(cycle,8
);
      end
      % linear exhaust fit 2
      if data(n,anglecolumn)>= curvefit(cycle,9) & data(n,anglecolumn)<
curvefit(cycle,10)

data(n,correctedpressurecolumn)=curvefit(cycle,11)*data(n,anglecolumn)+curvefit(cycle,
12);
      end
   end
end
%---------------------- loop for volume and pv work calculation ----------
for n=m:dataamount-1
    data(n,workcolumn) =
(data(n,correctedpressurecolumn)+data(n+1,correctedpressurecolumn))*abs(data(n+1,vol
umecolumn)-data(n,volumecolumn))/(2*10);
end
% this loop finds each zone (compression and expansion) and then sums the
% pv_work within each zone
work=0;
prev_zone=0;
zone_half=1;
```

```
cycle=1;
for n=m:dataamount-1
   if data(n,anglecolumn)>180 & cycle < max_cycle;
      angle = data(n,anglecolumn);
      zone = fix(angle/180);  %odd zones are compression
      %data2(n,1)=angle;
      %data2(n,3)=zone;
      if zone ~= prev_zone
         results(cycle,zone_half) = work;
         work=0;
         prev_zone =zone;
      end
      cycle = data(n,cyclenumbercolumn);
      %data2(n,2)=cycle;
      %data2(n,5)=data(n,workcolumn);
      %data2(n,6)=work;
      %data2(n,7)=data(n,correctedpressurecolumn);
      zone_half = fix(zone/cycle);
      %data2(n,4)=zone_half;
      work = work + data(n,workcolumn);
   end
end
%---------------------------- loop to get times at start of cycle ------------
old_cycle=0;
t1=0;
k=0;
for n=m:dataamount-1
   if data(n,cyclenumbercolumn)~=old_cycle
     k=k+1;
     time(k,1)=data(n,1);
     old_cycle = data(n,cyclenumbercolumn);
   end
end
%------------------- loop for rpm --------------
 for n=1:cycle-1
   results(n,4) = 60/(time(n+1,1)-time(n,1));% calculates engine rpm for each cycle based
on the time matrix
end
%------------------- loop to get power ------------------
vd = pi*(b^2)*s/4; %displacement volume
for n=1:cycle-1
   results(n,3)= results(n,2)-results(n,1); %calculates gross indicated work per cycle
   results(n,5)= results(n,3)*results(n,4)/(60*1000); %calculates gross indicated power
per cycle #of cylinders=1
   results(n,6)= results(n,3)/(2*pi); %calculates gross indicated torque
   results(n,7)= results(n,5)*60*1000000/(vd*results(n,4)); %calculates imep
```

```
end
%----------------- fuel calculations -------------
% pulsewidth = curvefit(1,13)
% fuelrate = curvefit(1,14)
% heatingvalue = curvefit(1,15)
% fuel energy = results
for n=1:cycle-1
   results(n,8) = curvefit(1,13)*curvefit(1,14)*results(n,4)*curvefit(1,15)/(60*1000000);
% calculates fuel energy in kW
   results(n,13) = curvefit(1,13)*curvefit(1,14)*results(n,4)*60/(results(n,5)*1000); %
calculates the specific fuel consumption
end
%----------------- efficiency calculations ----------
% brakepower = curvefit(1,16)
for n=1:cycle-1
   results(n,10) = curvefit(1,16)*0.7457; %brake power converted to kW
   results(n,9) = results(n,5)/results(n,8); %indicated thermal efficiency
   results(n,11) = results(n,10)/results(n,8); %brake thermal efficiency
   results(n,12) = results(n,11)/results(n,9); %mechanical efficiency
end
%----------------- engine stats -------------------
average = mean(results); %average of all result columns
std_dev = std(results); %standard deviation of all results column, use N-1 standard dev
cov_imep = std_dev(1,7)/average(1,7)*100; % coefficient of variance for the imep
%----------------- output -------------------
outputfile1 = strrep(datafile1,'.txt','_with_IMEP.txt');
save (outputfile1,'data','-ascii','-double','-tabs');
outputfile2 = strrep(datafile1,'.txt','_results.txt');
save (outputfile2,'results','-ascii','-double','-tabs');
outputfile3 = strrep(datafile1,'.txt','_average.txt');
save (outputfile3,'average','-ascii','-double','-tabs');
outputfile4 = strrep(datafile1,'.txt','_cov_imep.txt');
save (outputfile4,'cov_imep','-ascii','-double','-tabs');
disp('done');
plot(data(1:dataamount-50,8),data(1:dataamount-50,12));
xlim([180,6500]);
ylim([-5,45]);
end
```

Appendix E: Intake Compressor Power Consumption Estimate

An estimate for the power consumed to pressurize the scavenging charge is necessary to determine if the novel engine produces a net power. A simple estimate based on isentropic compression is developed below.

The power required to compress air isentropically is calculated from Eq. (E.1). Where, $\dot{m}$, is the air mass flow through the compressor, C_p, is the specific heat at constant pressure, T_{amb}, is the entrance air temperature, p_r, is the pressure ratio, and γ is the ratio of specific heats for air.

$$P_s = \dot{m} C_p T_{amb}\left(p_r^{\frac{\gamma-1}{\gamma}} - 1 \right) \qquad \text{(E.1)}$$

For an estimate, the operating conditions from section 5.2.5 will be used. For an air mass flow of 31 g/s, T_{amb} of 294 K, C_p of 1.005 kJ/kg-K, p_r of 1.5, and γ of 1.4, the resulting isentropic power required is 1.13 kW. To find the actual power required to compress the air, an isentropic efficiency and mechanical efficiency of 0.80 and 0.85 respectively, are applied. The resulting power required is 1.7 kW. This estimate assumes that the compressor is adiabatic and also estimates the two efficiencies used in the calculation.

The difference between the indicated power and brake power from the dynamometer at 2000 rpm is 0.4 kW, yielding a rough estimate for friction losses. Therefore the net power equals the indicated power minus the compressor power estimate and the friction. The resulting net power is about 4.4 kW. Therefore with an efficiently designed compressor, the engine would produce a net positive power.

Appendix F: Uncertainty Estimation

An estimation of the uncertainty associated with the indicated torque, indicated power, IMEP and ISFC is developed here. The uncertainty in the work done per cycle is required first since it is the basis for the subsequent calculations. It is assumed that the largest source of uncertainty would come from the determination of TDC, since the volume calculation is based on this. An error in TDC location would alter the area under the pV curve and hence the work done per cycle. Therefore, the uncertainty in work per cycle was calculated using the uncertainty extremes from the TDC index angle.

The following example uses test 130 in section 5.2.5 and all uncertainties are at 95% confidence. The nominal TDC index angle is 266° with an assumed bias uncertainty ±0.5° or 0.2%. The work per cycle at 266° is 192.0 J. If the actual angle is 0.5° lower at 265.5°, the work per cycle is 195.1 J an overshoot of 3.1 J or 1.6% from the nominal work. If the angle is 0.5° higher at 266.5°, the work per cycle is 187.1 J an undershoot of 4.9 J or 2.6% from the nominal work. Therefore, the bias uncertainty in work per cycle is as high as 4.9 J or 2.6%.

The precision uncertainty in the work per cycle can be estimated using a student t-distribution [47]. For a sample of 26 cycles, sample standard deviation of 11.3 J, and a confidence of 95%, the precision uncertainty is ±4.6 J or 2.4%. Combining the precision and bias uncertainties in a root-mean-square method yields a total uncertainty in the work per cycle of ±6.7 J or 3.5%.

The engine speed is calculated from the trigger wheel signal time data. The bias uncertainty is assumed negligible since the speed measurement is relative. The precision uncertainty can be estimated using the student t-distribution. For a sample of 26 cycles,

sample deviation of 12.2 rpm, and a confidence of 95%, the precision uncertainty is 4.9 rpm or 0.2%. Therefore, the total uncertainty in the engine speed is ±4.9 rpm or ±0.2%.

From these the two total uncertainties found above, the uncertainty in the torque and power can be found using uncertainty propagation. The resulting total uncertainty for the indicated torque is ±1.1 N-m or ±3.5% and the uncertainty for the indicated power is ±0.2 kW or ±3.1%.

The uncertainty in the IMEP requires the uncertainty in the displacement volume calculation. The bias uncertainty is ±0.005 mm and the precision uncertainty is estimated as negligible. Therefore propagating the uncertainty through the displacement calculation yields a total uncertainty of ±0.6 cm^3 or ±0.1%. The total uncertainty in IMEP is then ±16.5 kPa or ±3.5%.

The ISFC uncertainty is dependent on the fuel pulse width uncertainty and the fuel flow uncertainty. The total uncertainty in the fuel pulse width can be assumed to be 0.2 ms arising from any opening and closing delay that would bias the data. The fuel flow rate has a total uncertainty of ±4% taken from the specifications sheet. With these uncertainties, the resulting total uncertainty in ISFC is ±58.0 g/kW-h or ±6.1%.

Table F.1: Uncertainty summary for example test 130.

Result	**Uncertainty**
Work per cycle	±6.7 J / ±3.5%
Indicated Torque	±1.1 N-m / ±3.5%
Indicated Power	±0.2 kW / ±3.1%
Displacement	±0.6 cm^3 / ±0.1%
IMEP	±16.5 kPa / ±3.5%
ISFC	±58.0 g/kW-h / ±6.1%